Doctoral Dissertation

STUDIES ON STABILIZATION OF POWER SYSTEM WITH DISTRIBUTED GENERATIONS USING VIRTUAL SYNCHRONOUS GENERATOR

Jaber Alipoor

January 2015

Graduate School of Engineering,
Osaka University

To my Wife and Parents

Acknowledgments

During my stay as a PhD candidate at Osaka University, I have received an enormous amount of support from various people and it is my great pleasure to take this opportunity to express my sincere gratitude to them all.

First and foremost, I would like to express my deepest gratitude and appreciation to my principal supervisor, Professor Toshifumi Ise for the opportunity of working under his supervision, his excellent guidance, and grate support. It is a great honor for me to have been a member of his laboratory. I present my sincere appreciation to Dr. Yushi Miura, the associate professor of Ise laboratory, for his patience, kindness, and precious advices during my doctoral studies. Without the indispensable guidance of my supervisors, the completion of this thesis would not have been possible.

I extend my appreciation to Professor Tsuyoshi Funaki in the Division of Electrical, Electronic and Information Engineering, Osaka University, for his careful review on my thesis and many useful comments.

I present my sincere thanks to Professor Tetsuzo Tanino, Professor Shigemasa Takai, and Professor Hiroyuki Shiraga in the Division of Electrical, Electronic and Information Engineering, Osaka University, for serving as members of my dissertation committee.

I am also grateful for the helpful and constructive advices of Dr. Yuji Shindo in Kawasaki Heavy Industries.

I gratefully acknowledge the scholarship provided by Mitsubishi Corporation and Nikki-Saneyoshi foundation during my tenure as PhD student.

My cordial appreciation goes to Taisei Nomura, the Professor Emeritus of Osaka University and the leader of Nomura Project of the National Institute of Biomedical Innovation of Japan, for his invaluable help and support. I addition, I wish to thank Dr. Haruko Ryo and Dr. Shigeki Adachi, and other members of Nomura Project for their support, kindness and warm friendship.

I would like to thank the members of Ise laboratory for the friendly atmosphere, help, and cooperation. Especially, I want to thank my colleague at Ise laboratory, Mr. Kenichi Sakimoto for his helps. In addition, I am thankful to all academic and non-academic staff of Osaka University for the support given to me in a countless number of ways. A special thanks to Ms. Yuri Okunishi in the Advisory Division for International Students (ADIS) for her kind helps.

Hearty thanks go to my parents, sister, and brothers for the support and encourage I received from them in every possible way.

Last but not least, my special thanks to my wife Ayumi who has been there for me through the worst of times and who has the patience of a saint. Thank you for all of your love, support, sacrifice, encouragement, and dedication.

Abstract

In centralized electric power generation, the electric power is generated mainly by enormous Synchronous Generators (SGs). In the power system with huge SGs, the frequency is determined by the rotational frequency that itself depends on the prime mover power. In case of a fault or disturbance, the kinetic energy preserved in massive rotors and associated equipment is injected to the power system to maintain the energy balance. Moreover, the inertia of the rotating masses prevents sudden changes in frequency and enhances the stability of power system. The decentralization of the electric power generation increased the number of inverter-based power sources. If these inverter-based units are operated and controlled similar to SGs, a large portion of problems involved with distributed generation (DG) and microgrids such as frequency regulation, islanded operation, and parallel operation of inverter-based DGs will be solved. The Virtual Synchronous Generator (VSG) is an inverter based generating unit that uses a synchronous generator model to emulate the dynamic behavior of a SG with a specific value of virtual inertia. By such scheme, the inverter-based generator can benefit the advantage of a SG in frequency stabilization, preserving its original features. In the first chapter of this dissertation, the merit of the VSG concept is discussed and the basic structure that is used in this research is elaborated. Besides, the majority of the existing VSG topologies are reviewed.

The VSG control uses the swing equation of a synchronous machine to express a virtual inertia property. Unlike a real synchronous machine, the parameters of the swing equation of the VSG can be controlled in real time to enhance the fast response of the generator in tracking the steady-state frequency. Based on this concept, the VSG with alternating inertia is introduced in chapter two. This scheme adopts the suitable value of the moment of inertia of the VSG considering its virtual angular velocity and its rate of change during oscillations. The damping effect of the Alternating Inertia scheme is investigated by transient energy analysis. In addition, the performance of the proposed inertia control in stability of nearby machines in power system is addressed in this chapter.

In chapter three, the parameters of the VSGs of the microgrid with multiple VSG units are tuned to obtain the desired response. In this dissertation, the multi-VSG microgrid is introduced and the Voltage Angle Deviation (VAD) of generators respect to the angle of the center of inertia is defined as a tool for transient stability assessment of the multi-VSG microgrid. Afterwards, particle swarm optimization is implemented to tune the parameters of the VSG units in order to achieve a smooth transition after a change or disturbance and also to keep the VAD of generators within the stability limit. Moreover, alternating inertia is applied to the VSGs of the multi-VSG microgrid to suppress the oscillation quickly and improve transient stability after a large disturbance.

Because of the limitation in inverter power and current, their operation under disturbances should be evaluated and enhanced. In chapter four, the VSG unit response to the symmetrical and unsymmetrical voltage sags is assessed. A theoretical analysis that traces the trajectory of the state variable of the system during voltage sag is represented. By this analysis, the effect of the characteristics of symmetrical and unsymmetrical voltage sags on the severity of their consequences is justified. In addition, it is detected that two sorts of transients appear that must be mitigated: one is the transients during voltage sag and the other one is the transient after voltage recovery. To prevent the overcurrent during voltage sags, voltage amplitude control and output power control, and to suppress the transients after voltage recovery, alternating inertia control are implemented.

Table of Contents

Chapter 1

Introduction

1.1- The origin of the Virtual Synchronous Generator

The portion of Distributed Generating (DG) units in power systems respect to its total power capacity is increasing rapidly; and a high penetration level is expected for the next two decades. For example only in Japan, 14.3 GW photovoltaic (PV) electric energy is planned to be connected to the grid by 2020, and it will be increased to 53 GW by 2030. In European countries, the USA, China, and India significant targets are also aimed for using the DGs and renewable energy sources (RESs) in their power systems up to next two decades.

In the conventional centralized power generations, in which the synchronous machine dominates, enormous synchronous generators (SGs) comprise rotating inertia due to their rotating parts. The intrinsic kinetic energy (rotor inertia) and damping property (due to mechanical friction and electrical losses in stator, field and damper windings) of the bulk synchronous generators play a significant role in the grid stability. These generators are capable of injecting the kinetic energy preserved in their rotating parts to the power grid in the case of disturbances or sudden changes. Moreover, the slow dynamic of the huge generators, allows the system to damp the transients after a change or disturbance through oscillations and thereby, keep balance between the power generation and demand within the required time scale.

The growing DG/RES units have either very small or no rotating mass (which is the main source of inertia) and damping property and therefore, the grid dynamic performance and stability is affected by insufficient inertia and damping of DGs/RESs. The most challenging issue with the inverter-based units is to synchronize the inverter with the grid and then to keep it in step with the grid even when disturbances or changes happen [1]-[3]. A power system with a big portion of inverter based DGs is prone to instability due to the lack of adequate balancing energy injection within the proper time interval [4]. The instability may happen in form of frequency variation with high rate, low/high frequency, and out-of-step of one or a group of generators. Voltage rise due to reverse power from PV generations [5], excessive supply of electricity in the grid due to full generation by the DGs/RESs, power fluctuations due to variable nature of RESs, and degradation of frequency regulation (especially in the islanded microgrids [6]), can be considered as some negative results of mentioned issue.

A solution towards stabilizing such a grid is to provide additional inertia, virtually. A virtual inertia can be established for DGs/RESs by using short term energy storage together with a power electronics inverter/converter and a proper control mechanism. By controlling the output of an inverter, it can emulate the behavior of a real synchronous machine. In this idea, the inverter-based interface of the DG unit is controlled in a way to exhibit a reaction similar to that of a synchronous machine to a change or disturbance. This concept is known as *virtual synchronous generator* (VSG) [7] or *virtual synchronous machine* (VISMA) [8]. This design is expected to operate like a synchronous generator, exhibiting amount of inertia and damping properties, by controlling the amplitude, frequency, and the phase angle of its terminal voltage. Therefore, it can contribute to the regulation of grid voltage and frequency. In addition, synchronizing units, such as phase-locked loops, can be removed [9]. As a result, the virtual inertia concept may provide a basis for maintaining a large share of DGs/RESs in future grids without compromising system stability.

In this chapter, first the fundamentals and the structure of VSG system are introduced, emphasizing the VSG scheme implemented in this dissertation. Then, the energy storage considerations are mentioned briefly. In continuation, the application of VSGs in microgrids control is explained. Afterward, the major VSG topologies with a brief review on their structure are presented.

1.2- Fundamentals and Structure of VSG

The objective of the VSG scheme is to reproduce the dynamic properties of a real synchronous generator (SG) for the power electronics-based DG/RES units, in order to inherit the advantages of a SG in stability enhancement. The principle of the VSG can be applied either to a single DG, or to a group of DGs. The first application may be more appropriate to individual owners of DGs, whereas the second application is more economical and easier to control from the network operator point of view [10]. The dynamic properties of a SG provides the possibility of adjusting active and reactive power, dependency of the grid frequency on the rotor speed, and highlighting the rotating mass and damping windings effect as well as stable operation with a high parallelism level [11].

The VSG consists of energy storage, inverter, and a control mechanism as shown in Fig. 1.1. In this scheme, the VSG serves as an interface between the DC bus and the grid. The virtual inertia is emulated in the system by controlling the active power through the inverter in inverse proportion of the rotor speed. Aside from higher frequency noise due to switching of inverter's power transistors [12], there is no difference between the electrical appearance of an electromechanical SG and electrical VSG, from the grid point of view.

In the VSG control block, generally a dynamic equation similar to the swing equation of the SGs is embedded that determines the output power based of the rate of the change of frequency and the frequency mismatch with respect to the nominal frequency. The block diagram of the VSG system used in this research is shown in Fig. 1.2. In this scheme, a distributed resource (DR) is

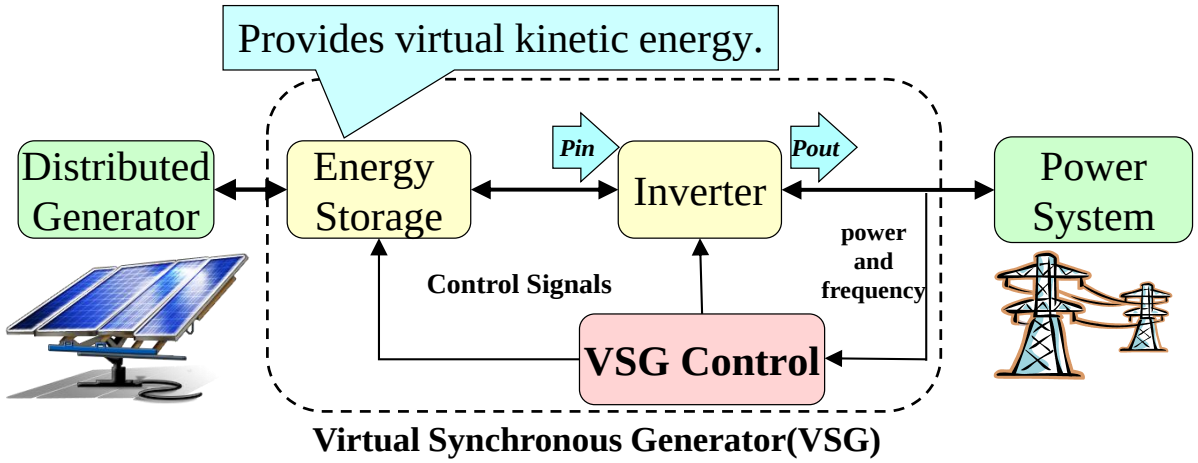

Fig. 1.1- General structure and concept of the VSG.

connected to the main power system via an inverter controlled based on the VSG concept. The model of synchronous generator that is used in this dissertation is a cylindrical-rotor type synchronous generator connected to an infinite bus as shown in Fig. 1.3. The well-known swing equation of synchronous generators is used as the heart of the VSG model:

$$P_{out} = P_{in} - J\omega_m \, d\omega_m / dt - D\Delta\omega \tag{1.1}$$

where P_{in}, P_{out}, J, ω_m, and D are the input power (as same as the prime mover power in a synchronous generator), the output power of the VSG, the moment of inertia of the virtual rotor, the virtual angular velocity of the virtual rotor, and the damping factor, respectively. $\Delta\omega$ is given by $\Delta\omega = \omega_m - \omega_{grid}$, ω_{grid} being the grid frequency or the reference frequency when the grid is not available. Using voltage and current signals measured at the VSG terminals, its output power and frequency are calculated. A governor model shown in Fig. 1.4 is implemented to tune the input power command based on the frequency deviation. The grid frequency is detected by a frequency detector block that can be a (Phase Locked Loop) PLL. The block diagram of a PLL is shown in Fig. 1.5. Having the essential parameters, (1.1) is solved by numerical integration. Runge-Kutta method is an appropriate approach. The procedure of calculating ω_m by Runge-Kutta method is shown in Fig. 1.6. By solving (1.1), the momentary ω_m is calculated and by passing through an integrator, the virtual

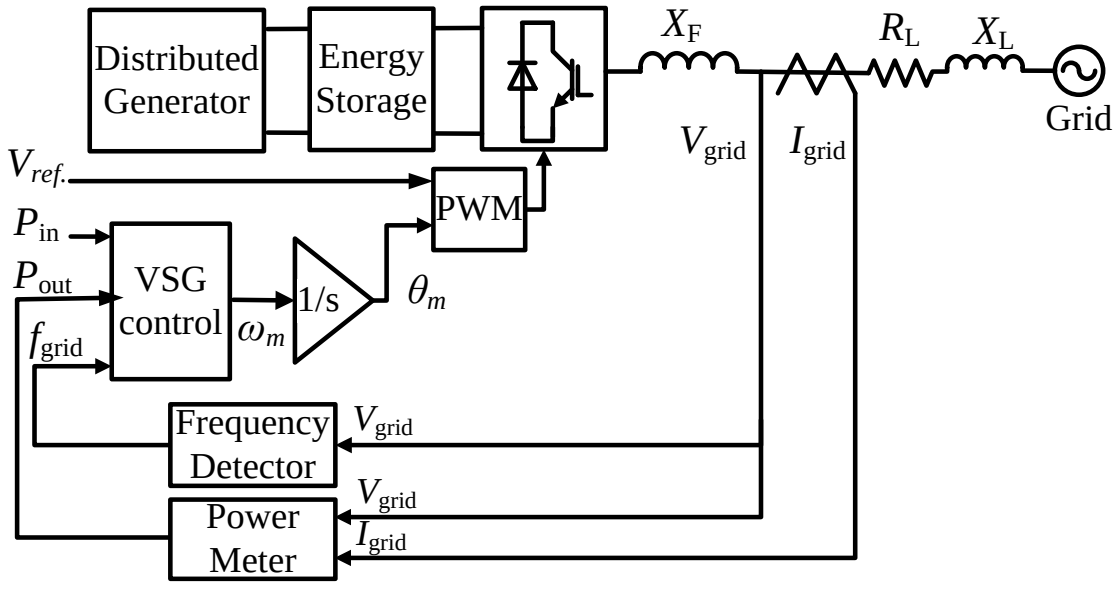

Fig. 1.2- Block diagram of the VSG unit.

mechanical phase angle θ_m is produced. $V_{ref.}$ in Fig. 1.1 is the voltage reference that determines the voltage magnitude at the inverter terminal. Implementing a controller for $V_{ref.}$ results in a regulated voltage and reactive power at the VSG terminal. The phase angle and the voltage magnitude reference are used as the VSG output voltage angle and magnitude commands to generate PWM pulses for the inverter.

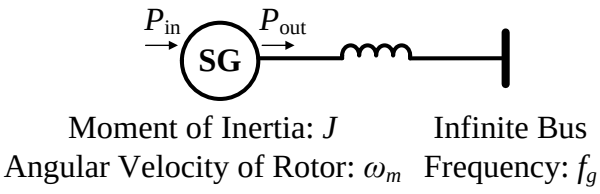

Fig. 1.3- Model of synchronous generator.

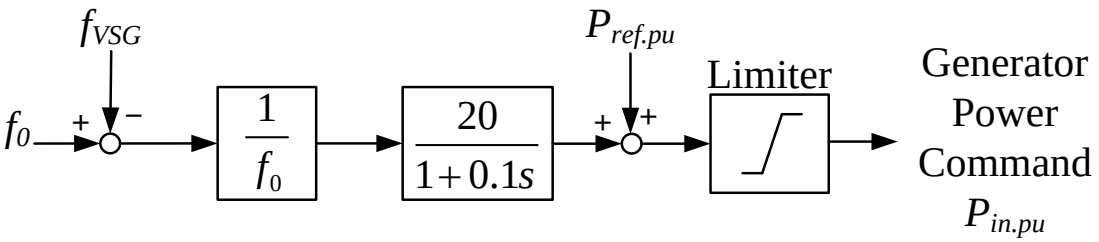

Fig. 1.4- Governor diagram.

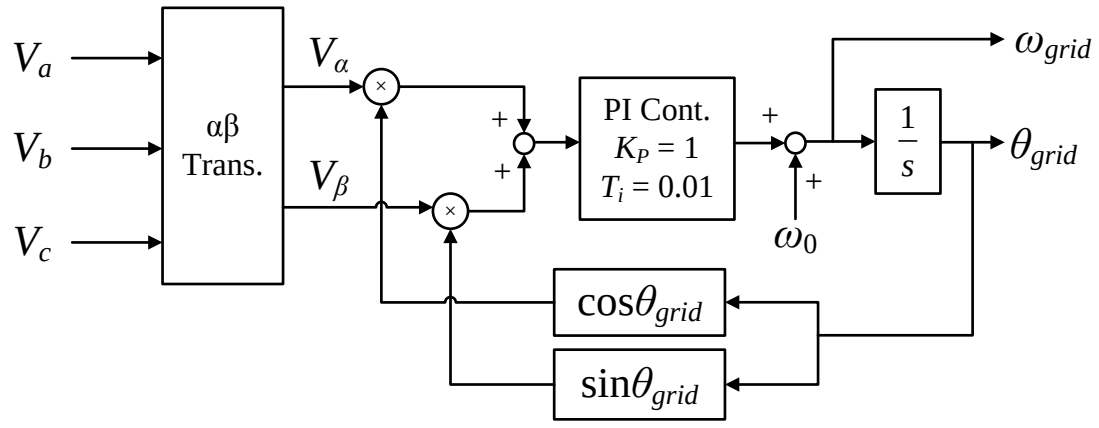

Fig. 1.5- Block diagram of PLL.

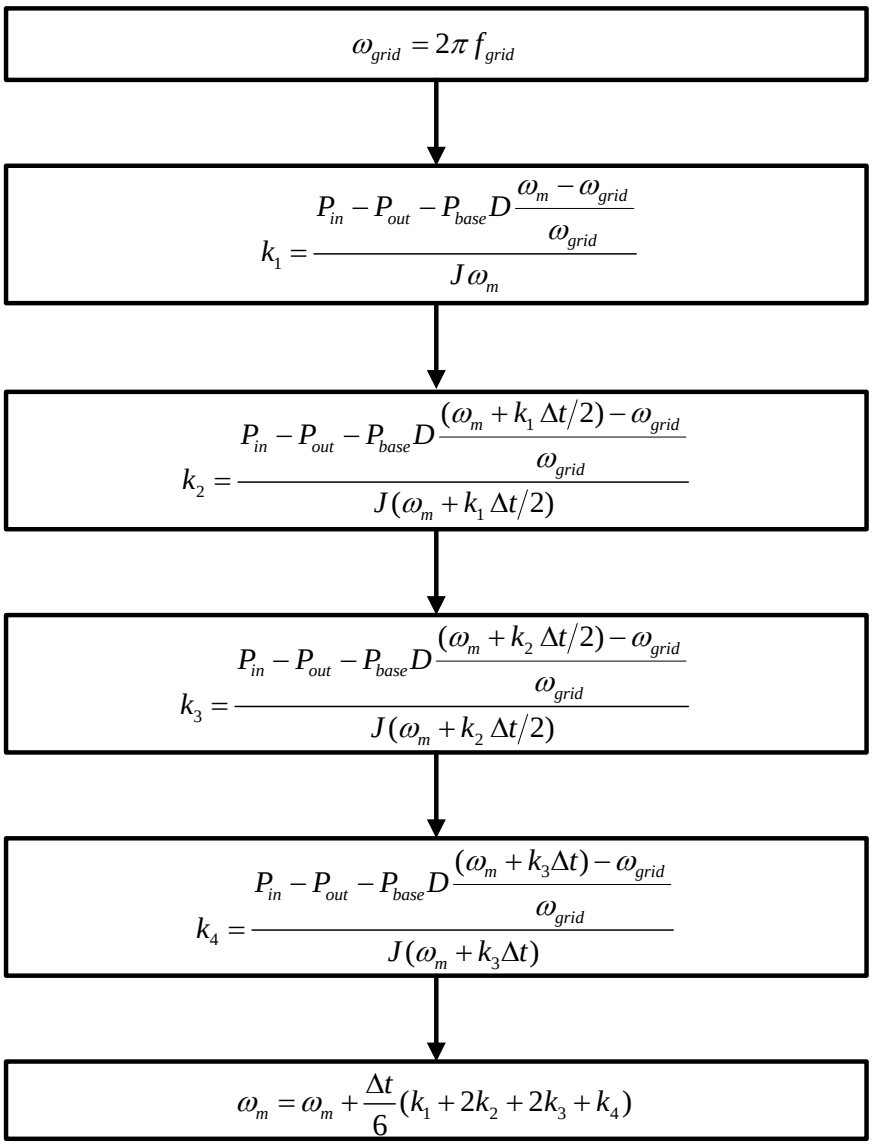

Fig. 1.6- Procedure of calculating ω_m by Runge-Kutta method.

The value of *J* together with *D* in (1.1) determines the time constant of the VSG unit. Selecting the proper value of them is a challenging issue without a routine. Mimicking a synchronous machine, *J* is the inertia emulating characteristic given by $J = 2HS_0/\omega_0^2$, where *H* is the machine inertia constant, S_0 is the nominal apparent power of the machine, and ω_0 is the system frequency. The parameter *H* tells that for which period of time the machine is able to supply the nominal load based solely on the energy stored in the rotating mass. The higher *H*, the bigger the time constant, resulting in a slower response but smaller frequency deviation after a change or disturbance. Although it depends on the machine size and power, for typical synchronous machines *H* varies between 2 and 10 s.

By (1.1), the initial rate of frequency change ($d\omega/dt$) provides an error signal (with equilibrium of zero). When this signal is zero and frequency matches ω_{grid}, the output power of VSG follows the power command P_{in}. When there is a frequency variation due to a change of disturbance, the error signal will be a non-zero value and causes power oscillations. If the term $D\Delta\omega$ is neglected, power will be exchanged only during the transient state without necessarily returning back the output frequency to the nominal value. In order to cover this issue, a frequency droop part $\Delta\omega$ is added as shown in (1.1). The $D\Delta\omega$ emulates the damper windings effect in a SG, and represents the linear damping. It must be chosen so that the P_{out} to be equal with the nominal power of the VSG when the frequency deviation is at the specified maximum value [13].

Considering only virtual inertia effect ($J\omega_m d\omega/dt$), increasing the moment of inertia, J reduces the maximum deviation of the rotor speed following a disturbance; however the natural frequency and the damping ratio of the system may be decreased [14].

In summary, the virtual mass counteracts the frequency drops by injecting/extracting active power and the virtual damper suppresses the oscillation so these features are equally effective to electromechanical synchronous machines. The J and D should be fixed so that the VSG exchanges its maximum active power when the maximum specified frequency variation and rate of frequency change occur. The larger J and D means that more power will be either injected or absorbed for the same amount of frequency deviation and rate of frequency change, respectively. However, oppositely, large values of J and D with specific power rating results in a small frequency excursion.

As mentioned, increasing of J provides a higher amount of equivalent inertia for the VSG, however there is a limit. This limit is mainly imposed by inverter capacity and PLL accuracy. The inverter capacity does not have the overload capacity of a synchronous machine. Thus, a high derivative term leads to bigger power overshoots during transients (frequency deviations), and the inverter must sustain an important overload. The accuracy in frequency-tracking depends on the performance of the implemented PLL. Therefore, the optimal value of derivative term in (1.1) can be obtained by a tradeoff between the virtual inertia, the inverter overload capacity, and the PLL characteristics.

1.3- Energy Storage Considerations

In a real synchronous generator, energy consumed by damping term is absorbed by resistance of damping windings. However, in the case of VSG, this power fluctuation should be absorbed by the energy storage device to balance the grid powers. In order to select the storage technology for an VSG application case, the most important parameters are: maximum power of the loads in the considered grid; the power of the controllable generation units; averaged State Of Charge SOC at normal operation; detection time; control delay; and maximum total response time delay [15].

Since the VSG should be able to inject or absorb power, the nominal SOC of the energy storage in the VSG should be operated at about 50% of its nominal capacity in a stationary situation [15]. Fully charged and/or relatively small capacity energy storage may result in an overvoltage failure in case of reverse power. The VSG operation states can be defined based on the SOC situation according to the specified lower and upper limits (e. g., 20 and 80 percent of maximum charge [23]). When the SOC is between about these limits, the VSG is working in its active (VSG) mode, when the energy in the system excesses, the VSG is working on the virtual load mode. The limits can be determined based on the used energy storage technology. In this research, the energy storage is not dealt with and a capacitor at the DC link is implemented as the energy storage unit assuming that the DG can supply sufficient power for the load during steady state and transients. The reverse power that may cause overvoltage failure will be dealt with by enhancing the VSG control.

1.4- VSG in Microgrids

A microgrid is an interconnection of domestic distributed loads and low voltage distributed energy sources, such as microturbines, wind turbines, PVs, and storage devices. The microgrids are placed in the low voltage (LV) and medium voltage (MV) distribution networks. This has important consequences. With numerous DGs connected at the distribution level, there are new challenges, such as system stability, power quality and network operation that must be resolved applying the advanced control techniques at LV/MV levels rather than high voltage levels which is common in conventional power system control [16, 17].

The VSG systems can be used as effective control units to compensate the lack of inertia and in result the control of active and reactive power as well as microgrid voltage and frequency. A

microgrid with VSG units is shown in Fig. 1.7. The VSGs can be connected between a DC bus/source and an AC bus, anywhere in the microgrid. These systems are going to be more vital to overcome fluctuations caused in the microgrid due to integration of large number of DGs with low or no inertia [16]. Some loads can be also locally controllable using the load controllers. The load controllers are usually used for demand side management.

In microgrids with small power capacity, a change or disturbance in the system (such as a temporary imbalance between production and demand after loss of a large generating unit) results in a high rate variation in the rotating speed of generators. Conventional technologies used for power generation are not always capable of responding quickly enough to prevent unacceptably low frequency in such cases, even when the available amount of frequency control reserve exceeds the power deviation [16]. It results in relatively frequent use of load-shedding, with subsequent consequences on the economic activity, to restore the power equilibrium and prevent frequency collapse [18]. With an appropriate control strategy, the VSGs equipped with fast-acting storage devices can help microgrids to mitigate the frequency excursions caused by generation outages, thus reducing the need for load-shedding [16].

During the grid-connected operation, all the DGs and inverters in the microgrid use the signals of grid voltage and frequency as reference for voltage and frequency. In this mode, it is not possible to highlight the VSG contribution to the grid inertia, due to system size differences. However, in islanding, the DGs lose that reference. In this case the DGs may use the VSG units, and may coordinate to manage the simultaneous operation using one effective control techniques such as master/slave control, current/power sharing control, and generalized frequency and voltage droop control techniques [17]. The balance between generation and demand of power is an important requirement of the islanded operation modes. In the grid-connected mode, the microgrid exchanges power to an interconnected grid to meet the balance, while, in the islanded mode, the microgrid should meet the balance for the local supply and demand using the decrease in generation or load shedding [16].

During the islanded mode, if there are local load changes, local DGs will either increase or reduce their production to keep constant the energy balance, as far as possible. In an islanded operation, a microgrid works autonomously, therefore must have enough local generation to supply

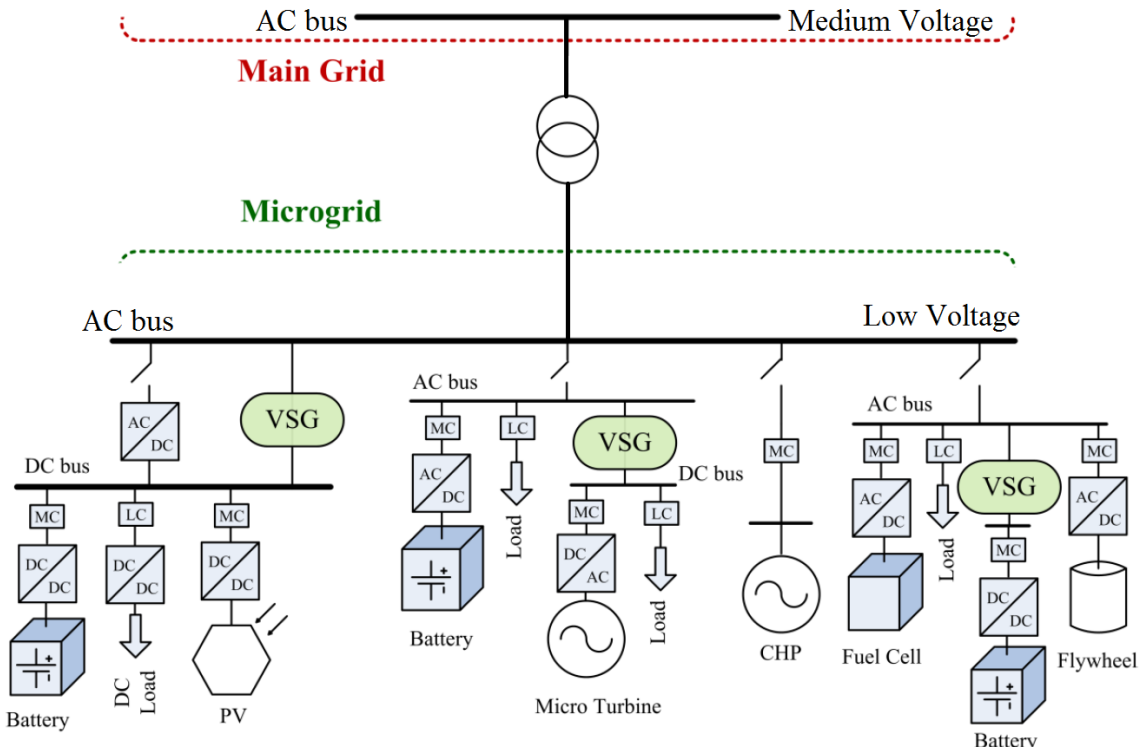

Fig. 1.7- Microgrid structure with VSG units [16].

demands, at least to meet the sensitive loads. In this mode, the VSG systems may present a significant role to maintain the active and reactive power [16].

Immediately after islanding, the voltage, phase angle and frequency at each DG in the microgrid change. For example, the local frequency will decrease if the microgrid imports power from the main grid in grid-connected operation, but will increase if the microgrid exports power to the main grid in the grid-connected operation [16]. The duration of islanded operation will depend on the size of storage systems. In this case they are sized to maintain the energy balance of the network for few minutes. The VSG control algorithms for islanding and grid-connected modes are different, as the islanded microgrid has to define its own frequency and voltage to maintain operation [19]. When the main grid has returned to normal operation, the frequency and voltage of the microgrid must be synchronized with and then reconnected to the main grid.

1.5- Existing VSG Topologies

The idea of VSG control emerged from October 2007 and up to now several groups developed various designs with the same fundamentals introduced in section 1.2. The VSG concept and application were introduced in [20], [21]. The same concept under the title of Synchronverter is

described in [22]. The VSYNC project under the 6th European Research Framework program [7, 10,13, 15, 19, 20, 23, 24, 25, 26], the Institute of Electrical Power Eng. (IEPE) at Clausthal University of Technology in Germany [11, 12, 27, 28], the VSG research team at Kawasaki Heavy Industries (KHI) [29], and the ISE Laboratory in Osaka University [4, 30, 31, 32, 33, 34, 35, 36] in Japan, can be addressed as the most active research groups in this area. In what follows, the overall frameworks of some developed VSG structures are explained.

1.5.1- VSYNC's VSG Design

The VSYNC research group is the initiator of the VSG concept in 2007 [37]. The initial VSG invented by this group with its full control connections is shown in Fig. 1.8. Here, energy storage unit connected to the grid through an inverter and LCL filter. The VSG control produces the current reference to be used in the current controller. The PLL is used to produce the rate of frequency change ($d\omega/dt$) using the grid terminal voltage *Vg*. In addition, it provides the phase angle reference for rotating frame for *dq* control of inverter quantities. The "Calculation" block produces the current reference in *dq*-coordinates from the measured grid voltage, SOC, $\Delta\omega$, $d\Delta\omega/dt$, and voltage reference through the following equations:

$$P = K_{SOC}\Delta SOC + K_P\Delta\omega + K_I\frac{d\Delta\omega}{dt} \tag{1.2}$$

$$Q = K_V\Delta V \tag{1.3}$$

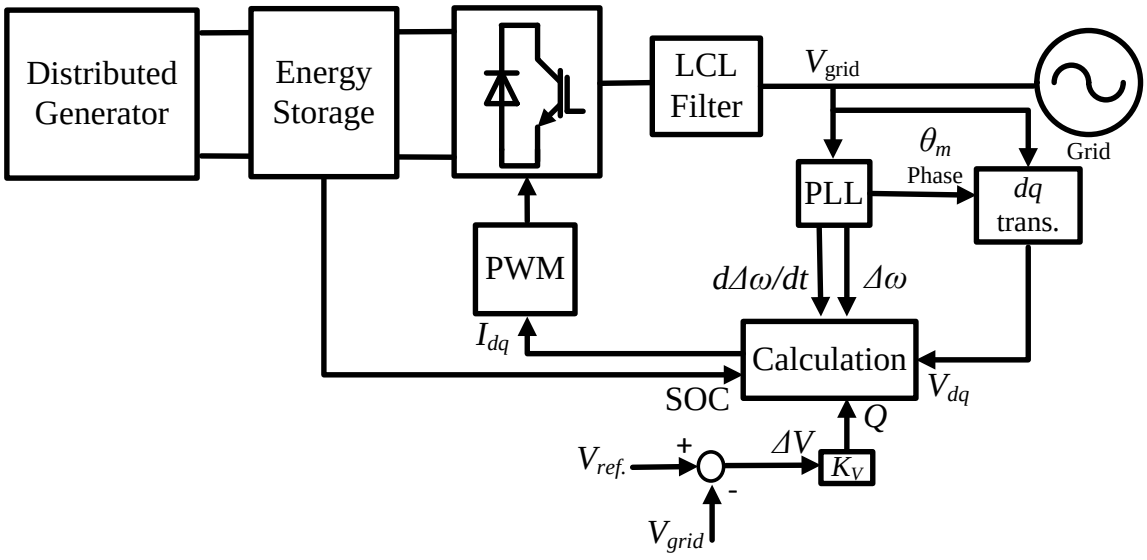

Fig. 1.8- VSG structure developed by VSYNC group.

$$i_d = \frac{v_d P - v_q Q}{(v_d + v_q)^2} \tag{1.4}$$

$$i_q = \frac{v_d Q - v_q P}{(v_d + v_q)^2} \tag{1.5}$$

K_{SOC} must be set such that the active power P is equal to the nominal VSG output power, when the SOC deviation (ΔSOC) is at its maximum level. Similarly, the K_V must be chosen such that the VSG produce its maximum reactive power for a specified voltage deviation (e.g., 10% [24]).

1.5.2- IEPE's VSG Topology

This group developed a VSG design and called it Virtual Synchronous Machine (VISMA) [11, 12, 28]. The main idea is shown in Fig. 1.9. The initial VISMA denoted as "Method 1" in Fig. 1.9 implements a linear and ideal model of a synchronous machine to produce current reference signals for the hysteresis controller of an inverter [11, 28]. The control diagram of this scheme is shown in Fig. 1.10. The grid voltage is measured and using a SG model, the current reference is produced to trigger the inverter switches through hysteresis controller. Furthermore, the authors developed another method, "Method 2" that uses the grid current signal to generate the Pulse-Width Modulation (PWM) pulses through a SG model. The signal flow diagram of this method is shown in Fig. 1.11. *E* and *M* in Figs. 1.10 and 1.11 are the voltage reference resembles the electromotive force of a SG and the virtual mechanical torque resembles the prime mover torque of a SG, respectively. Then the authors added an algorithm to compensate small disturbances and improve the quality of the grid voltage.

In Figs. 1.10 and 1.11, J is the moment of inertia, R_S is the stator resistance and L_s is the stator

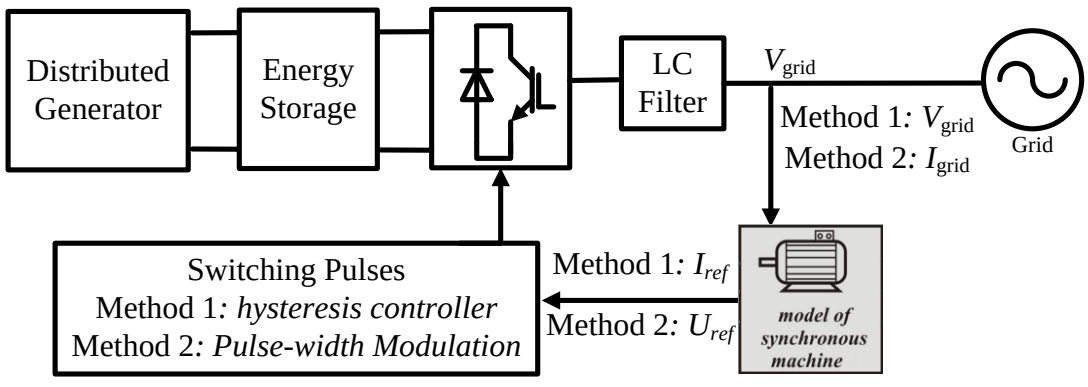

Fig. 1.9- VISMA structure using PLL to emulate the synchronous generator behavior.

inductance, K_d is the mechanical damping factor, $f(s)$ is the phase compensation term with the transfer function of $1/(0.5s+1)$, ω is the angular velocity, θ is the angle of rotation, M_d and M_{el} are the damping and electrical torques, respectively. The phase compensation term ensures that the virtual damping force counteracts any oscillating movement of the rotor in opposite phase. Despite of simplifying the excitation winding, the induced electromotive force is given by adjustable amplitude E_P and the rotation angle θ [12].

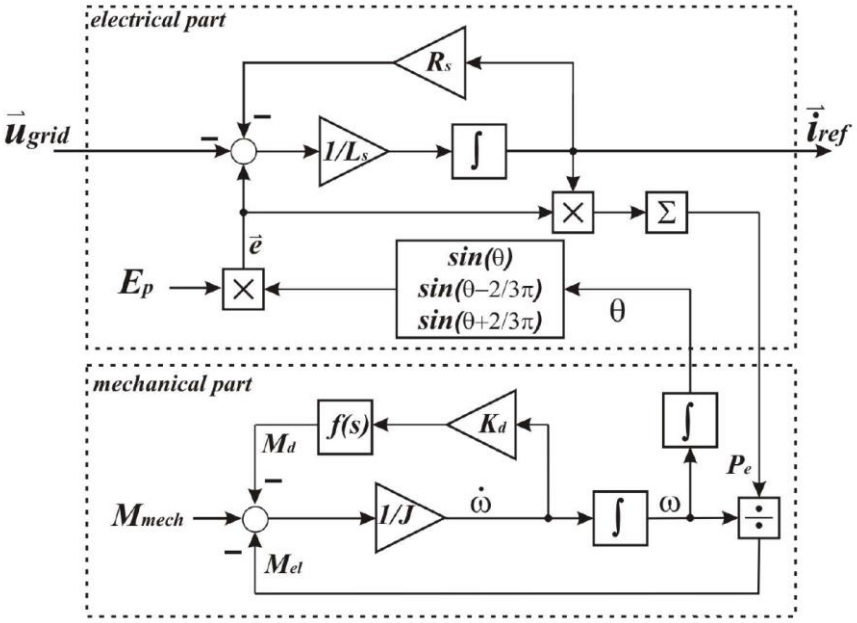

Fig. 1.10- Block diagram of the VISMA, Method 1 [11].

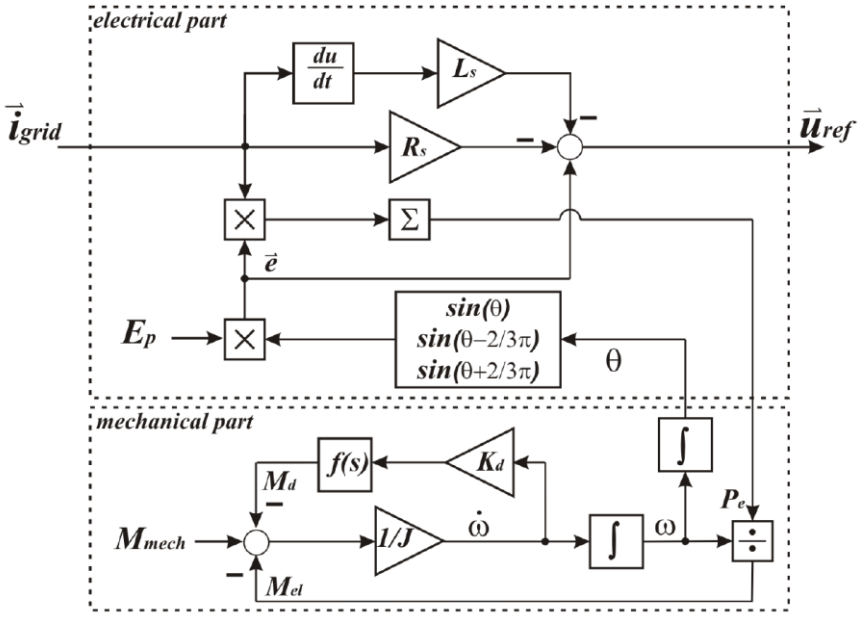

Fig. 1.11- Block diagram of the VISMA, Method 2 [11].

1.5.3- VSG System of Ise Laboratory

The VSG system of Ise Laboratory was described in Section 1.2. This group has introduced the new VSG design [30, 31], evaluated it in various voltage sag conditions [33], enhanced the voltage sag ride-through capability of the VSG [35], and finally added reactive power control to have a constant voltage at VSG terminals [32].

1.5.4- KHI's VSG

The KHI's VSG uses the phasor diagram of a SG to produce current reference [29]. The relation between voltage and current phasors of a SG is algebraic. The complete control diagram is shown in Fig. 1.12. The load angle δ is produced from the governor model that has the active power command, active power feedback signal and the reference angular velocity as inputs and uses a droop controller. The Automatic Voltage Regulator (AVR) produces the electromotive force E_f, from reactive power command, reactive power feedback signal, the voltage reference, and the voltage feedback signal through a droop controller. The δ, E_f, and grid voltage signals v_d, v_q are used to produce the current reference based on the phasor diagram shown in Fig. 1.12. The parameters r and x in the phasor diagram of Fig. 1.12 denote the virtual armature resistance and virtual synchronous reactance, respectively.

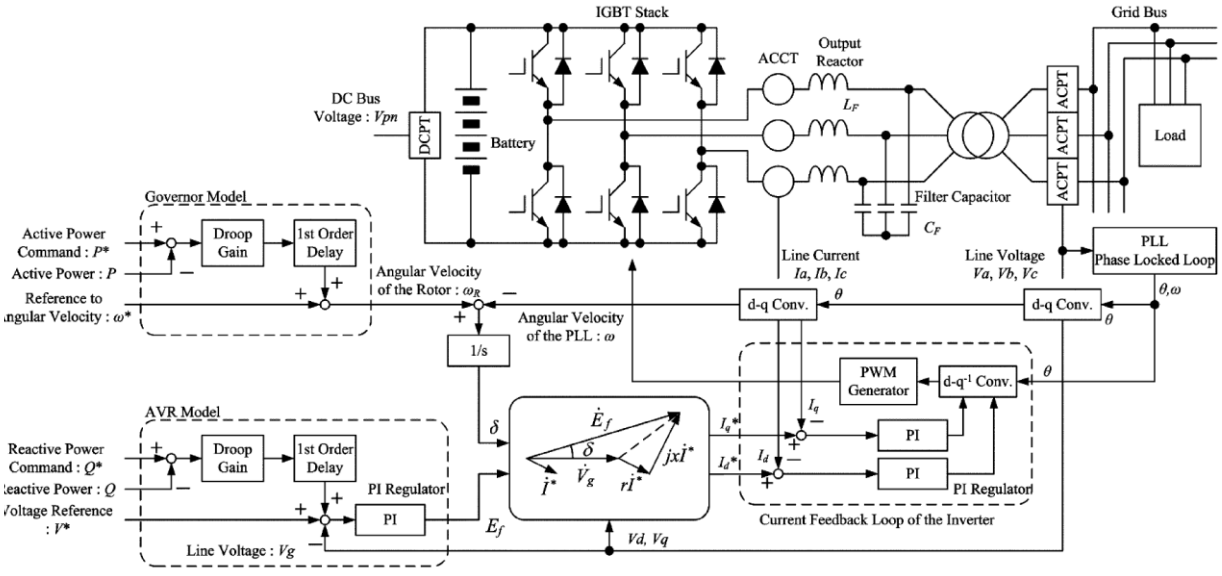

Fig. 1.12- Control diagram of algebraic type VSG introduced by KHI [29].

1.6- Conclusion

In the first chapter, the origin of the VSG concept and its importance for the new power systems with many DGs were discussed. The basics and the structure of the VSG were elaborated focusing on the VSG used in this research. In addition, practical aspects that are the energy storage considerations and the VSG operation in microgrids were mentioned briefly. Finally, the majority of the existing VSG technologies were reviewed.

References

[1] Q.-C. Zhong and T. Hornik, *Control of Power Inverters in Renewable Energy and Smart Grid Integration*. New York, NY, USA:Wiley, 2013.

[2] L. Zhang, L. Harnefors, and H.-P. Nee, "Power-synchronization control of grid-connected voltage-source converters," *IEEE Trans. Power Syst.*, vol. 25, no. 2, pp. 809–820, 2010.

[3] F. Blaabjerg, R. Teodorescu, M. Liserre, and A. Timbus, "Overview of control and grid synchronization for distributed power generation systems," *IEEE Trans. Ind. Electron.*, vol. 53, no. 5, pp. 1398–1409, 2006.

[4] J. Alipoor, Y. Miura, T. Ise, "Power system stabilization using virtual synchronous generator with alternating moment of inertia," *IEEE Journal of Emerging and Selected Topics in Power Electronics*, vol. PP, no. 99, pp. 1-8, 2014.

[5] K. Koyanagi, Y. Hida, Y. Ito, K. Yoshimi, R. Yokoyama, M. Inokuchi, T. Mouri, J. Eguchi, "A smart photovoltaic generation system integrated with lithium-ion capacitor storage," 46th Int. Universities' Power Engineering Conf., Soest, Germany, 2011.

[6] H. Bevrani, T. Hiyama, *Intelligent Automatic Generation Control*. CRC Press, NY, USA, 2011.

[7] M. P. N. van Wesenbeeck, S. W. H. de Haan, P. Varela, and K. Visscher, "Grid tied converter with virtual kinetic storage," in *PowerTech, 2009 IEEE Bucharest*, 2009, pp. 1-7.

[8] H.-P. Beck and R. Hesse, "Virtual synchronous machine", Int. Conf. on Electrical Power Quality and Utilisation, EPQU, pp.1-6, Barcelona, Spain, October 2007.

[9] Q.-C. Zhong, P.-L. Nguyen, Z. Ma, and W. Sheng, "Self-synchronized synchronverters: inverters without a dedicated synchronization unit," *IEEE Trans. Power Electron.*, vol. 29, no. 2, pp. 617-630, Feb. 2014.

[10] K. Visscher and S. W. H. De Haan, "Virtual synchronous machines (VSG's) for frequency stabilization in future grids with a significant share of decentralized generation," in *Smart Grids for Distribution, 2008. IET-CIRED. CIRED Seminar*, 2008, pp. 1-4.

[11] Y. Chen, R. Hesse, D. Turschner, and H. P. Beck, "Comparison of methods for implementing virtual synchronous machine on inverters," Int. Conf. on Renewable Energies and power quality- ICREPQ'12, Spain, March 2012.

[12] C. Yong, R. Hesse, D. Turschner, and H. P. Beck, "Improving the grid power quality using virtual synchronous machines," in *Power Engineering, Energy and Electrical Drives (POWERENG), 2011 International Conference on*, 2011 ,pp. 1-6.

[13] V. Karapanos, S. W. H. de Haan, K. H. Zwetsloot, "Testing a virtual synchronous generator in a real time simulated power system," Int. Conf. on Power Systems Transeints (IPST2011), Delft, Netherland, June 2011.

[14] M. Torres and L. A. C. Lopes" ,Virtual Synchronous Generator control in autonomous wind-diesel power systems," in *IEEE Electrical Power & Energy Conference*, 2009, pp. 1-6.

[15] M. Albu, A. Nechifor, and D. Creanga, "Smart storage for active distribution networks estimation and measurement solutions," in *Instrumentation and Measurement Technology Conference (I2MTC), 2010 IEEE*, 2010, pp. 1486-1491.

[16] H. Bevrani, T. Ise, and Y. Miura, "Virtual synchronous generators: A survey and new perspectives," *Electrical Power and Energy Systems*, vol. 54, pp. 244-254, 2014.

[17] H. Bevrani, M. Watanabe, and Y. Mitani, "Microgrid controls", in *Standard handbook for Electrical engineers*, Section 16, 16th Edition. H. W. Beaty and D. G. Fink (Ed), McGraw-Hill, 2012.

[18] I. Serban and C. Marinescu, "Frequency control issues in microgrids with renewable energy sources," in *Advanced Topics in Electrical Engineering (ATEE), 2011 7th International Symposium on*, 2011, pp.6-1.

[19] T. V. Van, K. Visscher, J. Diaz, V. Karapanos, A. Woyte, M. Albu, J. Bozelie, T. Loix, and D. Federenciuc, "Virtual synchronous generator: An element of future grids," in *Innovative Smart Grid Technologies Conference Europe (ISGT Europe), 2010 IEEE PES*, 2010, pp. 1-7.

[20] J. Driesen and K. Visscher, "Virtual synchronous generators," in *Proc. IEEE Power and Energy Society General Meeting - Conversion and Delivery of Electrical Energy in the 21st Century*, 2008, pp.1-3.

[21] T. Loix, S. De Breucker, P. Vanassche, J. Van den Keybus, J. Driesen, and K. Visscher , "Layout and performance of the power electronic converter platform for the VSYNC project," in *Proc. IEEE Powertech Conf.*, 2009, pp.1-8.

[22] Q.-C. Zhong, G. Weiss, "Synchronverters: inverters that mimic synchronous generators," *IEEE Trans. Ind. Electron.*, vol. 58, no. 4, pp.1259-1267, Apr. 2011.

[23] M. Albu, J. Diaz, V. Thong, R. Neurohr, D. Federenciuc, M. Popa, and M. Calin, "Measurement and remote monitoring for virtual synchronous generator design," in *Applied Measurements For Power Systems (AMPS), 2010 IEEE International Workshop on*, 2010, pp. 7-11.

[24] V. Karapanos, Z. Yuan, S. de Haan, "SOC maintenance and coordination of multiple VSG units for grid support and transient stability," 3rd VSYNC workshop, Cheia, Romania, June 2010.

[25] M. Albu, M. Calin, D. Federenciuc, and J. Diaz, "The measurement layer of the Virtual Synchronous Generator operation in the field test," in *Applied Measurements for Power Systems (AMPS), 2011 IEEE International Workshop on*, 2011, pp. 85-89.

[26] V. Karapanos, S. de Haan, and K. Zwetsloot, "Real time simulation of a power system with VSG hardware in the loop," in *IECON 2011 - 37th Annual Conference on IEEE Industrial Electronics Society*, 2011, pp. 3748-3754.

[27] Y. Chen, R. Hesse, D. Turschner, and H. P. Beck, "Dynamic properties of the virtual synchronous machine (VISMA)," Int. Conf. on Renewable Energies and Power Quality (ICREPQ´11), Las Palmas de Gran Canaria, Spanien, April 2011.

[28] R. Hesse, D. Turschner, and H.-P. Beck, "Micro grid stabilization using the virtual synchronous machine," in *Proc. International Conf. on Renewable Energies and Power Quality (ICREPQ'09)*, Spain, 2009.

[29] Y. Hirase, K. Abe, K. Sugimoto, and Y. Shindo, "A grid connected inverter with virtual synchronous generator model of algebraic type," IEEJ Trans. on Power and Energy, vol. 132, No. 4, pp. 371- 380, 2012.

[30] K. Sakimoto, Y. Miura, and T. Ise, "Stabilization of a power system with a distributed generator by a Virtual Synchronous Generator function," *IEEE 8th International Conference on Power Electronics and ECCE Asia (ICPE & ECCE),* pp. 1498-1505, 2011.

[31] K. Sakimoto, Y. Miura, T. Ise, "Stabilization of a power system including inverter type distributed generators by the virtual synchronous generator," IEEJ Trans. on Power and Energy, vol. 132, No. 4, pp. 341-349, 2012.

[32] T. Shintai, Y. Miura, and T. Ise, "Reactive power control for load sharing with virtual synchronous generator control," *7th IEEE Int. Power Electronics and Motion Control Conf.- ECCE Asia, pp. 846-853, Harbin, China, June 2012.*

[33] J. Alipoor, Y. Miura, T. Ise, "Evaluation of virtual synchronous generator (VSG) operation under different voltage sag conditions," in *Proc. IEE Japan Joint Technical Meeting on Power Engineering and Power Systems Engineering*, Tokyo, JAPAN, 2012, no. PE-12-60 PSE-12-76, pp. 41-46.

[34] J. Alipoor, Y. Miura, T. Ise, "Distributed generation grid integration using virtual synchronous generator with adoptive virtual inertia," in *Proc. IEEE Energy Conversion Congress and Exposition (ECCE),* 2013, pp. 4546-4552.

[35] J. Alipoor, Y. Miura, T. Ise, "Voltage sag ride-through performance of Virtual Synchronous Generator," in *Proc. IEEE Power Electronics Conference (IPEC-Hiroshima - ECCE-ASIA),* 2014, pp. 3298-3305.

[36] J. Liu, Y. Miura, T. Ise, "Dynamic characteristics and stability comparisons between virtual synchronous generator and droop control in inverter-based distributed generators," in *Proc. IEEE Power Electronics Conference (IPEC-Hiroshima - ECCE-ASIA),* 2014, pp. 1536-1543.

[37] The VSYNC Project website: http://www.vsync.eu/

Chapter 2

VSG with Alternating Moment of Inertia

The quantities of the VSG, such as its output frequency and power, oscillate after a change or disturbance similar to those of a synchronous machine. However, the transient condition tolerance (the severest transient that can be ridden -through) of an inverter-based generating unit is much less than a real synchronous machine. Therefore, a VSG system may stop working redundantly due to oscillations with high amplitude after a change or disturbance. On the other hand, VSG control has an advantage in that its swing equation parameters can be adopted in real time to obtain a faster and more stable operation. In this concept, the value of the virtual moment of inertia is changed based on the relative virtual angular velocity (the difference between virtual mechanical velocity generated by the VSG and grid angular frequency) and its rate of change [1]. Therefore, it is called Alternating Inertia scheme. This scheme removes the oscillations and thereby, increases the reliability of the VSG unit against changes or disturbances. Here, increase in reliability means operation with fewer failures after changes or disturbances in the system. This chapter goes into detail on the Alternating Inertia control with the objective of clarifying its damping and stabilizing effect [2]. The damping effect is investigated by the transient energy analysis and its stabilizing performance on the nearby machines in the power system is investigated by simulations. Finally, the performance is verified by experiments on a laboratory scale DSP controlled inverter.

The VSG system and the bang-bang control algorithm of Alternating Inertia control are reviewed in sections 2.1 and 2.2, respectively. In section 2.3, the stabilizing effect of Alternating Inertia is clarified by transient energy analysis. In section 2.4, the effect of Alternating Inertia on dissipated energy is addressed. In section 2.5, the impact of Alternating Inertia control on the stability of other machines in the microgrid is discussed. Experimental results are represented in section 2.6. Finally, the conclusion of this chapter is given in section 2.7.

2.1- Virtual Synchronous Generator Structure

The VSG system introduced in section 1.2 is used in this chapter. The control diagram is shown in Fig. 1.2 and the governor model of Fig. 1.4 is implemented. $V_{ref.}$ is set constant in the simulations and experiments of this chapter because voltage control does not affect the idea introduced in this chapter.

2.2- The Bang-Bang Control Strategy of Alternating Inertia

Consider the power-angle curve of Fig. 2.1. After a change in system, for example, a change in prime mover power from P_{in0} to P_{in1}, the operating point moves along the power curve, from point "a" to "c" and then from "c" to "a." One cycle of the oscillation consists of four segments indicated as ① to ④ in Fig. 2.1. The machine condition during each segment of an oscillation cycle is summarized in Table 2.1. During each segment, the sign of the $d\omega_m/dt$ together with the sign of the relative angular velocity $\Delta\omega$ defines the acceleration or deceleration. For example, in segment ③ of Fig. 2.1, during transition from points "c" to "b," both $d\omega_m/dt$ and $\Delta\omega$ are negative and act in the same direction; therefore, it is an acceleration period. Whereas, when they have opposite signs like segment ④**,** it is a deceleration period.

The objective is to damp frequency and power oscillation quickly by controlling the acceleration and deceleration term. The derivative of angular velocity, $d\omega_m/dt$ indicates the rate of acceleration or deceleration. Considering (1.1) of chapter 1, it is observed that this rate has a reverse relation to the moment of inertia, J. Based on this fact, one can select a large value of J during acceleration phases ("a" to "b" and "c" to "b") to reduce the acceleration and a small value of J during deceleration phases ("b" to "c" and "b" to "a") to boost the deceleration. The big moment of inertia J_{big} and the small one J_{small} can be chosen within a wide range depending on the rated power

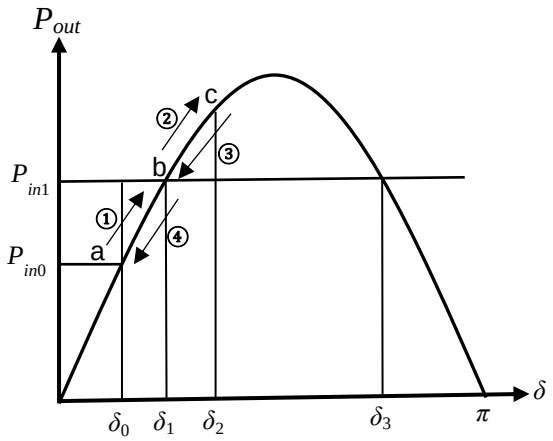

Fig. 2.1- Power-angle curve of a typical synchronous machine.

Table 2.1- Machine Modes During Oscillation.

Segment		$\Delta\omega$	$d\omega_m/dt$	Mode	Alternating J
①	a→b	$\Delta\omega > 0$	$d\omega_m/dt > 0$	Accelerating	Big value of J
②	b→c	$\Delta\omega > 0$	$d\omega_m/dt < 0$	Decelerating	Small value of J
③	c→b	$\Delta\omega < 0$	$d\omega_m/dt < 0$	Accelerating	Big value of J
④	b→a	$\Delta\omega < 0$	$d\omega_m/dt > 0$	Decelerating	Small value of J

so that the difference between J_{big} and J_{small} determines the damped power in each half-cycle of oscillation by Alternating Inertia. The value of J_{big} can be equal to the normal value of J (calculated by $J = 2HS_0/\omega_0^2$). However, applying a considerably larger value than the normal J will result in a smaller frequency excursion at the first quarter-cycle (segment ① of Fig 2.1) but a sluggish response. The value of J_{small} determines the transient of the second quarter-cycle of oscillation (segment ② of Fig 2.1). It will be shown that a very small value of J_{small} (1% of J_{big}) will result in a quick damping effect.

The bang-bang control strategy is summarized in Table 2.1. During each cycle of oscillations, the value of J is switched four times. Each switching happens at the points that the sign of either $\Delta\omega$ or $d\omega_m/dt$ varies. Before the disturbance, the VSG is operating with the normal value of J. When the disturbance happens, the transition from "a" to "b" starts with $\Delta\omega > 0$ and $d\omega_m/dt > 0$. In this condition, the J_{big} is adopted. At the end of the first quarter-cycle, that is point "b," the sign of $d\omega_m/dt$ changes. It means that the small value for J is adopted at this point. At point "c," the sign of $\Delta\omega$ changes and J retrieves it big value. It will be the end of the first half-cycle. During the second

half-cycle, the value of J is switched to the J_{small} at point "b," and again at the end of one cycle at point "a," J_{big} is adopted. This procedure is repeated for each cycle of oscillation until the transients are suppressed and $\Delta\omega$ equals zero at the new equilibrium point, that is, point "b." A threshold for $\Delta\omega$ can be applied to avoid the chattering of J during normal operation. However, this threshold is set to zero in this dissertation.

Figs. 2.2 and 2.3 show simulation results of this concept. Simulations were performed on the system model of Fig. 1.2 with the parameters of P_{base}=50 kW, f_{base}=60 Hz, R_L=12.5%, X_L=33.0%, X_F=42.4%, and D=17 pu at the base kW and the base voltage of 0.2 kV. The system was subjected to increase in the VSG power reference in two steps of 70% and 30% at t = 2 s and t = 8 s, respectively. Fig. 2.2 shows the output power and frequency of the VSG with the fixed value of J = 6 kgm^2. To show the effectiveness of the proposed idea, simulations were carried out on a weak system that VSG with fixed J is not able to track the grid frequency and keep up synchronism after the second step of power increase. Then, the control scheme of the VSG was changed to Alternating Inertia control, and the same scenario was applied. As it is observed in Fig. 2.3, Alternating Inertia selects the values of J out of J_{big} = 6 kgm^2 and J_{small} = 1 kgm^2 (the value for J_{small} is decided by

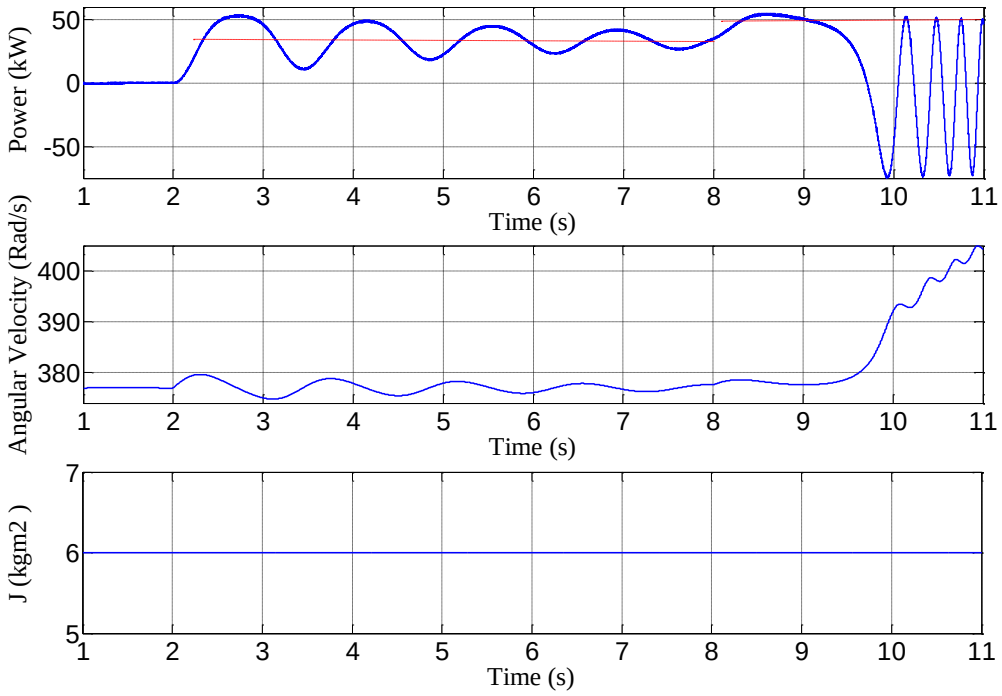

Fig. 2.2- Output power, virtual angular velocity, and virtual moment of inertia of VSG with fixed J = 6 kgm^2 and D = 17 pu.

experience. Any value that is smaller than J_{big} can be applied. However, the difference between J_{big} and J_{small} determines the suppressed energy at each half-cycle and thereby, decides the speed of oscillation damping). This process does not only stabilize the system, but also suppresses the frequency and power oscillations effectively. In Fig. 2.3, it is observed that the value of inertia is chattering during steady state operation. This chattering appears because of the slight variation of the angular velocity around the equilibrium point. However, the chattering can be removed by setting a threshold for the $\Delta\omega$ in the Alternating Inertia algorithm. It is carried out by replacing the $\Delta\omega > 0$ and $\Delta\omega < 0$ in Table 2.1 by $\Delta\omega > \varepsilon$ and $\Delta\omega < \varepsilon$, respectively which ε is a negligible positive value. It this research, this threshold is not applied since experience showed that the chattering J has a better performance in frequency regulation and voltage ripple reduction.

Damping factor is an important term that defines the VSG response. An inappropriate value of damping factor may result in a high magnitude of oscillation or a sluggish response. Besides, a proper value of the damping factor in a specific working point may not end up with an acceptable response in other conditions. The Alternating Inertia concept allows the VSG system to exert a suitable time constant in each phase of oscillation; therefore, the importance of the damping factor in

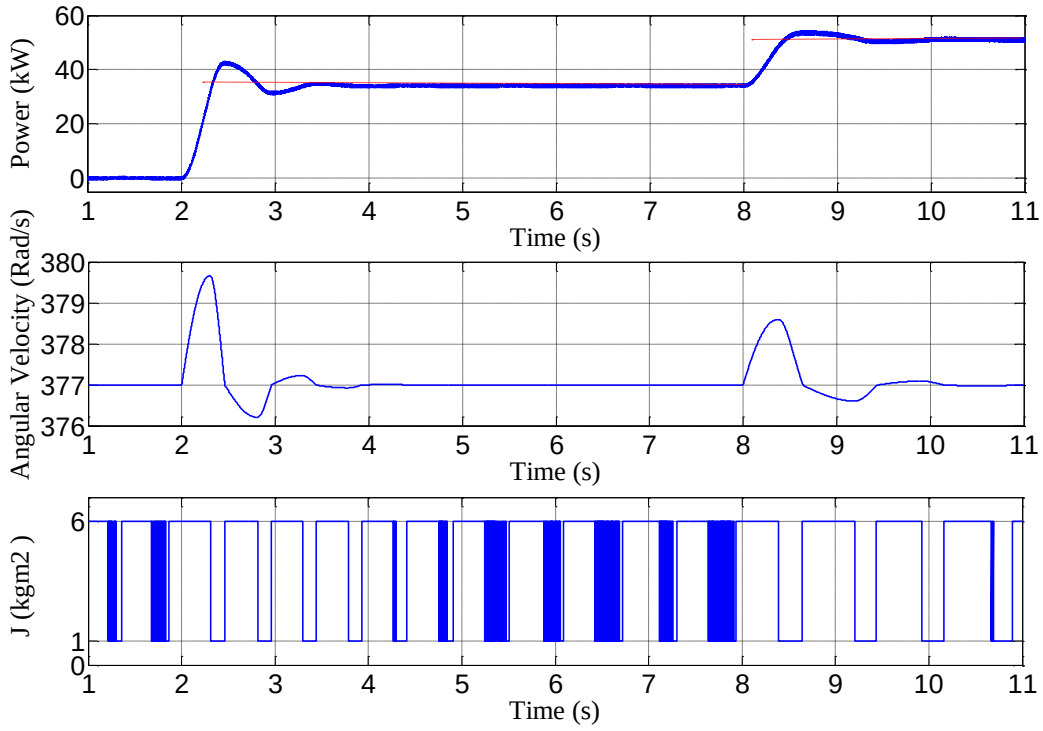

Fig. 2.3- Output power, virtual angular velocity, and virtual moment of inertia of VSG with Alternating J: 1and 6 kgm^2 and D = 17 pu.

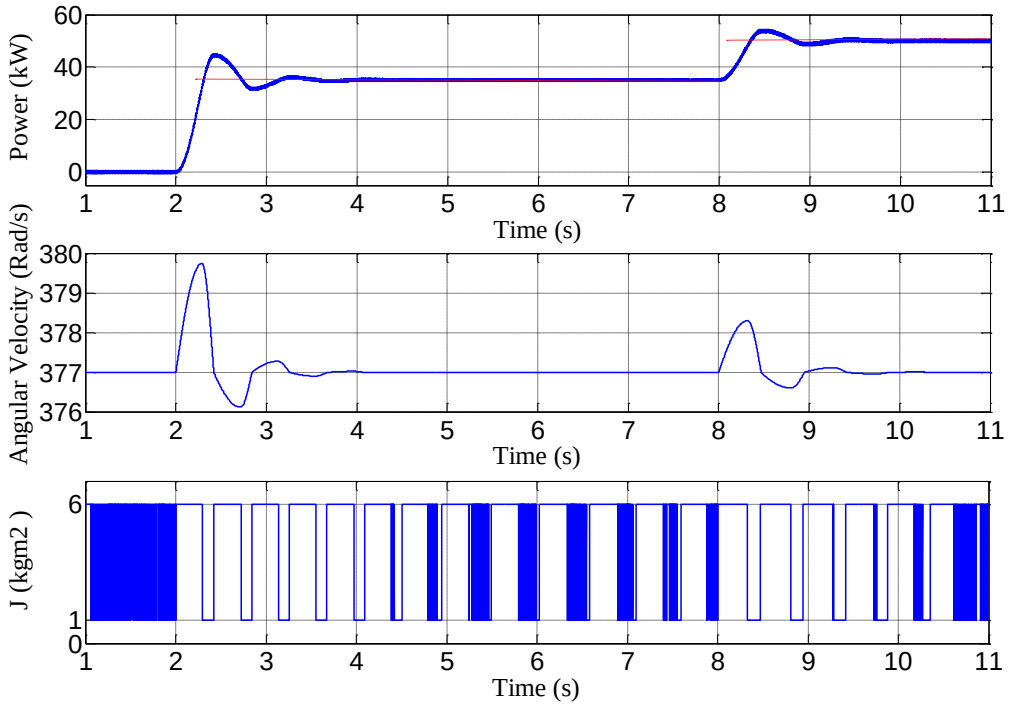

Fig. 2.4- Output power, virtual angular velocity, and virtual moment of inertia of VSG with Alternating J: 1and 6 kgm^2 and D = 0 pu.

the behavior of the VSG system is reduced considerably. To assess this matter, the damping factor was changed to zero, and the same scenario was applied. Fig. 2.4 shows the output power and angular velocity of the VSG in this condition. It is observed that the system operates stably, and the oscillations are eliminated by the Alternating Inertia idea even with a zero value for the damping factor.

2.3- Stability Assessment by Energy Function Analysis

Transient stability concerns the stability of the rotor angle of synchronous machines (voltage angle in the case of VSG) after a significant disturbance. Having the advantage of not solving the nonlinear differential equations, Lyapunov direct method has become the center of attention for transient stability analysis. Consider a system expressed by a set of nonlinear differential equations of the form $\dot{\boldsymbol{x}} = \boldsymbol{F}(\boldsymbol{x})$, $\boldsymbol{x}$ being a vector of state variables. The point $\hat{\boldsymbol{x}}$ for which $\boldsymbol{F}(\hat{\boldsymbol{x}}) = 0$ is the equilibrium point of the system in a state space. The solution of system state equations from initial point to the equilibrium point forms the system trajectory. The trajectory of an asymptotically stable system converges at the equilibrium point as time approaches infinity.

Based on the Lyapunov stability theorem, point $\hat{\boldsymbol{x}}$ is asymptotically stable if a continuous

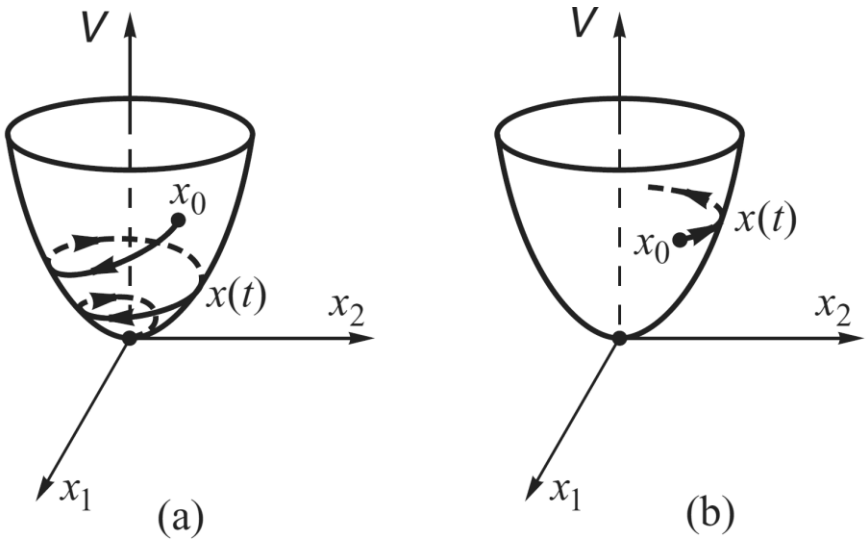

Fig. 2.5- Lyapunov's theorem on Stability [3]: (a) transient energy level descends in a stable case; (b) transient energy ascends in an unstable case.

differentiable function $V(\boldsymbol{x})$ exists and $\dot{V}(\boldsymbol{x}) \leq 0$. In the other words, the rate of change of $V(\boldsymbol{x})$ along the system trajectory is negative. The theorem is illustrated in Fig. 2.5. The $V(\boldsymbol{x})$ of Fig. 2.5(a) is declining during time as state variables converge to the equilibrium point that is a minimum stationary point. Whereas, for an unstable initial point, the value of $V(\boldsymbol{x})$ rises, and the trajectory diverges on the state variables plane as shown in Fig. 2.5(b).

Finding a candidate Lyapunov function is the next step of stability analysis. Reference [3] calculated the energy function through removing the damping factor, multiplying the swing equation by $\Delta\omega$, and integrating the product from the first equilibrium point, that is, point "b" in Fig. 2.1, with δ_1 and $\Delta\omega = 0$, to any point on the system transient trajectory. The resultant expression is:

$$V = E_k + E_p = \frac{1}{2}\omega_0 J \Delta\omega^2 - [P_{in}(\delta - \delta_1) + b(\cos\delta - \cos\delta_1)] \tag{2.1}$$

where V is the system transient energy after a change or disturbance, b is the amplitude of the power-angle curve, and ω_0 is the system frequency. The transient energy is the energy required to move the system states from a predisturbance operating point to the new stable operating point. This term can be considered as an energy gap. Depending on the form of change or disturbance, the transient energy may be needed to be injected or extracted. The transition of the system states to the new stable point (filling the energy gap) includes oscillation that may result in instability (transient instability evaluated by equal area criterion). Besides, the transients involve power oscillation that is

dissipated in resistive elements. It means that the high magnitude and the long duration oscillation results in power loss in the system. In the case of a VSG with energy storage, the dissipated power comes from the storage unit. It can be concluded that if the transient oscillation is removed, not only stabilization is achieved, but also the energy dissipation is prevented. Equation (2.1) has two terms. The first term, which is denoted as E_k, is the kinetic energy of the rotor of synchronous generator and virtual kinetic energy for the VSG system. The other term, E_P is the potential energy that is stored and released electromagnetically during the interaction between the electromagnetic fields of the rotor and stator of the machine. It is proved that V satisfies the Lyapunov function criteria that are: (i) it has stationary points at the equilibrium points (the gradient of V is equal to zero at the stationary points); (ii) it is positive definite in the vicinity of one of the equilibrium points (Its Hessian matrix is positive definite); and (iii) its derivative is not positive [3]. In the case of VSG with alternating moment of inertia, a presumption of $J > 0$ is needed. Moreover, the derivative of the V with Alternating Inertia should be checked to be negative.

When oscillation starts at point "a" of Fig. 2.1, $\Delta\omega$ is zero and $\delta–\delta_1$is maximum. Therefore, E_k = 0 and E_P is maximum. During the transition from point "a" to "b" with a large value of J, E_k is increasing, and E_p is decreasing as $\Delta\omega$ increases and $\delta–\delta_1$ decreases. All system transient energy is converted into the kinetic form at point "b" with maximum $\Delta\omega$ and J_{big}. At this point, the change in the moment of inertia to the small value is applied. Therefore, the system transient energy will be decreased to a smaller-value kinetic form with the same $\Delta\omega$ but J_{small}. Now this energy will be converted into the potential form during the transition from point "b" to "c" as $\Delta\omega$ decreases and $\delta–\delta_1$ increases. Because the total energy has decreased, the amplitude of oscillation will be reduced. In other words, $\delta_2–\delta_1$ will be much smaller than $\delta_0–\delta_1$. J adopts its big value at point "c." However, all of the system transient energy is in potential form at this point as $\Delta\omega$= 0 and $\delta–\delta_1$has its maximum value. Therefore, the increase in J does not increase the system energy level based on (2.1). This process happens in each half-cycle until $\Delta\omega$ becomes less than a desired threshold.

To see the damping effect of the alternating moment of inertia scheme, the third criterion of the Lyapunov function is considered. This criterion demands that the derivative of the energy function is negative. Thus, the system transient energy declines during time until the system state variables are

settled at the equilibrium point. For a VSG with variable J, by calculating the derivatives of E_k and E_p of (2.1) separately and considering the swing equation, the derivative of V is expressed as:

$$\frac{dV}{dt} = \frac{\omega_0}{2}\Delta\omega^2\frac{dJ}{dt} - D\Delta\omega^2 \tag{2.2}$$

This expression must be negative to have decay in the system transient energy during oscillation. The term $-D\Delta\omega^2$ is obviously negative for $D > 0$. Because J varies discontinuously, dJ/dt is approximated by its average value at the points at which J is switched. At points "a" and "c" at which J is varied from J_{small} to J_{big}, the variation of J is positive ($\Delta J = J_{big}–J_{small}$). However, dJ/dt is multiplied by $\Delta\omega^2$ in (2.2) and $\Delta\omega$ is zero at these points. It means that, the variation of J does not change the transient energy at these points. Inversely, at point "b," at which J is varied from J_{big} to J_{small}, ΔJ is calculated as $J_{small}–J_{big}$, and $\Delta\omega$ has its maximum value. Therefore, the term dJ/dt is effective at this point and it is estimated for each half-cycle as follows:

$$\frac{dJ}{dt} \approx \frac{\Delta J}{\Delta t} = \frac{J_{small} - J_{big}}{0.5T} \tag{2.3}$$

Assuming a zero damping factor D, (2.2) can be rewritten as:

$$\frac{dV}{dt} = \frac{\omega_0}{2}\Delta\omega^2\frac{J_{small} - J_{big}}{0.5T} < 0 \tag{2.4}$$

Equation (2.4) shows that an additional damping effect is imposed in each half-cycle by varying the value of the moment of inertia. This damping acts directly on the transient energy and cuts it to a desired level decided by the difference in the values of J. Fig. 2.6 illustrates the performance of the Alternating Inertia method in transient energy suppression. Simulations were performed on the system model of Fig. 1.1. Fig. 2.6(a) contains the system transient energy trajectory for a VSG with the fixed moment of inertia of 6 kgm^2 after a step increase of 1 pu (at 50 kW base power) in power reference. It is observed that the system transient energy declines by the damping factor as the state variables converge to the equilibrium point. When the Alternating Inertia scheme is applied, the transient energy drops to a desired level by applying the small J of 3 kgm^2 as shown in Fig. 2.6(b). By adopting a tiny J_{small}, fast decay of transient energy can be achieved, which bypasses the state variables to the stable stationary point in the first half-cycle.

There is another stationary point for the swing equation, with $\Delta\omega = 0$ and $\delta = \pi–\delta_1$ (that equals

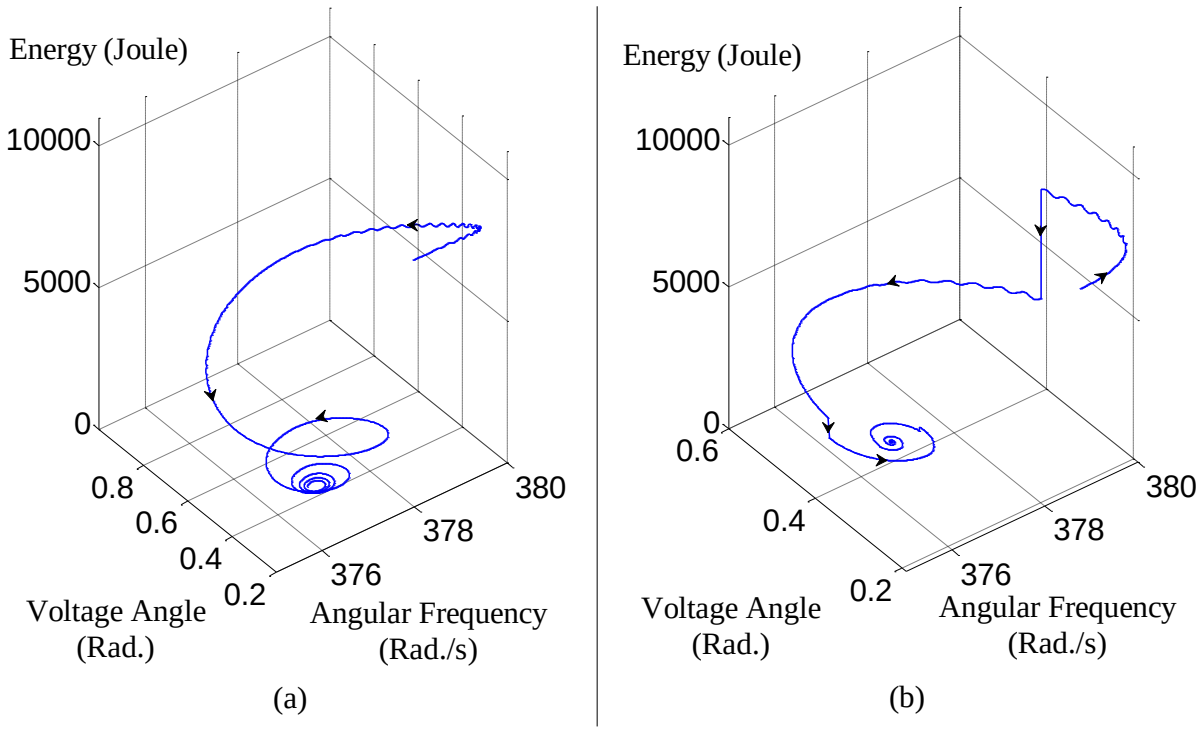

Fig. 2.6- Transient energy trajectory after a step change in power reference of VSG with: (a) Fixed moment of inertia; (b) Alternating Inertia.

δ_3 in Fig. 2.1). The value of the energy function at this point is the critical transient energy. For a synchronous generator and VSG with fixed inertia, the value of energy function at the initial point of oscillation must be smaller than the critical value. However, in the case of VSG with Alternating Inertia scheme, any initial energy gap can be reduced to nearly zero value at the end of the first quarter-cycle; therefore, the critical transient energy and thereby transient stability area will always have its maximum value, that is, $2b – \pi P_{in}$ from (2.1). Other corollaries regarding the transient stability area and the critical clearance time that can be inferred from the Alternating Inertia concept are forgone because of prolixity. The system kinetic, potential, and total energy in the same simulation condition as Fig. 2.6 are plotted in Fig. 2.7.

2.4- Effect of Alternating Inertia on Dissipated Energy

In the case of a real SG, during oscillation, the kinetic energy preserved in the rotor mass will be converted into the potential energy accumulated in the magnetic field of SG, and then in reverse, until the oscillation is damped and system states are stabilized at the equilibrium point. For the VSG system, the kinetic energy of the rotor and the potential energy are virtual quantities and the VSG scheme controls the inverter output similar to the output of a SG. For example, when $\Delta\omega$ is not zero,

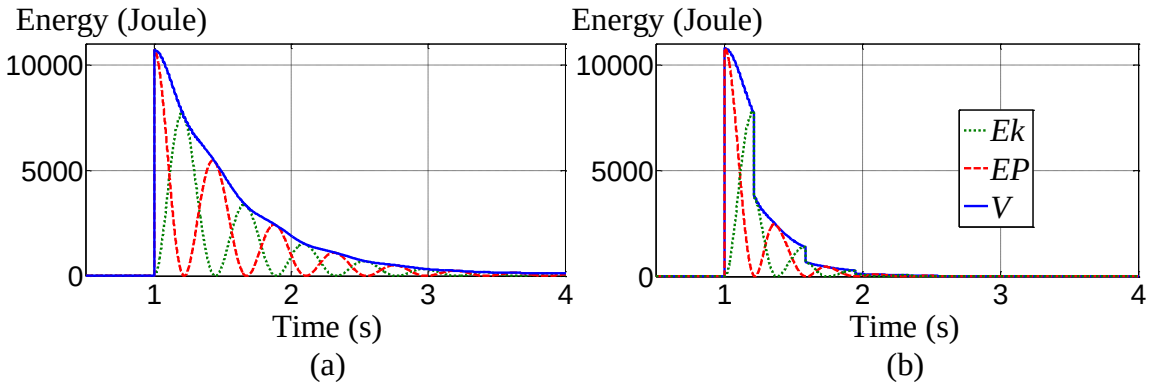

Fig. 2.7- The kinetic energy (*Ek*), potential energy (*EP*), and total transient energy (*V*) waveforms after a step increase in power reference of VSG with: (a) fixed moment of inertia; (b) Alternating Inertia.

the VSG imagines that there is a specific value of kinetic energy considering the value of J and oscillates the output power of the inverter (by changing the voltage angle) based on the swing equation of a SG that expressed in (1.1). When the Alternating Inertia switches the value of J to J_{small} at the maximum value of $\Delta\omega$, the VSG scheme just imagines that a smaller value of kinetic energy is available rather than the big value of it with the J_{big}. In the other words, the kinetic energy that is removed by Alternating Inertia is imaginary and is used by VSG algorithm to control the output of VSG and does not exist in reality. Thus, for quick convergence of the states of the system, the energy value can be varied at the proper time without concerning where the energy goes to.

Another issue is the effect of Alternating Inertia on the dissipated energy. The dissipated energy is different from the transient energy (energy gap) and refers to the energy that is dissipated in the system during oscillations of power and current. Hereafter, it is shown that Alternating Inertia reduces the energy dissipated in the system by monitoring the dc-link power and energy. Consider the VSG system of Fig 1.2. The system parameters are: P_{base} = 50 kW, f_{base} = 60 Hz, R_L = 12.5%, X_L = 33.0%, X_F = 42.4%, and D = 17 pu at the base kW and the base voltage of 0.2 kV. The energy storage is a 5 mF-capacitor. At t = 1 s, the VSG power command has been changed from 0 to 1 pu. The dc-link power it is injected to the grid though inverter is shown in Fig. 2.8 in two conditions: (a) VSG with fixed Inertia (J = 6 kgm^2) and (b) VSG with Alternating Inertia (J_{small} = 1 and J_{big} = 6 kgm^2). It is observed that Alternating Inertia removed the oscillation of dc-link power. The energy is calculated by integrating the dc-link power with respect to time and shown in Fig. 2.9. It is observed that the dc-link energy of VSG with Alternating Inertia is slightly less than the case with fixed

inertia. However, the difference is not considerable. The difference between the value of energy with Alternating Inertia and the value of energy without Alternating Inertia at any moment after settling time indicates the energy that is saved by Alternating Inertia. For example at t = 6 s, the difference in the value of the energy of two cases is 1.724 Wh that means this amount of energy has been saved by Alternating Inertia.

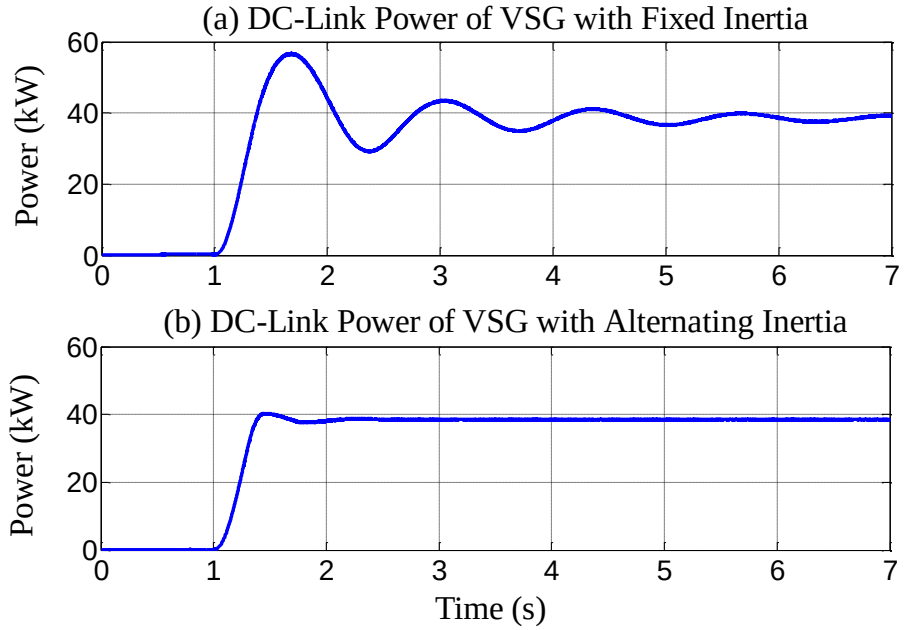

Fig. 2.8- DC-link power of VSG subjected to a step change in the power reference: (a) VSG with Fixed Inertia and (b) VSG with Alternating Inertia.

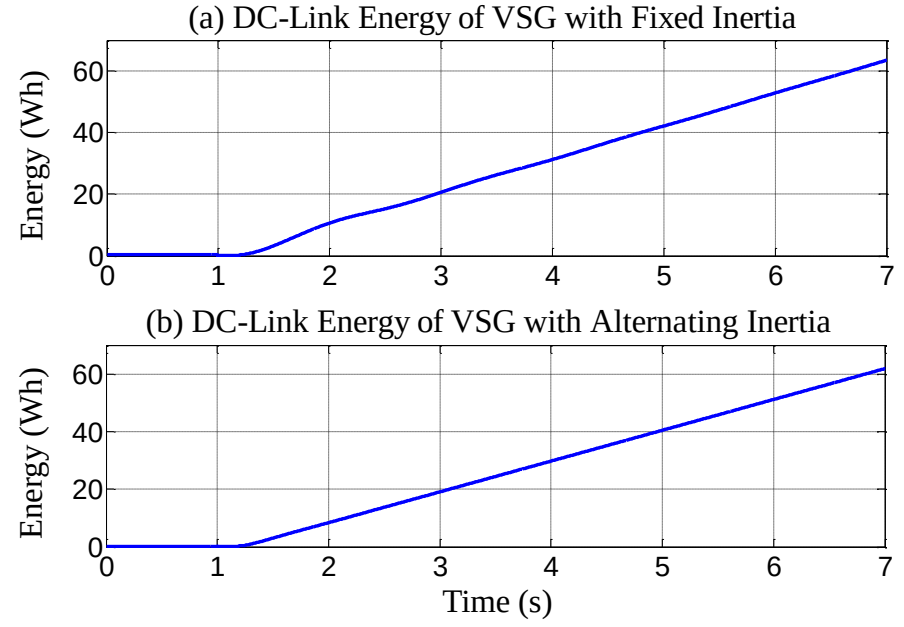

Fig. 2.9- DC-link energy of VSG subjected to a step change in the power reference: (a) VSG with Fixed Inertia and (b) VSG with Alternating Inertia.

2.5- Grid Stability Enhancement by Alternating Inertia

2.5.1- VSG in parallel with other machines

In microgrid applications, an inverter-based DG works in parallel with other DGs that may include synchronous machines. Consider the islanded microgrid of Fig. 2.10. The VSG block has the control scheme shown in Fig. 1.1 with the output filter reactance of 9.7%. The objective of this part is to assess the effect of the Alternating Inertia scheme of the VSG on the stability of the parallel SG. To clarify the effectiveness of the idea, the capacity of the VSG unit was assumed to be 20% of the SG that is insignificant. A symmetrical fault (3 L-G) happened at the load point at t = 0.2 s and lasted for 0.3 seconds. In this condition, the system comprising the VSG with the fixed value of moment of inertia J = 8.445 kgm^2 was not able to recover from the fault as shown in Fig. 2.11. The same scenario was applied to the system with Alternating Inertia of J_{big} = 8.445 and J_{small} = 0.0844 kgm^2. The waveforms of power, SG rotor angle, and angular frequency are shown in Fig. 2.12. As it is observed, the Alternating Inertia scheme improved the stability of the adjacent machine by the extra damping effect imposed on the transient energy directly.

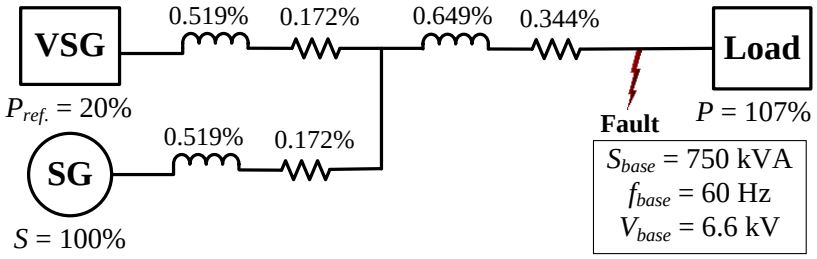

Fig. 2.10- VSG unit in parallel with the SG in microgrid.

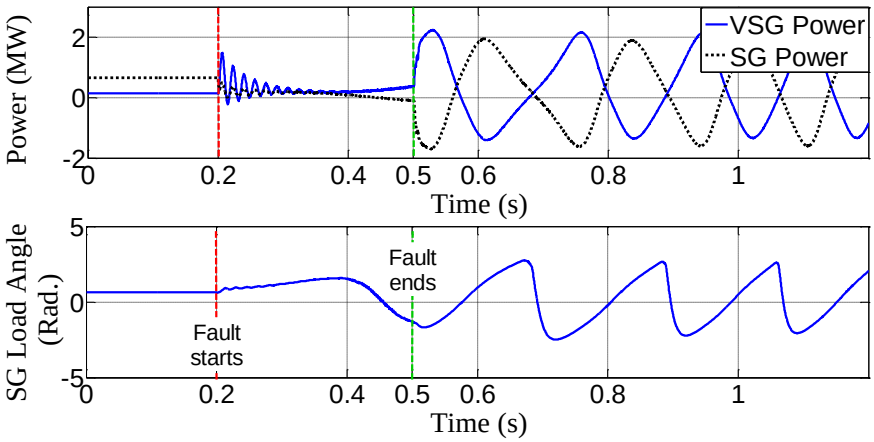

Fig. 2.11- VSG and SG powers and SG rotor angle waveforms of the system with fixed moment of inertia and D = 17 pu.

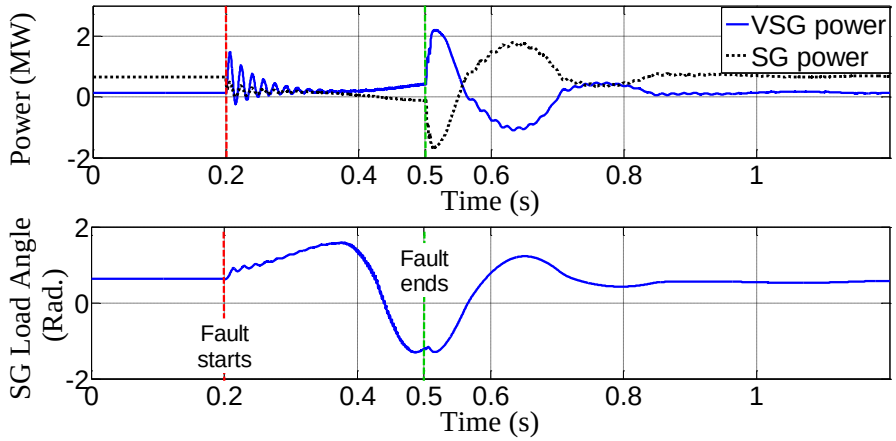

Fig. 2.12- VSG and SG powers and SG rotor angle waveforms of the system with Alternating Inertia control and D = 0 pu.

2.5.2- VSG as an interface between the SG and the grid

Another configuration is shown in Fig. 2.13. An SG is connected to the grid/microgrid through a VSG unit. The prime mover of the SG can be a gas or diesel engine, and an inverter interface is required to correct the generated power to be injected to the grid. If the VSG unit is not robust enough, the disturbances from grid/microgrid will affect the stable operation of the SG. To assess the effect of the Alternating Inertia control on the stability of such systems, a symmetrical three-phase voltage sag with 10% remained voltage magnitude and the duration of 0.2 seconds was applied from grid side, and the performance of the system was monitored. The reference power and damping factor of the VSG were 1 and 17 pu, respectively, and a fixed inertia factor equal to 5 kgm^2 was applied. Fig. 2.14 shows the SG rotor angle and DC link voltage were affected by the grid voltage sag considerably. The high-peak transient of DC-link voltage is mainly because of the oscillation of the VSG output power. The same scenario was applied to the system with the Alternating Inertia control with J_{big} = 5 and J_{small} = 0.05 kgm^2. To discriminate the stabilizing effect of Alternating Inertia as the only stabilizing effect in the system, the damping factor D was set to zero. It should be mentioned that the system with fixed inertia and a zero damping factor was unable to recover from much milder faults (higher remained voltage and shorter duration). As it is observed in Fig. 2.15, the oscillation was suppressed by the Alternating Inertia scheme, and the severe transient of DC-link voltage was also eliminated.

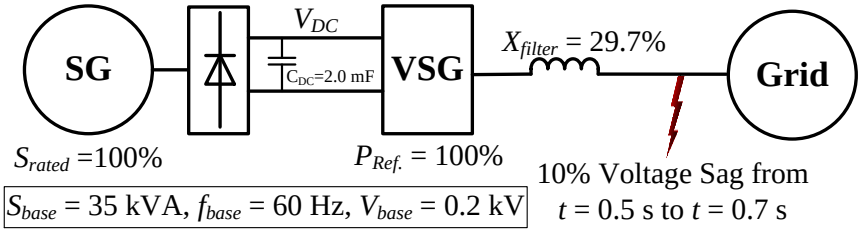

Fig. 2.13- SG connected to the grid via VSG unit.

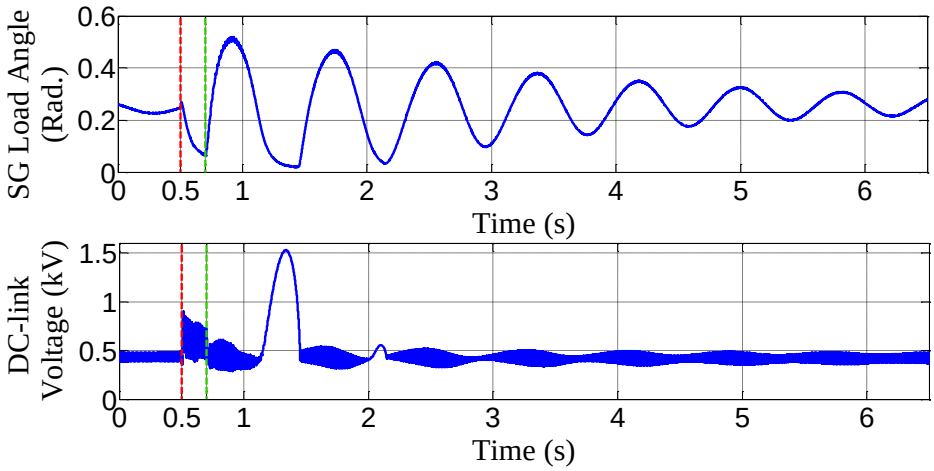

Fig. 2.14- SG load angle and DC-link voltage of the system of Fig. 2.13 containing VSG with fixed moment of inertia.

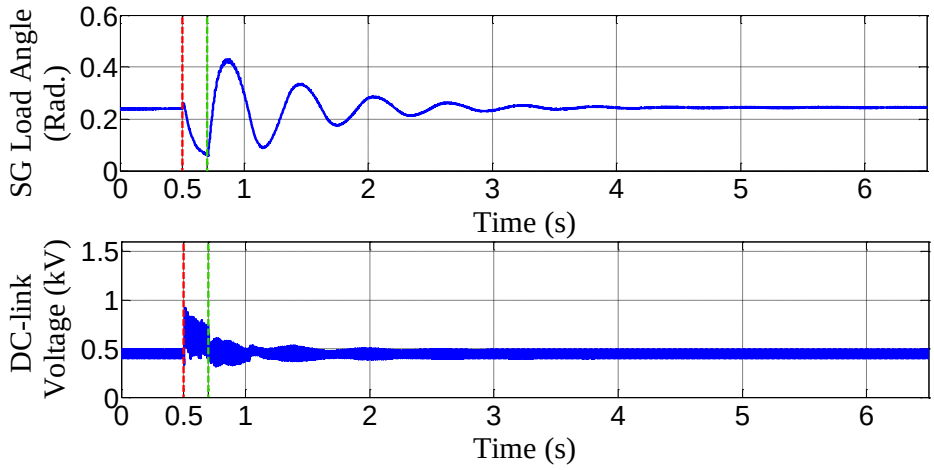

Fig. 2.15- SG load angle and DC-link voltage of the system of Fig. 2.13 containing VSG with Alternating Inertia.

2.6- Experimental Results

The damping effect of Alternating Inertia was verified by applying it to a laboratory-scale test system. The overall system configuration is depicted in Fig. 2.16, and the main parameters of the

system are presented in Table 2.2. The transmission unit (TU) in Fig. 2.16 simulates the π model of a 40 km transmission line shown in Fig. 2.17.

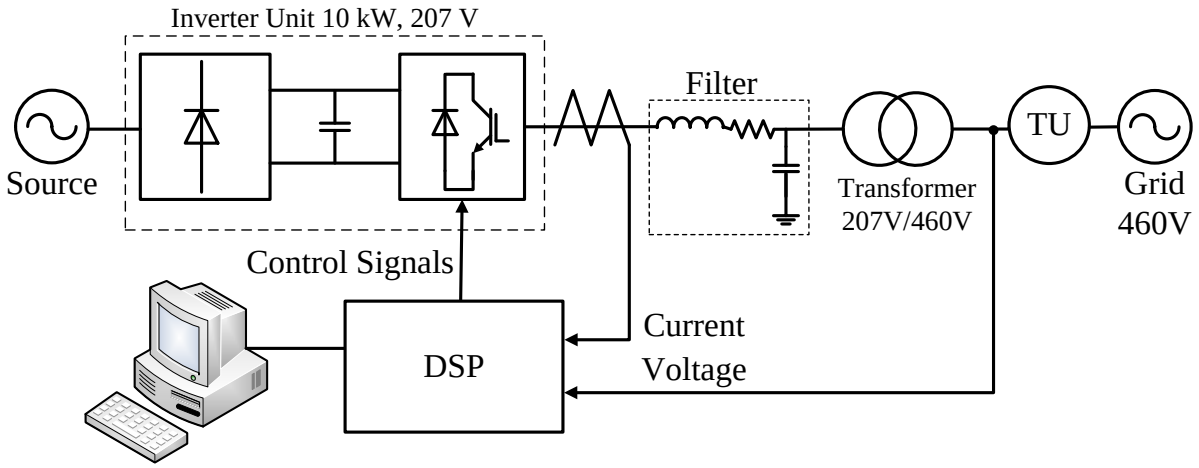

Fig. 2.16- Experimental system.

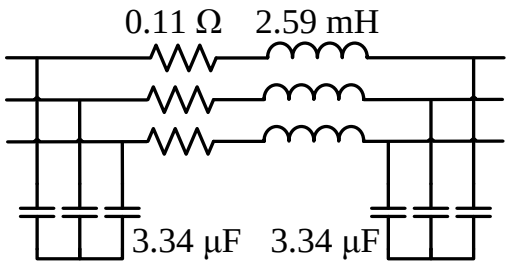

Fig. 2.17- The π model of a 40 km transmission line.

Table 2.2- Specifications of the Experimental System.

Base Power	10 kVA
Base Frequency	60 Hz
Base Voltage	207 V
Switching Frequency	14 kHz
Dc-link Voltage	320 V
Filter Stray Resistance	0.23%
Filter Inductive Reactance	8.8%
Filter Capacitor VAR	1.62%
Resonance Frequency of LC Filter	1.59 kHz
Transformer Reactance	9.68%

Initially, the VSG with the constant moment of inertia J = 0.563 kgm^2 was subjected to a step change of 3 kW in the power reference. This value of J is calculated by assuming the inertia constant H = 8 s at rated power and frequency. The output power and angular velocity of the VSG is shown in Fig. 2.18. When the power reference increased, the VSG output power followed the power command after passing severe oscillations with the amplitude of 2 kW. The VSG stopped operating by applying 3.6 kW power command. Fig. 2.19 shows the RMS values of the VSG voltage and current in this condition. Because of the severe oscillation, the VSG current exceeded its tolerable limit and the inverter was stopped at t = 1.43 s.

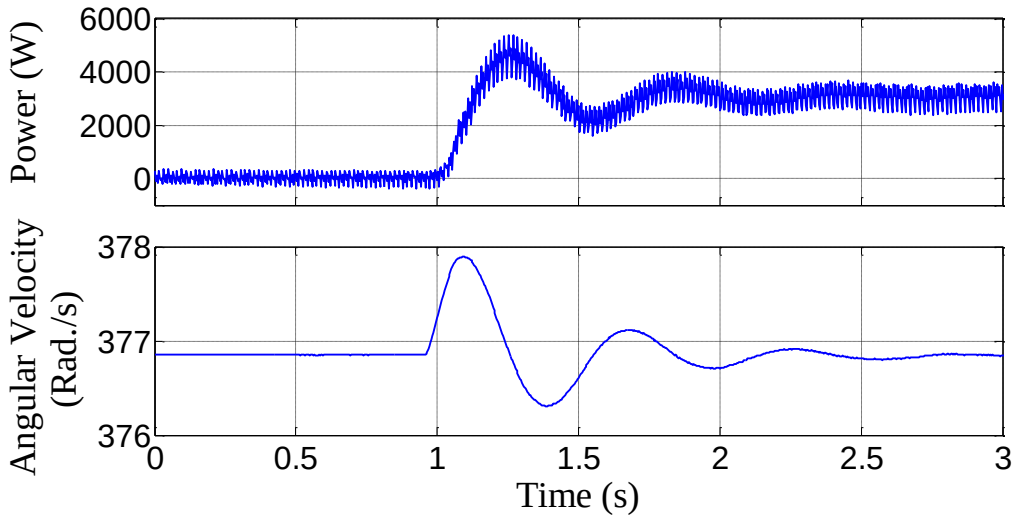

Fig. 2.18- Output power and virtual angular velocity of VSG with fixed moment of inertia of 0.563 kgm^2 and D = 17 pu.

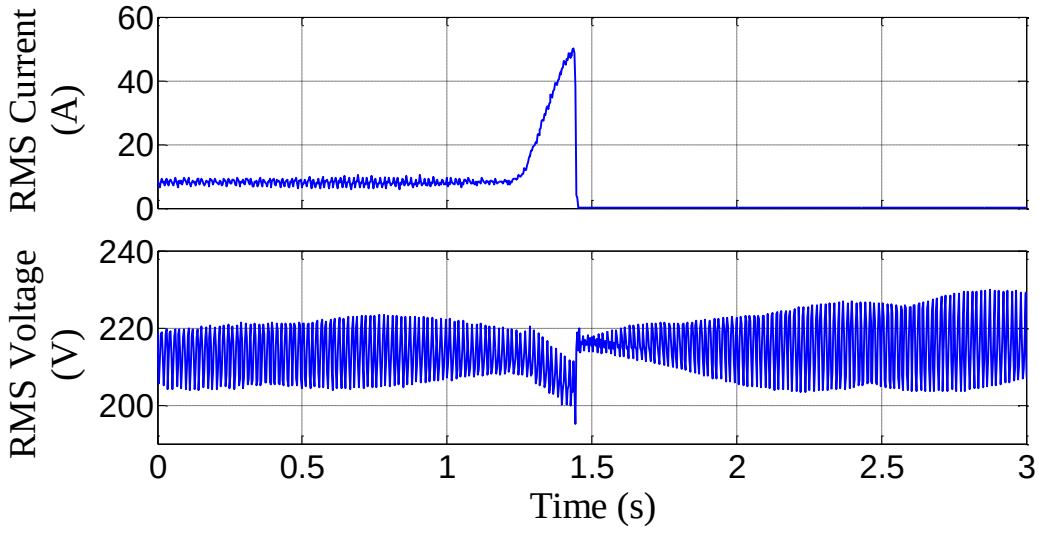

Fig. 2.19- The RMS values of the VSG current and voltage with the fixed moment of inertia of 0.563 kgm^2 and D = 17 pu subjected to a 3.6 kW step power increase.

Then the VSG control was changed to the Alternating Inertia scheme with J_{big} = 0.563 kgm^2 and J_{small} =0.1 kgm^2, and the step power change of 4.5 kW was applied. The result is shown in Fig. 2.20. It is observed that the VSG follows the power command without oscillations. It can be concluded that the VSG with Alternating Inertia can be loaded reliably at power levels close to its rating, and also can ride- through severer disturbances than the disturbances that VSG with fixed moment of inertia can ride-through them. The effectiveness of the Alternating Inertia in the smooth transition of current level and reducing the voltage ripples at the VSG terminal is obvious in this figure.

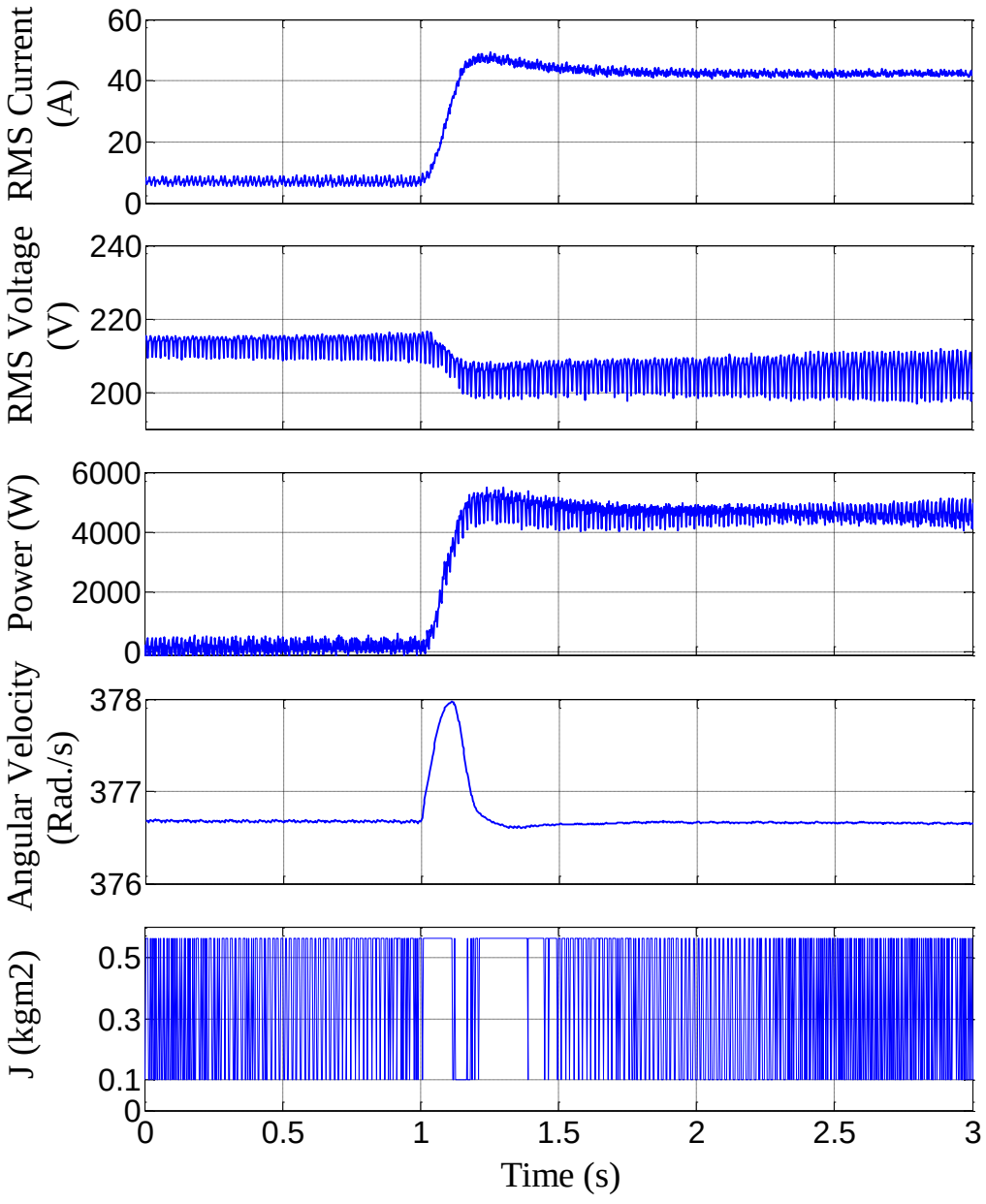

Fig. 2.20- RMS current, RMS voltage, output power, virtual angular velocity, and virtual moment of inertia of VSG with Alternating *J* and *D* = 17 pu after a power command of 4.5 kW.

To clarify the damping effect of the Alternating Inertia scheme, the VSG with Alternating Inertia and zero damping factor *D* is subjected to a change of 3 kW in the power reference. It must be noted that the VSG with fixed inertia and zero damping factor cannot keep in step with the grid frequency and fails to track power reference after any disturbance. Output power, virtual angular velocity, and the real-time adopted *J* are shown in Fig. 2.21. As it is expected, the VSG can track the power reference with negligible transients. However, VSG with a reasonable non-zero *D* that does not result in a slow response, has better performance. Therefore, in practical implementation zero value for *D* is not recommended.

2.7- Conclusion

In this chapter, the Alternating Inertia structure was elaborated. The Alternating Inertia scheme adopts the suitable value of the moment of inertia of the VSG considering its virtual angular velocity and acceleration/deceleration in each phase of oscillation. By selecting a big value for the moment of inertia during acceleration, the acceleration was mitigated, and on the other hand, during

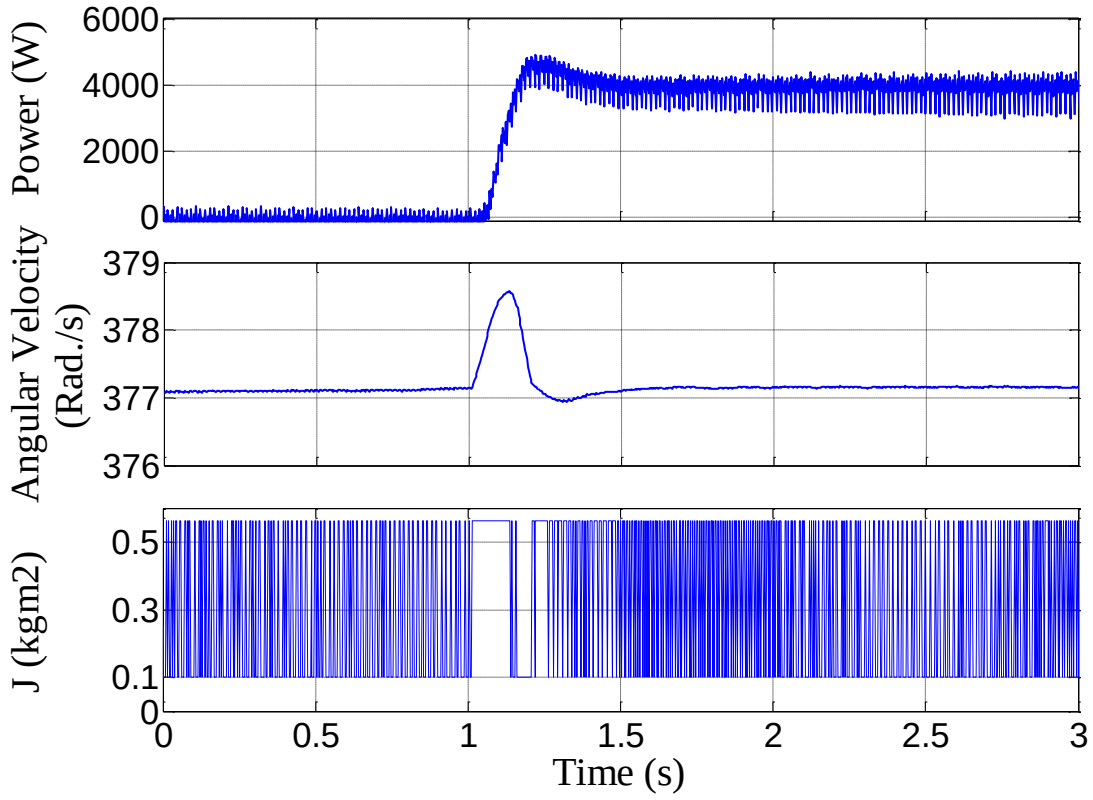

Fig. 2.21- Output power, virtual angular velocity, and moment of inertia of VSG with Alternating *J* and *D* = 0 pu.

deceleration, a small value for inertia factor was adopted to increase the deceleration effect. The system transient energy analysis was used to assess the stabilizing effect of Alternating Inertia control. It was clarified by the energy function analysis that the system transient energy is reduced promptly by the reduction in the value of the moment of inertia. Actually, in the case of a real synchronous machine, this transient energy is dissipated by damping terms during oscillations, whereas the Alternating Inertia control eliminates the transient energy directly and prevents its flow from dc storage and dissipation. Compared to normal damping factor *D*, the damping exerted by Alternating Inertia is considerably more effective and has identical results in any conditions. In addition, the transient energy can be reduced to zero at the end of the first quarter-cycle by Alternating Inertia control. Therefore, any transients can be eliminated instantaneously. The idea does not only stabilize the VSG unit but also enhances the stability of other machines in the system. Two configurations were assessed by simulation, and the stabilizing effect of Alternating Inertia on the adjacent machines was illustrated. The proposed scheme was realized on the experimental system, and the results affirmed the outstanding stabilizing effect of Alternating Inertia.

References

[1] J. Alipoor, Y. Miura, T. Ise, "Distributed generation grid integration using virtual synchronous generator with adoptive virtual inertia," in *Proc. IEEE Energy Conversion Congress and Exposition (ECCE)*, 2013, pp. 4546-4552.

[2] J. Alipoor, Y. Miura, T. Ise, "Power system stabilization using virtual synchronous generator with alternating moment of inertia," *IEEE Journal of Emerging and Selected Topics in Power Electronics*, vol. PP, no. 99, pp. 1-8, 2014.

[3] J. Machowski, J. w. Bialek, and J. R. Bumby, *Power System Dynamics: Stability and Control, 2nd ed*. Chippenham, Wiltshire, UK: Wiley, 2008, pp. 222-230.

Chapter 3

Stability Assessment and Optimization Methods for Microgrid with Multiple VSG Units

The main transient stability analysis tool for power system is the direct method that evaluates the transient energy function after a large disturbance [1], [2]. In this method, the transient energy or an index related to it is evaluated after a contingency or new dispatch configuration. If it is below the critical level, the stability is guaranteed. Evaluating the energy function required off-line simulation of the system and is not suitable for on-line monitoring and control. On the other hand, most of the practical works on the transient stability constrained optimization that needs a simple and real-time transient stability index, select Rotor Angle Deviation (RAD) [3-7]. This criterion is consistent with industry practice and has been found by utility engineers to be acceptable [3]. However, In the case of VSG units, the rotor angle is not available to be used in transient stability constrain. To solve this problem, Voltage Angle Deviation (VAD) of generators with respect to the angle of the Center Of Inertia (COI) is used to generalize the RAD security constrain for the multi-VSG microgrid applications.

In traditional power systems, in which all the machines are SGs, desired performance is achieved by including the power system security criteria in optimal power dispatch [3-6]. Besides, power system stabilizer is embedded in the system to enhance the stability. Once the power system

condition (the system topology and generation-loading dispatch) changes, the parameters of the controllers must be retuned; because the optimized parameters under specific condition might not result in the desired response in another condition. Artificial intelligences are implemented to readjust the parameters when system condition changes [8]. Major state quantities of a synchronous generator such as mechanical angular frequency and voltage angle can be found in VSG control. Moreover, VSGs have an advantage respect to SGs that the model parameters that determine their response can be tuned in real time to achieve the proper performance. The contribution of this chapter is to set the parameters of the VSG units in a multi-VSG system in real time to have the smooth transition after a change or disturbance in all operating points. To achieve this goal, Particle Swarm Optimization (PSO) is implemented to find the parameters of VSG units that result in the desired performance. Then, Alternating Inertia scheme will be applied to multi-VSG microgrid to not only damp the oscillation quickly, but also improve the stability of the system.

This chapter is organized as follows. The microgrid with multiple VSGs is introduced in section 3.1. In section 3.2, VAD constraint is introduced as a tool for transient stability assessment and confinement. In section 3.3, PSO is used to obtain the desired response of a multi-VSG microgrid. In section 3.4, the performance of Alternating Inertia in oscillation damping and stabilizing of a multi-VSG microgrid is investigated. In section 3.5, a comparison of the performance of PSO and Alternating Inertia methods is made. Finally, conclusion is given in section 3.6.

3.1- Microgrid with Multiple VSG Units

The multi-VSG system used in this research as case study is shown in Fig. 3.1. The parameters of the system are represented in Table 3.1 with the base power and frequency of 250 kVA and 60 Hz, respectively. The VSGs and SGs of this system have a governor similar to what shown in Fig. 1.4 of chapter 1. The automatic voltage regulator shown in Fig. 3.2 is used to keep the terminal voltage of the generators at the nominal value that is 2 kV.

The value of J together with D determines the time constant of the VSG unit. Selecting the proper value of them is a challenging issue without a routine. Mimicking a synchronous machine, J is given by:

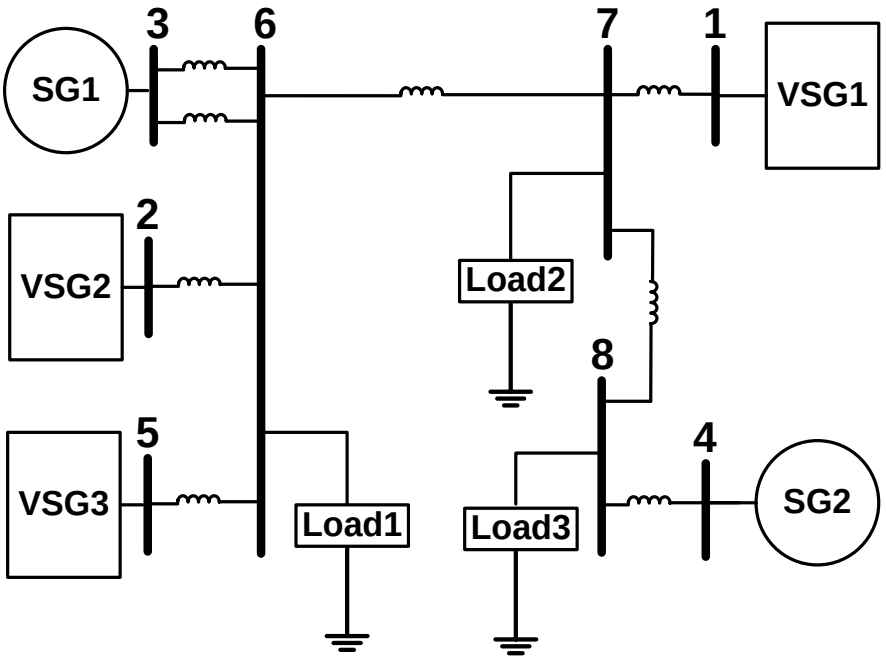

Fig. 3.1- Multi-VSG system.

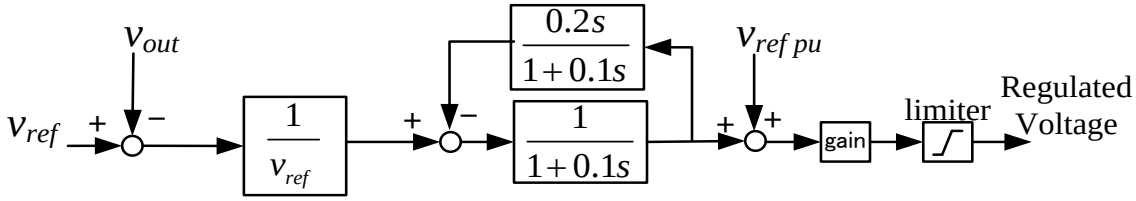

Fig. 3.2- Automatic Voltage Regulator diagram.

Table 3.1- The Parameters of the Multi-VSG System

Line	X (pu)	Line	X (pu)
3-6	0.170	6-7	0.696
3-6	0.170	1-7	0.058
2-6	0.025	7-8	0.038
5-6	0.127	4-8	0.064
VSG Filter inductance		0.353 pu	
H_{SG1} and H_{SG2}		4 s	

$$J = \frac{2HS_{base}}{\omega_0^2} \tag{3.1}$$

where H is the machine inertia constant, S_{base} is the base power of the machine, and ω_0 is the system frequency. The parameter H tells that for which period of time the machine is able to supply the nominal load based solely on the energy stored in the rotating mass. The higher H, the bigger

the time constant, results in a slower response but smaller frequency deviation after a change or disturbance. Although it depends on the machine size and power, for typical synchronous machines H varies between 2 and 10 s.

The VSG response at a specific output power and voltage is determined by parameters of its second order differential equation which are the real part of its eigenvalues σ_i and the damping ratio ξ_i. These parameters are calculated for a single VSG connected to a grid in Appendix A. The following equations indicate that the VSG response parameters are related to J and D directly:

$$\sigma_i = -\frac{D_i}{2J_i\omega_s},$$

$$\omega_{ni} = \sqrt{\frac{P_{\max i}\cos(\theta_{0i})}{J_i\omega_s}}, \tag{3.2}$$

$$\xi_i = \frac{-\sigma_i}{\omega_{ni}},$$

where $P_{max\,i}$ is the maximum transferable power from i-th VSG bus to the grid, θ_{0i} is the voltage angle of the i-th VSG with respect to the grid and ω_{ni} is the undamped natural frequency of the i-th VSG. At any working conditions, the desired system response parameters can be achieved by tuning J and D.

3.2- Multi-VSG Microgrid Stability Assessment Tool

In the traditional power systems, the difference between the rotor angle of each SG with respect to the angle of COI is observed for stability and optimization purposes. If the relative rotor angle of a SG exceeds RAD limit, the system will be prone to instability. Moreover, optimization methods tend to find the optimum configuration of the system which keeps RADs of all SGs below the RAD limit.

The VSG units are designed to emulate the behavior of SGs. However, unlike a real SG, the rotor angle of a VSG is not available to be used in stability considerations. On the other hand, having the specific value of inertia, VSG units can contribute in the calculation of the angle of COI and the angle deviation. Consider the multi-VSG microgrid of Fig. 3.1. The voltage angle at the VSG connected buses are determined by the connected VSG. For the SG-connected buses, the

voltage angle follows the variations of the load angle or rotor angle of the SG. The voltage angle can be calculated by a (Phase Locked Loop) PLL unit to be used in the calculation of the angle of COI and VAD. The voltage angle of a generating bus is denoted as:

$$\theta_i = \omega_i t + \theta_{0i} . \tag{3.3}$$

In the study system, all of the generators comprise an amount of inertia. For general application of this method, the generators that are not controlled based on the VSG concept are assumed not to contribute in the frequency and angle regulation. In the other words, they have zero value of inertia. The angle of COI is calculated as:

$$\theta_{coi} = \frac{\sum_{i=1}^{Ng} J_i \theta_i}{\sum_{i}^{Ng} J_i} = \omega_{coi}(t) + \theta_{0coi} \tag{3.4}$$

where N_g is the number of the generators. ω_{coi} is the speed of COI and considered as the grid frequency to calculate $\Delta\omega$ of (1.1) of chapter 1. The VAD of each generator is the voltage angle of the corresponding generator with respect to the angle of COI and calculated as follows:

$$\Delta\theta_i = \theta_i - \theta_{coi} \tag{3.5}$$

In order to guarantee the stable operation, (3.6) must be valid:

$$\left|\Delta\theta_i\right| \le \theta_{MAX} \tag{3.6}$$

where θ_{MAX} is the maximum allowable VAD. There are some points that justify this criterion. At first, it should be mentioned that there is no general method for evaluating the large disturbance stability region of a dynamic system consisting of swing and power flow equations. Secondly, after a disturbance, the angle of one or a group of generators will deviate from the rest of the system. Based on the equal area criteria, if the relative angle between the two groups of generators remains below 180 degrees, the system preserves its stability [3]. Thirdly, in practical power systems, if the rotor angle of a generator with respect to the angle of COI exceeds a threshold, the generator will be tripped by out-of-step relay [9]. The value of the θ_{MAX} depends on the system modeling precision

(the details of the model of system elements that are included and the precision of the calculated or estimated parameters) and is selected as 100, 120, 70, and 110 degrees for RAD limit in literatures [3-7].

To evaluate the performance of multi-VSG microgrid with untuned VSGs, J =14.07 kgm^2 is calculated via (3.2) assuming H is 4 s for all VSG units of Fig. 3.1. Although the VSG units are not supposed to be tuned in real time, nevertheless, a reasonable value for D is applied to see the performance of the system. To calculate a suitable value of D resulting a smooth response (a response that is fast enough and has minimum oscillation), ξ_i is set equal to $\xi_0 = 0.7$ in (3.2) and D is calculated by assuming $\theta_{0i} = \pi/6$ and $P_{max\,i}$ calculated at rated voltage, which results in $D_1 = 3.0$, $D_2 = 3.1$, and $D_3 = 2.7$ at system base KVA that is 250 KVA.

The system was simulated in PSCAD/EMTDC and the simulation scenario according to Table 3.2 was applied. First at $t = 1$ s the power reference of the VSG units were increased simultaneously by a step. Then the impedance type load increased at $t = 4$ s. Fig. 3.3 shows the output angular frequencies of the VSG units. As it is observed, small frequency oscillations appeared after the increase in power references at 1 s. The parameters calculated for the VSG units are very close to the optimum values (values that result in a critically damped response); therefore the response is not terrible (it does not have severe oscillation or slow rise time). However, the response is not perfect since it has oscillation that can be eliminated by tuning the parameters. When the load

Table 3.2- Simulation Scenario.

	t < 1 s	t ≥ 1 s
SG1	0.8 pu 200 kW	0.8 pu 200 kW
SG2	1 pu 250 kW	1 pu 250 kW
VSG1	0.8 pu 200 kW	1 pu 250 kW
VSG2	0.6 pu 150 kW	1 pu 250 kW
VSG3	0.4 pu 100 kW	1 pu 250 kW
	t < 4 s	t ≥ 4 s
Load 1	R 0.669 pu, 373.8 kW at rated voltage L 0.636 pu, 270.9 kVA at rated voltage	R 0.444 pu, 564.2 kW at rated voltage L 0.636 pu, 322.5 kVA at rated voltage
Load 2	R 1.137 pu, 219.8 kW at rated voltage L 0.990 pu, 165.8 kVA at rated voltage	R 0.594 pu, 419.7 kW at rated voltage L 0.990 pu, 216.5 kVA at rated voltage
Load 3	R 0.513 pu, 487.8 kW at rated voltage L 0.542 pu, 355.2 kVA at rated voltage	R 0.375 pu, 662.3 kW at rated voltage L 0.542 pu, 378.6 kVA at rated voltage

increased at 4 s, the generators of the system try to converge at the frequency of COI. Although the frequencies are very close to each other at t = 5 s, the small difference in frequency and the sluggish transition result in violations of VAD from the stability limit as observed in Fig. 3.4 and therefore, the frequency of the generators cannot converge at the equilibrium point.

Other disturbances that can result in large disturbance instability (transient instability) are faults in power system. To investigate the stability of multi-VSG microgrid in fault condition, a symmetrical fault with fault resistance of 1 Ω was stablished at bus No. 8 of Fig. 3.1 and lasted for 0.13 s. The system loading condition when fault happened is presented in Table 3.3. The angular frequencies of generators are shown in Fig. 3.5. It is observed that with such fault, the angular velocity of a group of generators increased and the ones of the other group decreased until the two

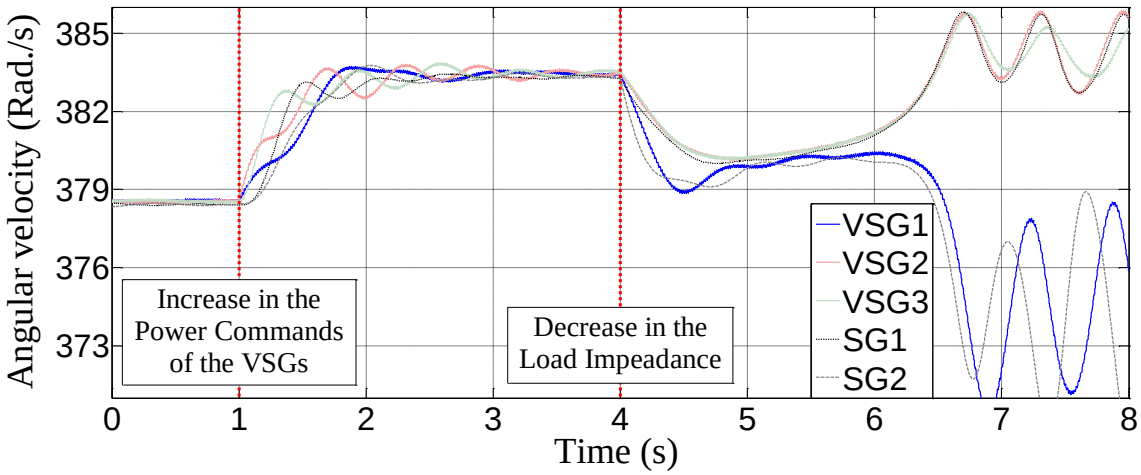

Fig. 3.3- Angular Frequency of the generators with untuned parameters.

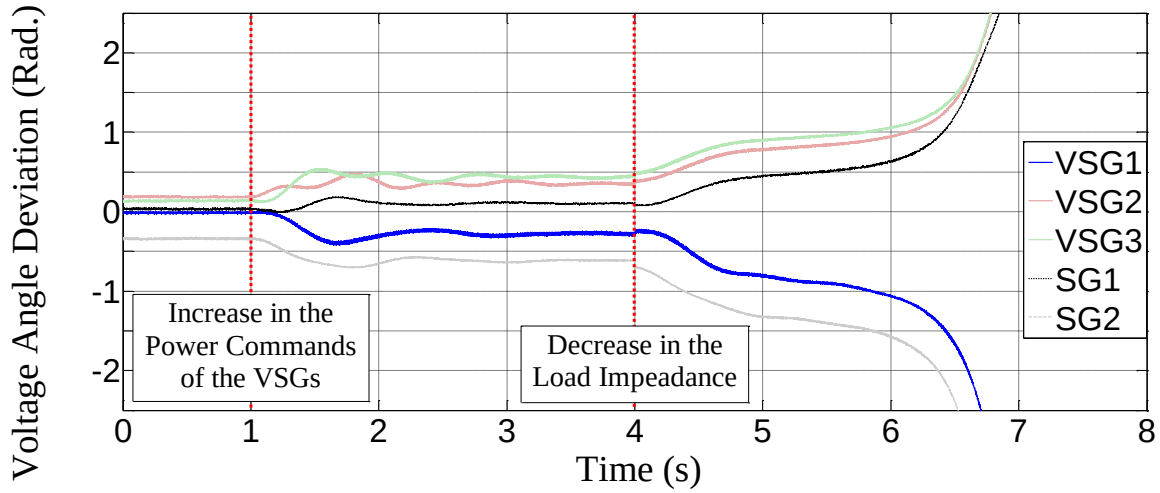

Fig. 3.4- VAD of the generators with untuned parameters.

groups of generators went out-of-step. The VADs of generators are shown in Fig. 3.6. In this figure, the breakup of VADs of two groups of generators and instability after the fault is obvious.

3.3- Multi-VSG Microgrid Optimization by PSO

Particle swarm optimization (PSO) is a distributed behavioral algorithm that performs multidimensional search [10]. The general algorithm modified for multi-VSG system is shown in Fig. 3.7. In this algorithm, the behavior of each individual (each VSG unit) is affected by the best local answer (best parameters values for each VSG during one search) and the best global individual (the best answer among all VSG units). The best answer means the values of parameters

Table 3.3- System condition when the fault happens.

SG1	0.8 pu	200 kW
SG2	1 pu	250 kW
VSG1	1 pu	250 kW
VSG2	1 pu	250 kW
VSG3	1 pu	250 kW
Load 1 (pu)	R 0.494 pu	506.3 kW at rated voltage
	L 0.636 pu	310.6 kVA at rated voltage
Load 2 (pu)	R 0.706 pu	354.0 kW at rated voltage
	L 0.990 pu	205.7 kVA at rated voltage
Load 3 (pu)	R 0.393 pu	634.9 kW at rated voltage
	L 0.542 pu	373.2 kVA at rated voltage

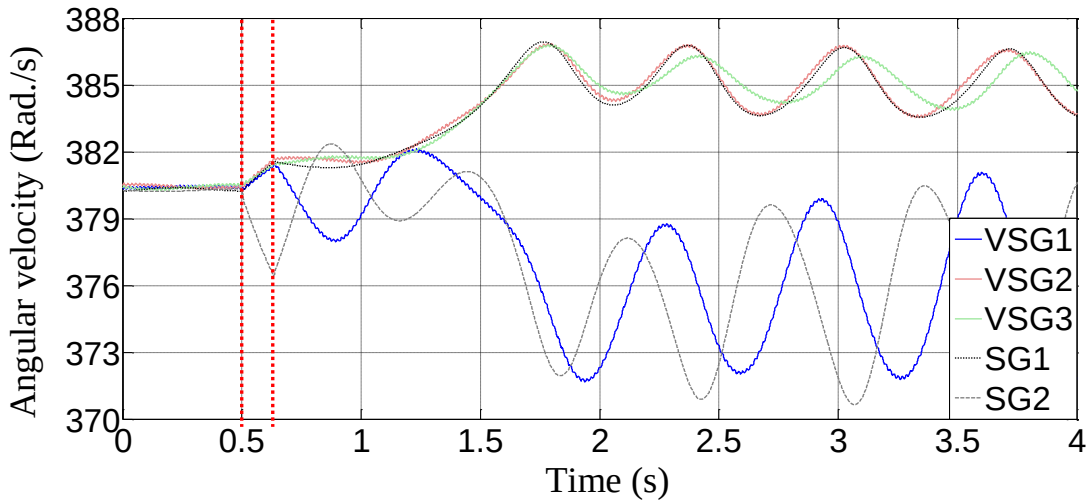

Fig. 3.5- Angular Frequency of the generators with untuned parameters subjected to a fault at bus No. 8.

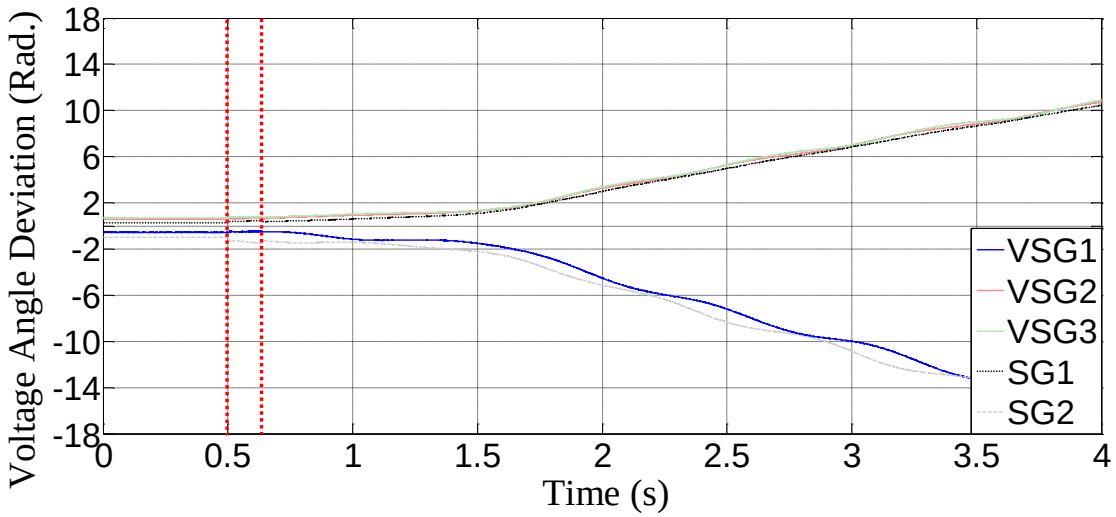

Fig. 3.6- VAD of the generators with untuned parameters subjected to a fault at bus No. 8.

1. For i = 1 to M (M = population size i.e. the number of VSG units)
   Initialize (J_i, D_i) for each VSG from interval
   Initialize $V_{(Ji, Di)} = 0$ (V = speed of each particle)
2. End For
3. For i = 1 to M
   $(J_i, D_i)_{BESTS} = (J_i, D_i)$ (Initialize the "memory" of each particle)
4. End For
5. Repeat
   For i = 1 to M
   $V_{(Ji, Di)} = w \times V[i] + C1 \times R1 \times ((J_i, D_i)_{BESTS} - (J_i, D_i))$
   $+C2 \times R2 \times ((J, D)_{GBEST} - (J_i, D_i))$
   (Calculate speed of each particle)
   (W = Inertia weight, $C1$ & $C2$ are positive constants)
   ($R1$ & $R2$ are random numbers in the range [0,1])
   $(J_i, D_i)_{new} = (J_i, D_i) + V_{(Ji, Di)}$
   If a particle gets outside the pre-defined limit
   then it is reintegrated to its boundaries
   Evaluate $(J_i, D_i)_{new}$ of each VSG by calculating the fitness function
   If $(J_i, D_i)_{new}$ is better than $(J_i, D_i)_{BESTS}$ then $(J_i, D_i)_{BESTS} = (J_i, D_i)_{new}$
   If $(J_i, D_i)_{new}$ is better than $(J, D)_{GBEST}$ then $(J, D)_{GBEST} = (J_i, D_i)_{new}$
   End For
6. Until stopping condition is reached

Fig. 3.7. The PSO algorithm for multi-VSG system.

that result in the minimum value of a fitness function. The PSO algorithm will be implemented with two different objectives combined in its fitness function: first the smooth transition after a

large disturbance will be aimed and second, the stability constraint will be included in the PSO algorithm fitness function to see whether the VAD constrained dispatch of the moment of inertia will improve the stability of the system.

The fitness function that is embedded in the algorithm will aim the objective. To have a smooth transition after a change or disturbance, the values of the parameters of each VSG units that corresponds the desired values of quantities introduced in (3.2) should be discovered by algorithm. The penalty type fitness function can be written as:

$$Min \quad fit_{1i} = P_{\xi} \times \left|\xi_i - \xi_0\right| + P_{\sigma} \times \left|\sigma_i - \sigma_0\right|\Big|_{\sigma_i > \sigma_0} \tag{3.7}$$

where P_σ and P_ξ stand for the penalty factors and σ_0 and ξ_0 are the desired real part of eigenvalues and the damping ratio, respectively (equation 3.2). The proper values of constants in (3.7) are slightly different from theoretical calculated values because of modeling approximations and simplifications. However, with a brief experience, the constants of (3.7) can be tuned finely.

The other constrain is needed to keep the VAD of all generators within the limits by finding the appropriate values of J of the VSG units. For this purpose, the second part of fitness function can be written as follows:

$$fit_{2i} = P_{VAD} \sum_{\substack{i=1 \\ |\Delta\theta_i| > \theta_{MAX}}}^{Ng} \left(\left|\Delta\theta_i\right| - \theta_{MAX}\right) \tag{3.8}$$

The overall fitness function that aims the smooth transition after a change or disturbance and limiting the VAD of all generators is embedded in the PSO algorithm:

$$fit_i = fit_{1i} + fit_{2i} \tag{3.9}$$

By this fitness function, when the VAD of a generator exceeds the limit, the algorithm compromises between the smooth transition and keeping the VAD of generators below the limit. The algorithm searches for the best values of J_i and D_i by evaluating the fitness function at each iteration until the maximum number of iterations is reached. Then $(J_i, D_i)_{\text{BESTS}}$ are extracted as the optimum values for i-th VSG parameters.

The algorithm was embedded into the case study system and the same simulation scenario as section 3.2 was applied. The optimum values of parameters calculated by algorithm were passed through a low-pass filter with the cut-off frequency of 16 Hz to remove its chattering.

Fig. 3.8 shows the calculated values of the moment of inertia, J and the damping factor, D by PSO. When these values of J and D were applied in real time, the mechanical angular velocity of the generators will have a transition shown in Fig. 3.9. As it is observed, by the optimized value of the parameters of the VSG units, they have a smooth response. Since this algorithm calculated the values of parameters in real time, even when system operating point changes, the VSG units will have the similar smooth operation. However, when the load increased at t = 4 s, again the VAD exceeded the stability limit as shown in Fig 3.10. It is observed that when the VAD of SG2 reached the specified limit, that is 1.75 Rad., at t = 6 s, the values of J and D of VSG2 and VSG3 were reduced by PSO algorithm. This reduction will move the position of the angle of COI toward the angle of the other group of generators that are SG2 and VSG1and thereby, the growth in the absolute value of the VAD of the SG2 will be prevented. This process on the other hand will increase the VAD of the SG1, VSG2, and VSG3 until they reach to the limit. At this point, the algorithm became confused between two groups of generators and tried to keep constant the VAD

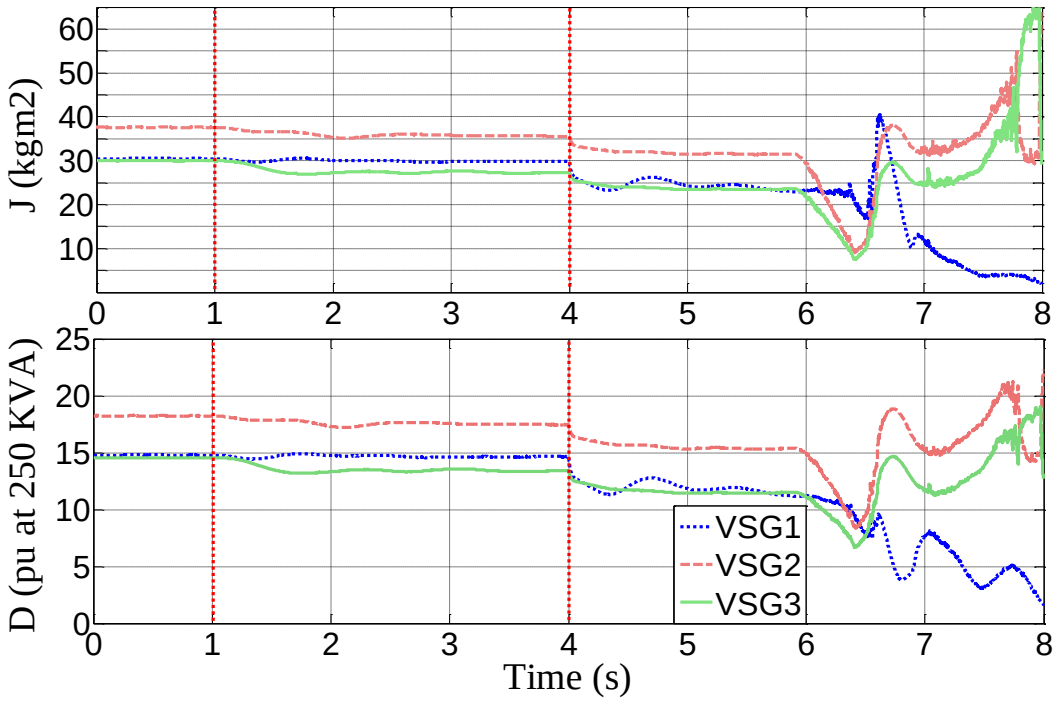

Fig. 3.8- J and D calculated by PSO.

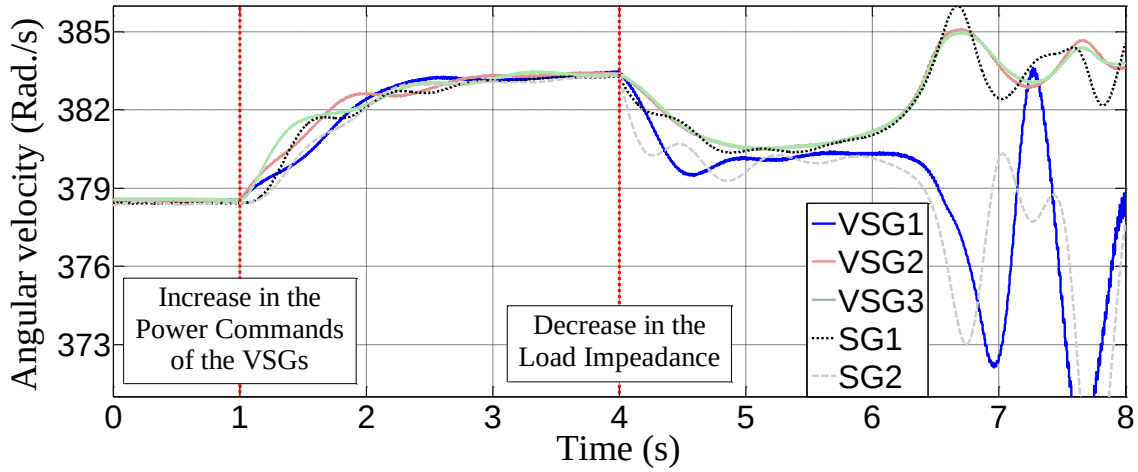

Fig. 3.9- Angular Frequency of the generators optimized by PSO.

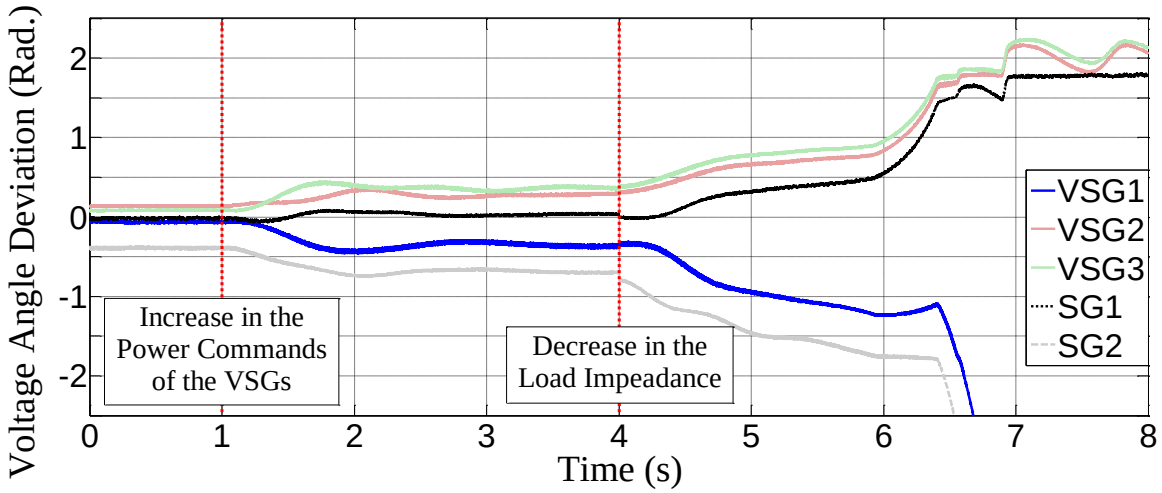

Fig. 3.10- VAD of the generators optimized by PSO.

of the generator group that has more influence on the fitness function, whereas the VAD of the other group passed the limit and the microgrid lost the stability.

It can be concluded that the smooth transition after a change or disturbance can be achieved by optimizing the parameters of the VSG units using PSO algorithm. However, limiting the VAD of generators by adjusting the values of the moment of inertia will not improve large disturbance stability of the microgrid when the system is seriously unstable.

It must be noted that if out-of-step happens when the VAD of a generator exceeds the stability limit during transient oscillations (when the generator has relatively small power rating compared to the system), it may be possible to keep the generator in-step by adjusting the inertia in the system. To investigate this possibility, a fault disturbance simulation similar to previous section

was performed on the system with PSO-optimized VSGs. The fault and system condition at the fault moment is similar to the previous section mentioned in Table 3.3. Fig. 3.11 depicts the values of J and D calculated by PSO during simulation. As it is observed, around t = 1.5 s, the value of J and D of VSG2 and VSG3 is reduced in order to keep the VAD of SG2 within the limit that is 1.57 Rad. Figs. 3.12 and 3.13 show the angular frequency and VAD of generators, respectively. It is observed that the angular frequencies of generators converged at predisturbance system frequency value and all generators remained in-step. Moreover, in Fig. 3.13, the VAD of SG2 was kept at the limit via adjusting the inertia of VSGs until the transients were passed and the VAD of SG2 went into the limit.

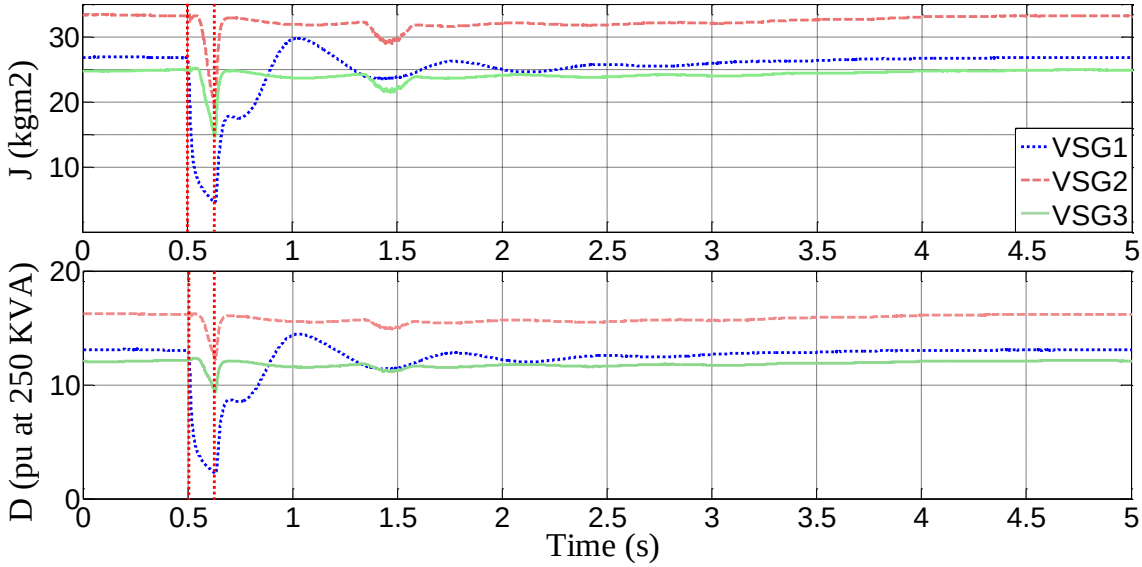

Fig. 3.11- J and D calculated by PSO for faulted system.

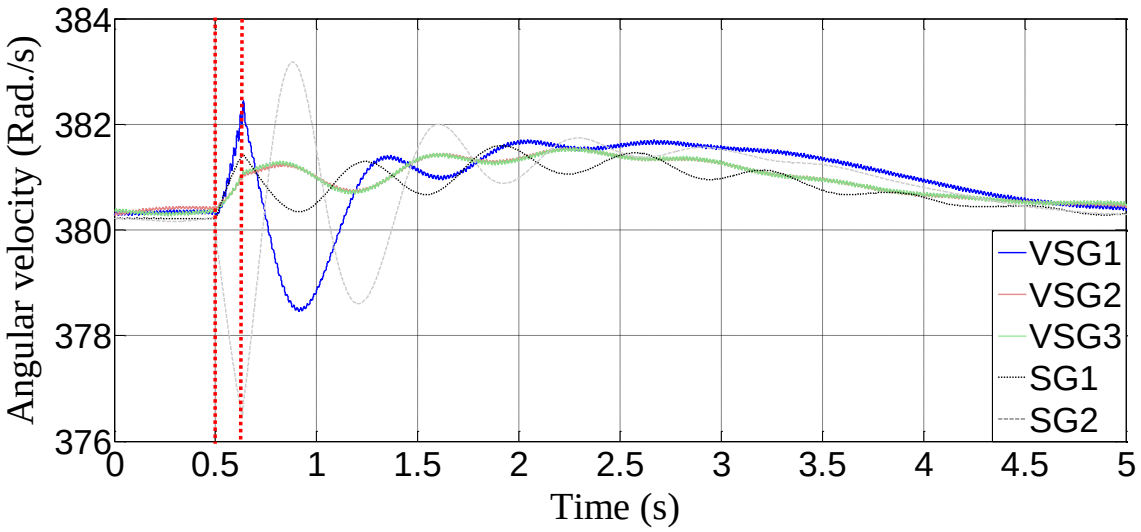

Fig. 3.12- Angular Frequency of the generators optimized by PSO subjected to a fault at bus No. 8.

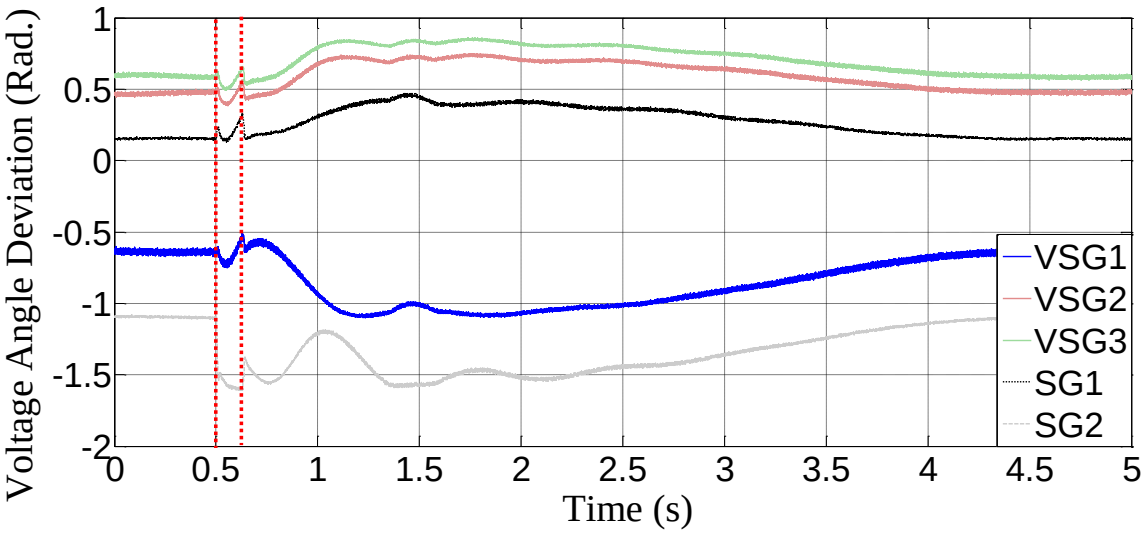

Fig. 3.13- VAD of the generators optimized by PSO subjected to a fault at bus No. 8.

3.4- Multi-VSG Microgrid Stabilization by Alternating Inertia

In chapter 2, the Alternating Inertia scheme was introduced and its oscillation damping effect for a single VSG unit was proved. However, the performance of this scheme in a multi-VSG system which each generator has a different oscillation mode was not clear. In this section, the Alternating Inertia is applied to the multi-VSG microgrid to investigate its oscillation damping and large disturbance stabilization performance.

The Alternating Inertia scheme was applied to each VSG of the microgrid of Fig. 3.1. In this chapter J_{big} is selected to be the value calculated in section 3.2 and the J_{small} is set to be 10% of J_{big}. Besides, the damping factors, D of VSG units are set to be equal to ones calculated in section 3.2. The simulation with the same scenario was performed and the values of J that calculated by this method are shown in Fig. 3.14. Fig. 3.15 shows the angular velocity of the generators of the microgrid. It is observed that by the virtual inertia control, the frequency oscillation damped fast and effectively by the damping inserted by the Alternating Inertia scheme. The VAD of the generators during this simulation are shown in Fig. 3.16. The effectiveness of the Alternating Inertia in stabilization is clear in this figure. The Alternating Inertia directly removes the transient energy that must be damped during the sluggish response. Fast elimination of the transient energy bypasses the system state variables (that are the angle and frequency of the generators) to the equilibrium point. After both of the disturbances of the simulation, VAD of generators increased smoothly and stabilized quickly at a smaller absolute value. It can be concluded that the Alternating Inertia enhances the consistency of the system by quick frequency adjustment.

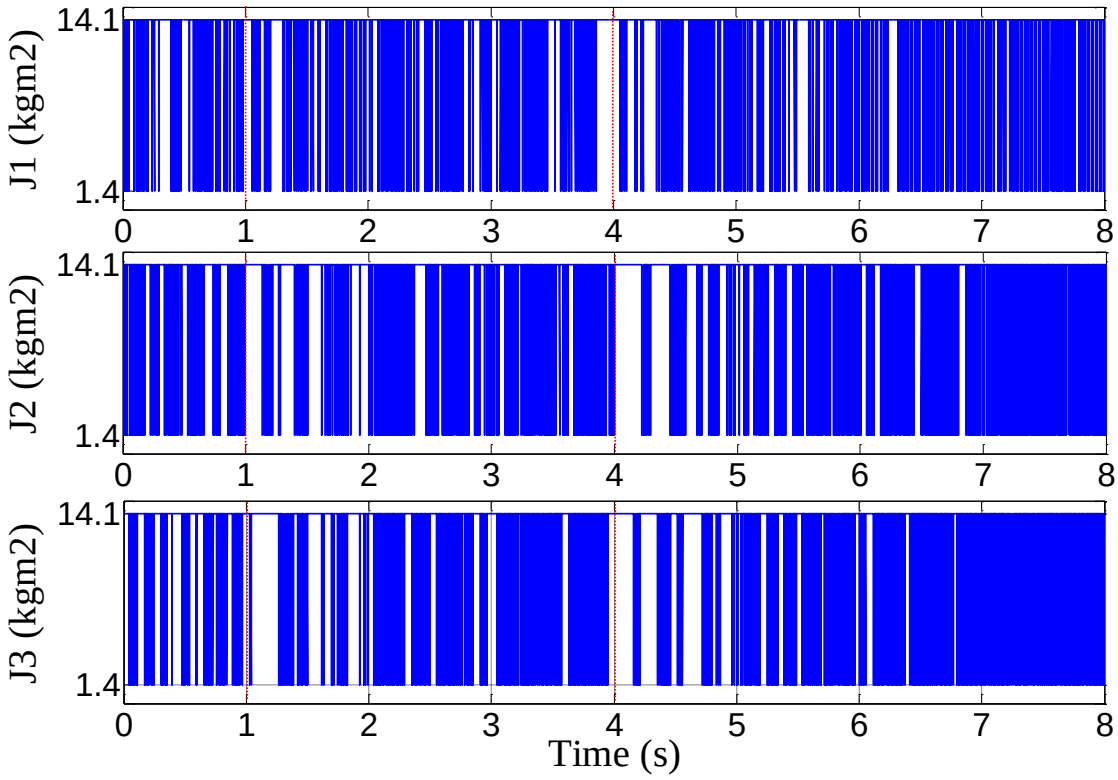

Fig. 3.14- J calculated by Alternating Inertia scheme.

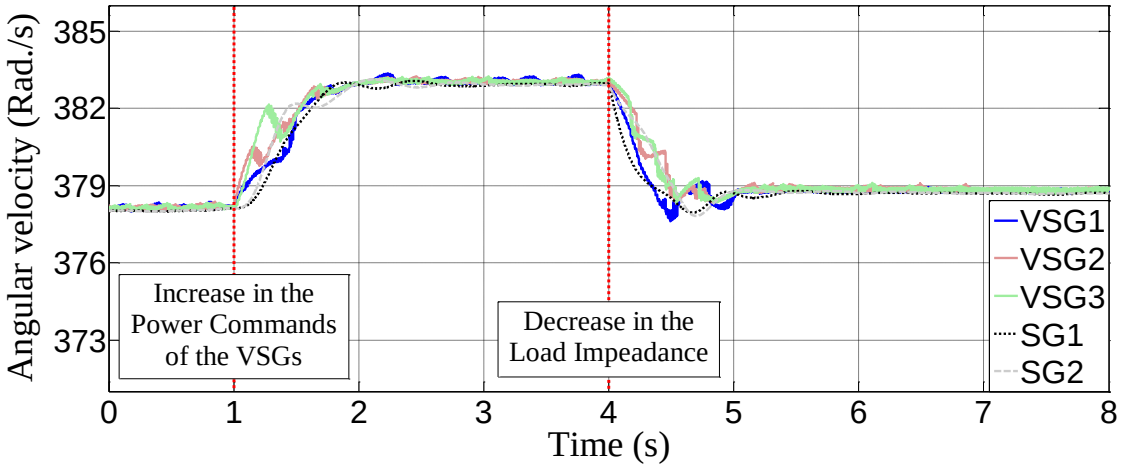

Fig. 3.15- Angular Frequency of the generators with Alternating Inertia control.

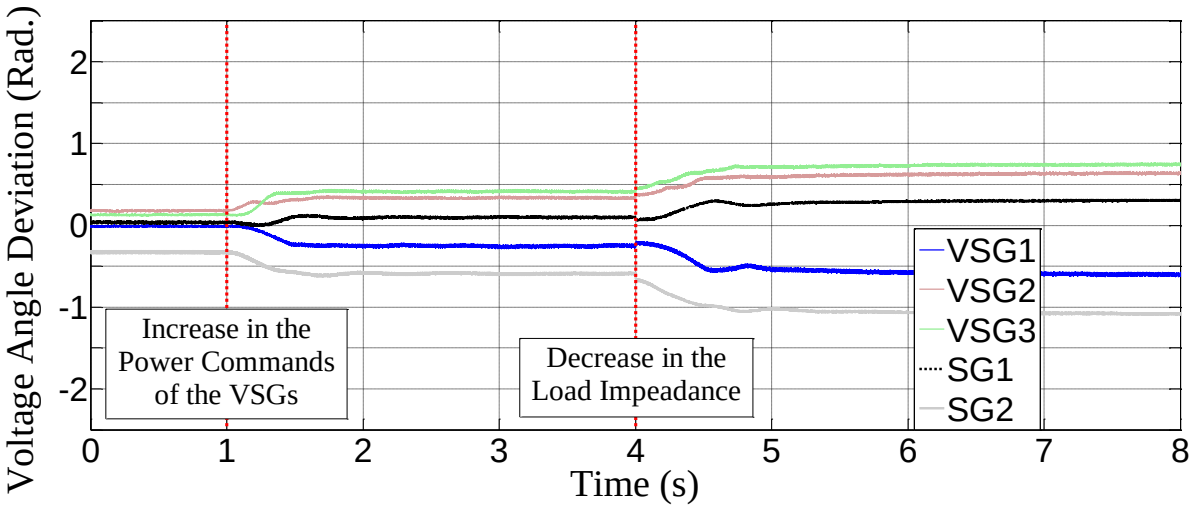

Fig. 3.16- VAD of the generators with Alternating Inertia control.

The performance of Alternating Inertia in fault condition was investigated. The same fault in the same system condition happened while VSGs are equipped with Alternating Inertia. The values of J of VSG units calculated by Alternating Inertia, angular frequencies, and the VADs of generators during simulation are shown in Figs. 3.17, 3.18, and 3.19 respectively. It is observed that in fault condition also, Alternating Inertia is effective in stabilization of multi-VSG system.

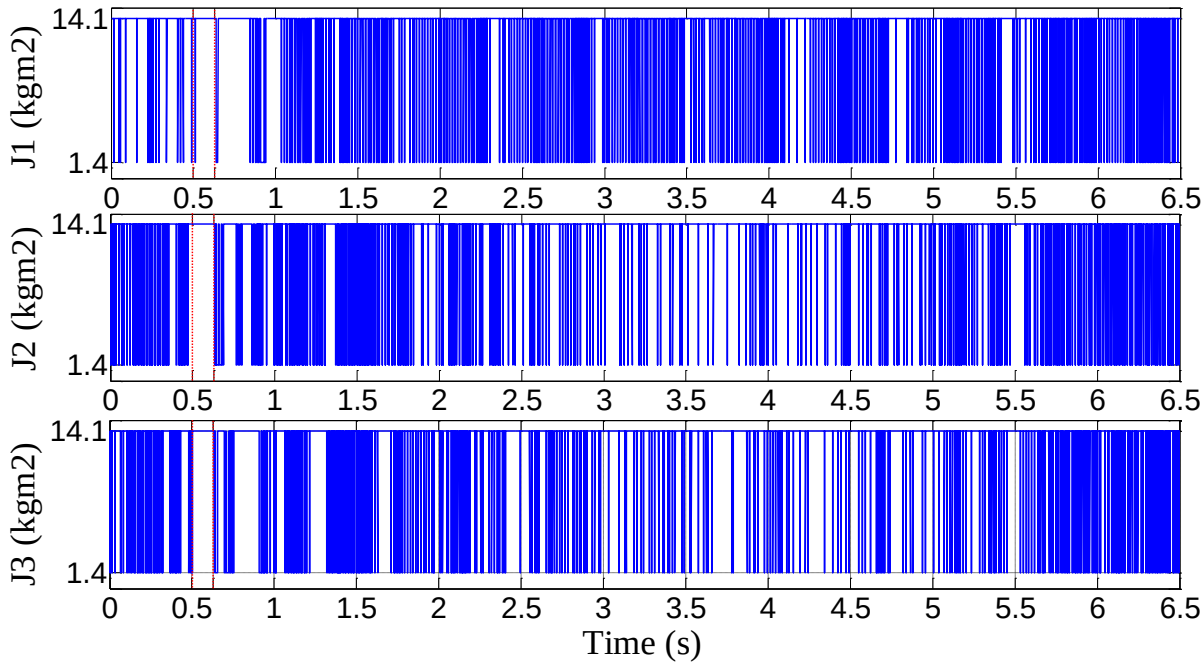

Fig. 3.17- *J* calculated by Alternating Inertia scheme when a fault happened at bus No. 8.

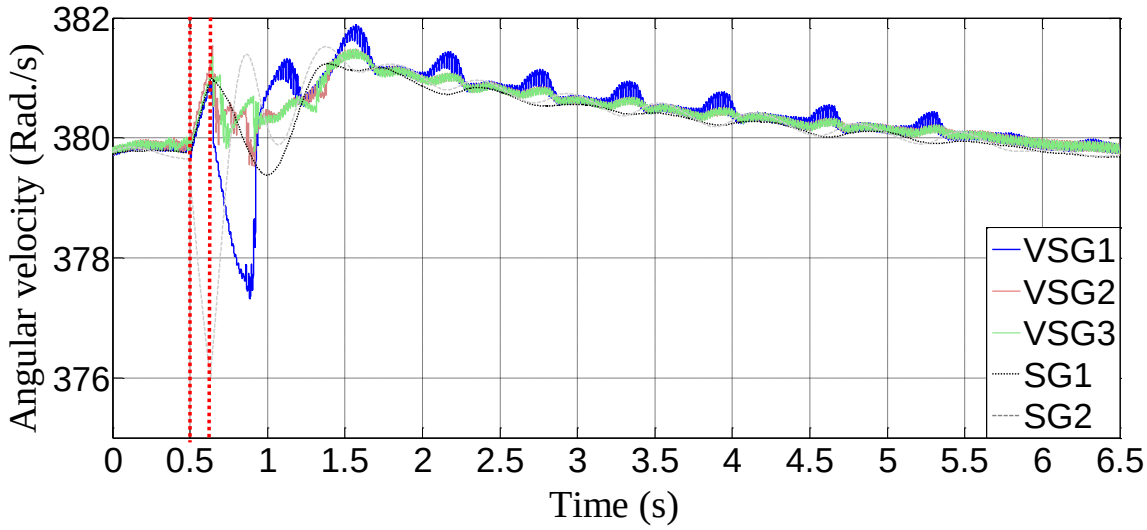

Fig. 3.18- Angular Frequency of the generators with Alternating Inertia control.

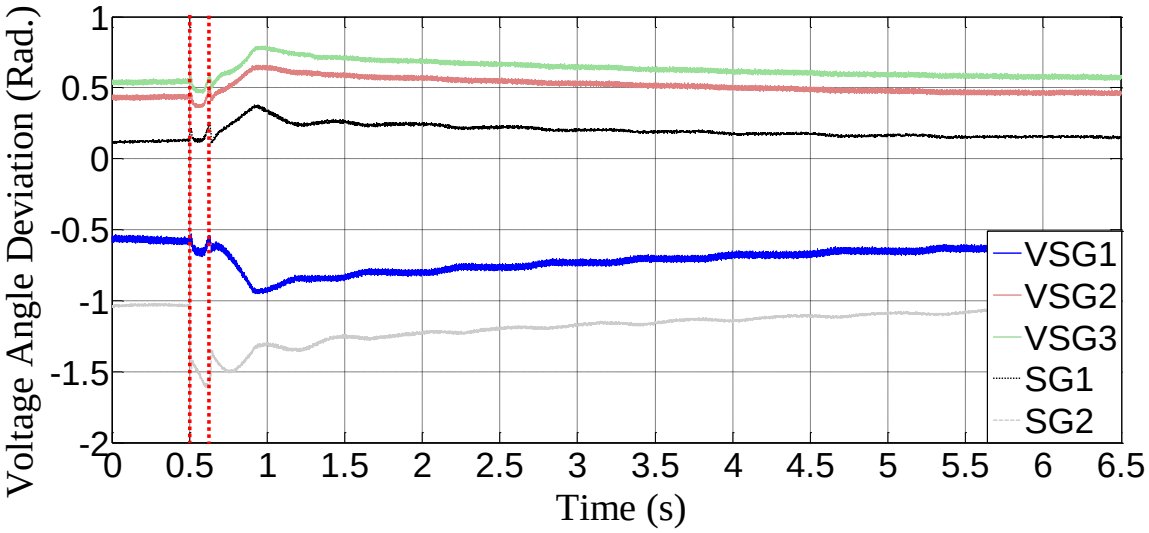

Fig. 3.19- VAD of the generators with Alternating Inertia control.

3.5- Comparison of PSO and Alternating Inertia

For a smooth transition after a change or disturbance, PSO has a good response. As shown in Fig. 3.9 after first disturbance (step increase in power commands) the transition has almost no oscillation. However, for the system with Alternating Inertia, small non-sinusoidal oscillation appeared that was suppressed quickly (Fig. 3.15). Regarding stabilization, PSO was not able to solve the instability due to heavy load. However it stabilized the system after a fault whereas the system with untuned VSGs lost the stability. On the other hand, Alternating Inertia was effective in stabilization of the system for all of the tested disturbances. It should be mentioned that the PSO includes communication between VSG units and considered as a global control that the conditions of all elements of the system can be included in its objectives. In addition, it is very flexible and various constraints can be implemented in it. Therefore it is suitable for optimizing large systems. Whereas, Alternating Inertia is a local control that optimizes the designated VSG. Having no additional calculation burden (the required quantities are calculated in the VSG control algorithm) is the advantage of Alternating Inertia method.

3.6- Conclusion

This chapter concentrated on the optimization and stabilization of VSG units in a microgrid. The basis of this chapter was founded on the advantage of VSGs with respect to SGs that is the variable physical model parameters in real time. Firstly, a simple and applicable transient stability

criteria that is used for optimal power dispatch with security constraint, was generalized to be used in a multi-VSG microgrid. Then PSO algorithm was used to find the optimum values of moments of inertia and damping factors of VSG units that bring in a smooth transition after a large disturbance at any working condition. Further, the fitness function of the algorithm is modified to make a compromise between the smooth transition objective and keeping the VAD within the stability limit. The simulation results show that the smooth transition was achieved. Although the algorithm managed to keep the VAD of generators within the limit to some extent; however, because of the slip between the two groups of the generators, the angle deviation became very large and the two generator groups fell out-of-step. The PSO method was investigated in fault disturbance that the instability may happen when the VAD of a generator passes the stability limit during transient oscillation. The results indicated that the PSO method prevented VAD of generators to pass the stability limit during transient oscillation and it was effective in stabilization of system in such condition that the transient oscillation causes instability.

Finally, the Alternating Inertia scheme was applied to the VSG units of the multi-VSG system. This scheme switches the value of the moment of inertia four times during a cycle of oscillation considering the relative angular frequency and its rate of change. By this method, a damping effect is imposed at the moment that the inertia factor is changed from the large value to the small one. The simulation results of Alternating Inertia showed that although the frequency transients include irregular oscillations, but the oscillation were damped exceptionally quickly and the system stability was achieved readily.

The PSO algorithm involves some calculation burden; however it is known as one of the simplest optimization algorithms. Moreover, PSO algorithm is flexible and other constraints such as the state of charge of the energy storage unit of the DGs, the total inertia of system, and the economic power dispatch can be embedded in the algorithm. The Alternating Inertia method has no additional calculation burden since the quantities required by algorithm are calculated in the VSG control.

References

[1] M. A. Pai, *Energy Function Analysis for Power System Stability*, Norwell, MA: Kluwer, 1989.

[2] M. La Scala, M. Trovato, and C. Antonelli, "On-line dynamic preventive control: An algorithm for transient security dispatch," *IEEE Trans. Power Syst.*, vol. 13, no. 2, pp. 601–610, May 1998.

[3] D. Gan, R. J. Thomas, and R. D. Zimmerman, "Stability-constrained optimal power flow," *IEEE Trans. Power Systems*, vol. 15, no. 2, pp. 535–540, May 2000.

[4] K. Tangpatiphan and A. Yokoyama, "Adaptive evolutionary programming with neural network for transient stability constrained optimal power flow," in *Proc. 15th International conference on Intelligent System Applications to Power System* (ISAPPS), 2009, pp. 1-6.

[5] L. Hakim, J. Kubokawa, Y. Yuan, T. Mitani, Y. Zoka, N. Yorino, Y.Niwa, K. Shimomura, and A. Takeuchi, "A study on the effect of generation shedding to total transfer capability by means of transient stability constrained optimal power flow," *IEEE Trans. Power Syst.*, vol. 24, no. 1, pp. 347–355, Feb. 2009.

[6] G. Guangchao, V. Ajjarapu, and J. Quanyuan, "A hybrid dynamic optimization approach for stability constrained optimal power flow," *IEEE Trans. Power Systems*, vol. 29, no. 5, pp. 2138–2149, Sept. 2014.

[7] Q. Jiang, Y. Wang, and G. Geng, "A parallel reduced-space interior point method with orthogonal collocation for first-swing stability constrained emergency control," *IEEE Trans. Power Systems*, vol. 29, no. 1, pp. 84–92, Jan. 2014.

[8] M.A. Abido, "Optimal design of power-system stabilizers using particle swarm optimization," *IEEE Trans. Energy Conversion*, Vol. 17, No. 3, pp. 406-413, Sep. 2002.

[9] A. A. Fouad and V. Vittal, *Power System Transient Stability Analysis Using the Transient Energy Function Method*. Englewood Cliffs: Prentice-Hall, 1991.

[10] C. A. Coello, G. B. Lamont, and D. A. Van, *Evolutionary Algorithms for Solving Multi-Objective Problems*. Second Edition, Springer, NY, 2007.

Chapter 4

Voltage Sag Ride-through Improvement of VSG

Faults on transmission lines cause voltage drops in several points in power system that affects electrical equipment. Voltage sags (drops) are classified in several types based on the fault type. Three-phase fault on power line produces symmetrical voltage sag, while other fault types cause various unsymmetrical sags. Several works addressed the effect of inverter based DG units on voltage sags in power system focusing on compensation effect of DGs [1, 2]. Reference [3] compared the performance of two control strategies in voltage sag ride-through improvement of a single phase converter-connected DG.

Since the VSG is inherently a power electronics-based unit, it is extremely sensitive to grid side faults and disturbances. Consequently, before practical usage, their operation must be evaluated under disturbances conditions. In this chapter, VSG is tested under symmetrical and unsymmetrical voltage sags and the influence of the characteristics of voltage sags on the VSG transient current is investigated. To verify the results by equations, current trajectory analysis in phase plane is introduced. The trajectory of system state variable (VSG current) is monitored in phase plane and its equations are extracted for during and after the sag. The effects of the characteristic of voltage sags can be observed clearly by this method. High magnitude transient current is the major hazardous consequence of voltage sags on inverter based DGs. To limit the

overcurrent, three additional controllers of voltage amplitude control, output power control and Alternating Inertia control are embedded in the model and tested. Experiments were performed on a 10 kVA VSG-controlled inverter and the results showed that the additional controllers enhanced the voltage sag ride-though capability of the VSG system.

The voltage sag types and characteristics are explained in section 4.1. In section 4.2, the consequences of voltages sags on the VSG unit is monitored by simulation. In section 4.3, the effect of the characteristics of voltages sags on its consequences is clarified by a theoretical analysis. In section 4.4, three additional controllers are introduced to improve the voltage sag ride-through performance of the VSG system. In section 4.5, simulations corresponding to the experimental system were carried out and the performance of the proposed controllers was tested on it. Experimental results are presented in section 4.6. Finally, conclusion is given in section 4.7.

4.1- Voltage Sags Types and Characteristics

Voltage sag (dip) is a momentary drop in the RMS voltage of at least one of the three phases or line voltages. Voltage sags originate from short-term increase in current in power system due to fault or starting large loads [4]. Severity of the effects of voltage sags on equipment depends on the sag characteristics. Sag magnitude and duration are major characteristics. In this dissertation, it is assumed that the implemented sags have rectangular shape. At the instant when the sag begins, voltage of phase "*a*", v_a is expressed by:

$$v_a(t)\big|_{t=t_{sag}} = V_m \sin(\theta_0) \tag{4.1}$$

Where V_m is the phase voltage amplitude. Voltage phase angle at the sag beginning instant, θ_0 is called initial point-on-wave. θ_0 is considered as a characteristic of voltage sag that affects the response of appliance to voltage sag. For both symmetrical and unsymmetrical voltage sags, sag duration is the time interval between sag beginning and ending.

Voltage sags can be either symmetrical or unsymmetrical. If the individual phase voltages are equal and the phase angle relationship is 120°, the sag is symmetrical. Otherwise, the sag is unsymmetrical. Reference [5] classified the voltage sags based on the remained voltage condition. Four major types are addressed in this research.

Three-phase short circuits produce symmetrical sags classified as type A. In this type, voltage magnitudes of three phases decrease equally. For symmetrical sags, the magnitude of sag is the remained RMS voltage in per unit or percent of rated voltage that expressed by a parameter denoted as "h".

Type B voltage sags are one kind of unsymmetrical voltage sags that originate from single line-to-ground faults. Single line-to-ground faults after passing through a "Δ-Y" transformer and line-to-line faults on power lines produce voltage sags of type C. In this type, relative phase angles between voltages vectors also change. If the voltage sag of type C passes through a "Δ-Y" transformer, it will be converted into type D voltage sag.

For unsymmetrical sags, "h" is a coefficient that appears in voltage equations and causes difference in their magnitude and/or phase angles as shown in Fig. 4.1. In the case of a real SG, voltage sags create torque oscillations, overcurrent, and magnetic saturation [6]. The consequences severity depends on the voltage sag type and characteristics. Lightest and severest characteristics of each voltage sag type are listed in Table 4.1 [7].

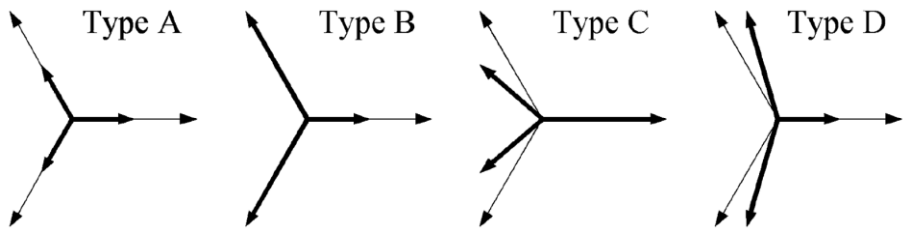

Fig. 4.1- Phasor diagram of voltage sag types for h = 0.5.

Table 4.1- Lightest and severest characteristics of voltage sags.

Sag type	Lightest characteristics		severest characteristics	
	duration	θ_0	duration	θ_0
A	$k^{*}T^{**}$	-	$(k\text{-}1/2)T$	-
B	kT	π/2, 3π/2	$(k\text{-}1/2)T$	0, π
C	kT	0, π	$(k\text{-}1/2)T$	π/2, 3π/2
D	kT	π/2, 3π/2	$(k\text{-}1/2)T$	0, π

$*k \in \mathbb{N}$

$**T$: One cycle time period

4.2- VSG Subjected to Voltage Sags

The VSG model discussed in section 1.2 was simulated in PSCAD/EMTDC software. The parameters of the system are: S_{base} = 35 kVA, f_{base}= 60 Hz, X_F = 42.4%, J = 5.63 kgm^2 and D = 17 pu. Voltage sags were applied to the VSG and its transient currents were investigated. In this section, results are summarized to voltage sags of types A and B. For all cases of simulation the voltage sag intensity parameter, h is set to 0.1.

Fig. 4.2 shows the current waveforms of VSG subjected to voltage sag of type A with the duration of 2 cycles. Since this is the lightest characteristic of voltage sag, overcurrent happens only during voltage sag. Whereas, as shown in Fig. 4.3, for voltage sag of type A with the duration of 1.5 cycles there are current oscillations which appear after voltage recovery.

Initial point-of-wave must be taken into account for voltage sag of type B. Fig. 4.4 shows the VSG response to a voltage sag of type B with the duration of 2 cycles and initial point-on-wave of $\pi/2$ that is the mildest condition. Slight overcurrent happens in two phases during voltage sag. On

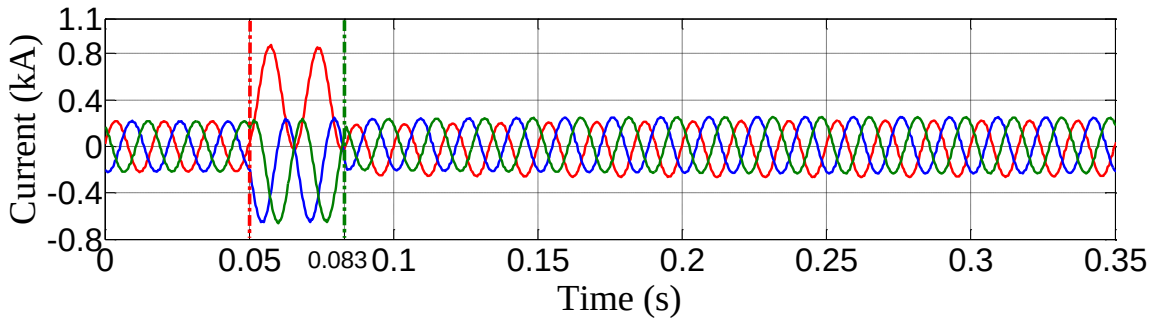

Fig. 4.2- Currents of the VSG subjected to a voltage sag of type A with the duration of 2 cycles and h = 0.1.

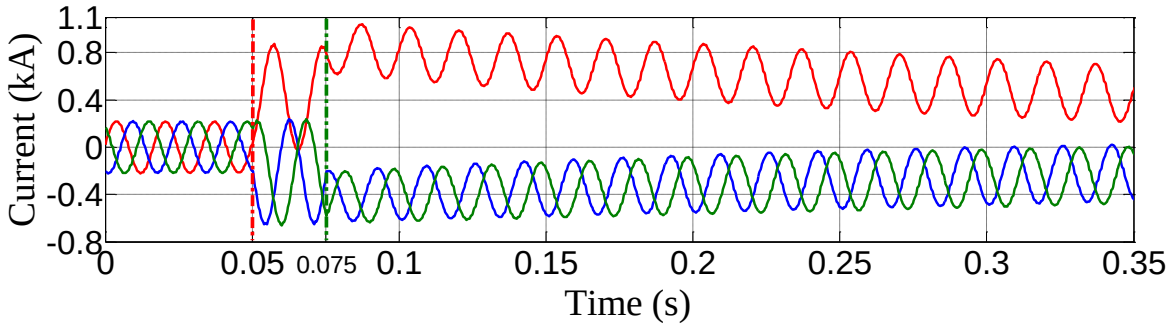

Fig. 4.3- Currents of the VSG subjected to a voltage sag of type A with the duration of 1.5 cycles and h = 0.1.

the other hand, for the severest characteristics, which are the duration of 1.5 cycles and initial point-on-wave of zero, there are significant current oscillations during and after the voltage sag observed in Fig. 4.5.

The point achieved by simulations is that there are two sorts of transients that should be considered: one during the voltage sag and the other one after voltage recovery. In the next part, the effect of the voltage sag characteristics will be clarified analytically.

4.3- State Variable Analysis in Phase Plane

The disparity of the VSG responses to various sags and their characteristics can be illustrated by VSG state variable (current) analysis in phase plane. In addition, the origin of the transients after voltage recovery can be explained by this analysis.

4.3.1- Symmetrical Voltage Sags (Type A)

Inverter output current during voltage sag is calculated by integrating the voltage in polar coordinate in stationary frame (the inverter current before voltage sag is not considered). To obtain

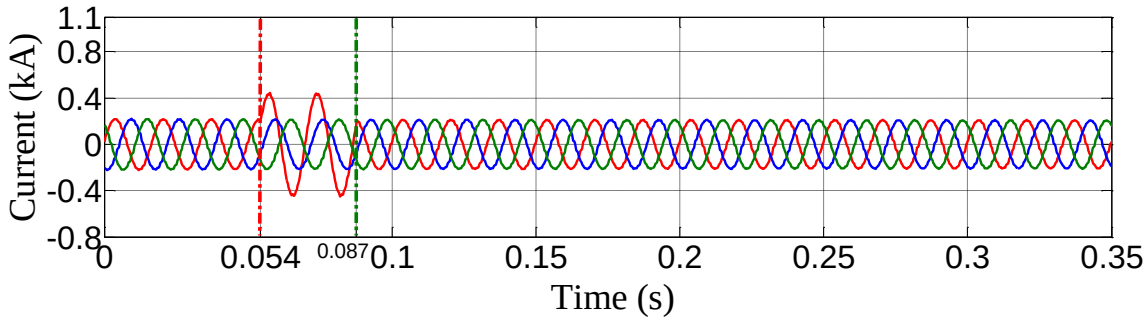

Fig. 4.4- Currents of the VSG subjected to a voltage sag of type B with the duration of 2 cycles, initial point-on-wave of $\pi/2$ and h = 0.1.

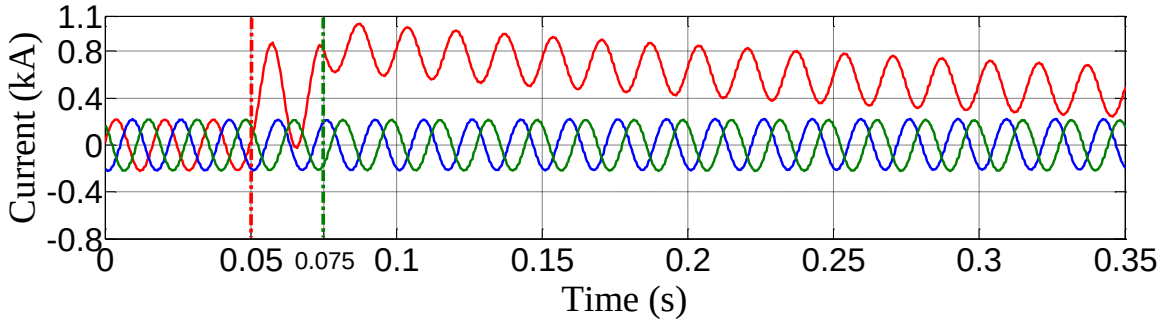

Fig. 4.5- Currents of the VSG subjected to a voltage sag of type B with the duration of 1.5 cycles, initial point-on-wave of zero and h = 0.1.

the voltage equation in polar form, three-phase gird voltage is transferred into the stationary *dq*-frame and expressed in the form of:

$$v(t) = v_d(t) + jv_q(t) = V_m e^{j(\omega_{grid}t+\theta_0-\pi/2)} \tag{4.2}$$

where V_m is the voltage vector magnitude in polar plane. This voltage vector rotates with the synchronous frequency on the stationary phase plane with the initial angle of $\theta_0-\pi/2$. Using this transformation, the voltage equation of sag type A in the stationary polar coordinate is expressed as:

$$v_{sag}(t) = hV_m e^{j(\theta_0-\pi/2)} e^{j\omega_{grid}t} \tag{4.3}$$

where hV_m is the remained voltage amplitude and θ_0 is the initial point-on-wave. As mentioned before, h is the voltage sag intensity parameter varies from zero (zero remained voltage magnitude) to 1 (normal voltage). The fault current is calculated by integrating the voltage difference as:

$$i_{sag}(t) = \frac{1}{L}\int_0^{t_{sag}} (1-h)V_m e^{j(\omega_{grid}t+\theta_0-\pi/2)} dt \tag{4.4}$$

where i_{sag}, L and t_{sag} are the fault current in the stationary reference frame, the interconnecting inductance and the sag ending time, respectively. Solving (4.4) and transferring to the synchronous reference frame yields:

$$i_{sag}^{synch}(t) = (1-h)\frac{V_m}{\omega_{grid}L} e^{j(\theta_0-\pi)}(1-e^{-j\omega_{grid}t}) \tag{4.5}$$

Based on (4.5), during voltage sag, current vector is circulating in the synchronous *dq*-frame phase plane with fixed radius as shown in Fig. 4.6. The damping terms is neglected in this figure. The radius of the circle, $(1-h)V_m/L\omega_{grid}$, determines the oscillation magnitude during voltage sag. It is independent of the θ_0 obviously.

If the duration of voltage sag is a multiple of full cycles, the state variable position at the sag ending moment will reach to its normal point (pre-sag point) after passing through circles in phase plane. When the voltage recovered from the sag, the state variable has to move to its normal point and since it is extremely close to it, minimum oscillations happen after voltage sag. Whereas if the

duration is half a cycle more than any number of full cycles, the state variable position has maximum distance to its normal point at the sag ending moment based on (4.5). It means that transient current has its maximum magnitude. The transient current must settle down on the origin of coordinate (current before fault is neglected) after voltage recovery. The second transient can be expressed as:

$$i_{after\ sag}^{synch}(t) = 2(1-h)\frac{V_m}{\omega_{grid}L}e^{j(\theta_0-\pi)}e^{-j\omega t} \tag{4.6}$$

Equation (4.6) is a circular trajectory with the center coinciding with the origin. The radius of trajectory after voltage sag has its maximum possible value proving that the assumed duration is the severest one. Fig. 4.6 includes the current paths in phase plane. In this dissertation, *d*-axis is taken as the reference axis and phase "*a*" and *q*-axis lead *d*-axis by θ_0 and $\pi/2$, respectively. Part (a) of Fig. 4.6 is related to the sag with the duration of 1.5 cycles and $h = 0.1$. At the sag ending point the state variable goes through circles with a large radius (dotted line) that causes severe current transient. While in part (b) of the figure, when the duration is one full cycle, there is a small distance between the position of the variable after and before the sag and light transient happens.

It must be noted that the transient during voltage sag is not affected by the sag duration. However, the sag magnitude parameter *h*, determines the transient severity during voltage sag. If the voltage sag is shallow (*h* close to unity) and/or if the sag lasts for a relatively long time, the

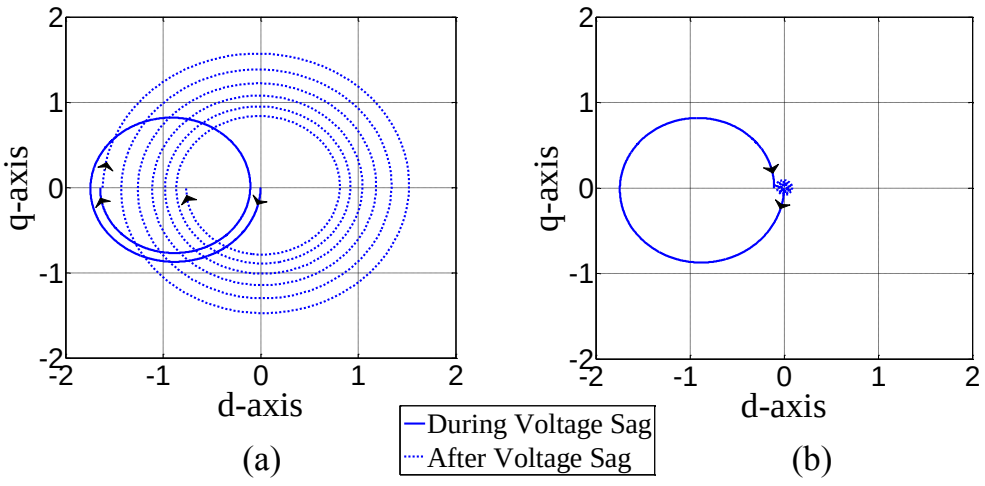

Fig. 4.6- VSG current trajectory in phase plane during (solid line) and after (dotted line) voltage sag type A with $h = 0.1$: (a) Voltage sag with the duration of 1.5 cycles and (b) Voltage sag with the duration of 1 cycle.

state variable transient during voltage sag will settle down at the center of the solid-line circles before voltage sag ends. Afterwards, when voltage amplitude is recovered, the state variable has to move to its normal point from the center of the first transient circles. It means that the oscillations will have identical amplitude regardless of the duration of the voltage sag.

4.3.2- Unsymmetrical Voltage Sags

The same analysis with more intense mathematical work is performed for voltage sag of type B as the representative of unsymmetrical voltage sags. The three-phase phasor expressions of voltage sag type B are as follows:

$$\begin{cases} V_a = hV_{rms} \\ V_b = -\frac{1}{2}V_{rms} - j\frac{\sqrt{3}}{2}V_{rms} \\ V_c = -\frac{1}{2}V_{rms} - j\frac{\sqrt{3}}{2}V_{rms} \end{cases} \tag{4.7}$$

Transforming into polar form in the stationary coordinate yields:

$$v_{sag}(t) = \frac{V_m}{3}((h+2)e^{j(\omega_{grid}t+\theta_0-\pi/2)} + (h-1)e^{-j(\omega_{grid}t+\theta_0-\pi/2)}) \tag{4.8}$$

After integrating the voltage difference between the inverter and grid, the fault current in the synchronous frame is given as follows:

$$i_{sag}^{synch}(t) = \frac{V_m(1-h)}{3L\omega_{grid}}(-e^{j\theta_0} + 2\cos\theta_0 e^{-j\omega_{grid}t} - e^{-j\theta_0}e^{-2j\omega_{grid}t}) \tag{4.9}$$

It is observed that the coefficient $\cos\theta_0$ appears in the current equation and affects its magnitude during oscillation. The form of (4.9) on the phase plane is not exactly circular and depends on θ_0. The characteristics of the voltage sags that result in the maximum absolute value of (4.9) are the critical characteristics for this type of voltage sag. The initial points-on-wave of zero and π bring forth the maximum oscillations during voltage sag type B and with these values of θ_0, when the duration of the sag is a multiple of a half-cycle, the state variable position has maximum distance to its normal point. When voltage is recovered at this moment, the state variable returns to

its normal point with severest oscillation similar to one of the symmetrical voltage sag, i.e., the circular trace in the phase plane. The terms $e^{-2j\omega_{grid}t}$ in (4.9) indicates that the current oscillates with twice of the system frequency during unsymmetrical voltage sags (in the other words, negative phase sequence component exists).

The mildest characteristics of voltage sag type B can be deduced from (4.9) as well. The initial points-on-wave of π/2 and 3π/2 result in the lightest oscillations during voltage sag. For these initial points-on-wave, the duration of a multiple of a half-cycle and the duration of an odd multiple of a quarter-cycle have the mildest and severest consequences after sag, respectively (only the oscillatory component with double system frequency exists in (4.9)). For unsymmetrical voltage sags also, if the duration is long or if the sag is shallow, the transient will settle down before voltage recovery. When voltage is recovered in this condition, the transients after voltage sag has fixed magnitude only related to *h*, in regardless of the duration and initial point-on-wave.

4.4- Voltage Sag Ride-through Enhancement

Three approaches are added to the VSG system to limit the overcurrent during and after voltage sag. Fig. 4.7 shows the VSG system with the additional controls.

4.4.1- Voltage Amplitude Control

Subsystem A in Fig. 4.7 calculates the Root Mean Square (RMS) value of grid voltage and uses it as the reference voltage for inverter output. By this control, when grid voltage drops during voltage sag, inverter output voltage also will be reduced to prevent overcurrent. The RMS voltage is calculated by the following equation:

$$V_{RMS} = \sqrt{V_{grid\ d}^2 + V_{grid\ q}^2} \tag{4.10}$$

During unsymmetrical voltage sags, the calculated RMS voltage has oscillation as mentioned in section 5. A first order Low Pass Filter (LPF) shown in subsystem A of Fig. 9 is used to remove the oscillation.

4.5.1- Output Power Control

Since inverter output power is proportional to the product of the inverter and grid voltages, once the output voltage follows the grid voltage, inverter output power must be limited proportional

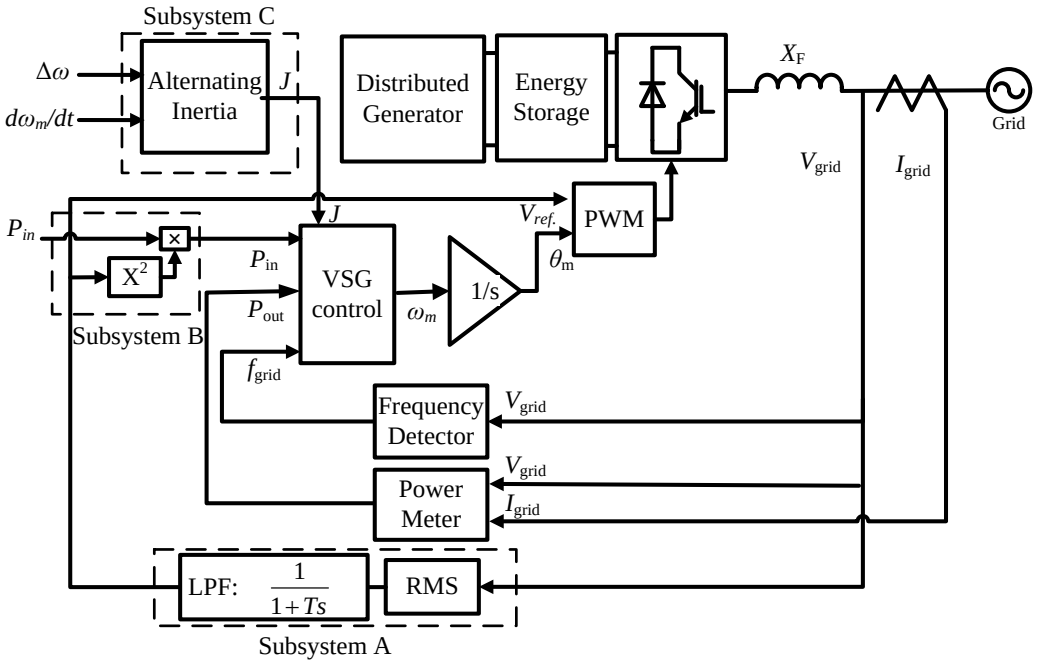

Fig. 4.7- VSG unit with the additional controls for voltage sag ride-through enhancement.

to the square of the grid voltage based on the power transfer equation that is:

$$\begin{aligned} P &= P_{\max} \sin\delta \\ &= \frac{V_{vsg} V_{grid}}{X} \sin\delta \end{aligned} \tag{4.11}$$

where δ is the voltage angle difference between the VSG and the grid. Subsystem B calculates the output power reference of VSG proportional to the square of the grid voltage.

4.4.2- Alternating Inertia Control

The Alternating Inertia control introduced in chapter 2 is used to quickly suppress the oscillation after voltage recovery. The disturbance in this case is different from the power reference change shown in Fig. 2.1. In the case of voltage sag, the power-angle curve follows a new curve in which the maximum transferable power decreases due to voltage drop based on (4.11). In this condition, the power-angle relation follows the dotted line curve shown in Fig 4.8 and load angle moves to the point δ_0. After the fault clearance, operating point moves along the original power-angle curve and load angle oscillates around the equilibrium point δ_1. The machine condition during each phase of an oscillation cycle is summarized in Table 4.2. Here also the derivative of angular velocity, $d\omega_m/dt$ indicates the rate of acceleration or deceleration. The only difference from

the oscillation of power reference change discussed in chapter 2 is the starting point of oscillation and the order of the oscillation phases. To suppress the oscillation, the Alternating Inertia is applied that selects a large value of J during acceleration phases ("a" to "b" and "c" to "b") to reduce the acceleration, and a small value of J during deceleration phases ("b" to "c" and "b" to "a") to boost the deceleration. Using the transient energy function analysis, it is proved that the proposed algorithm brings in a damping effect that suppresses the transient quickly [8]. The subsystem C in Fig. 4.7 adopts the value of the virtual inertia based on the stated algorithm summarized in Table 4.2.

The simulations of section 4.2 were repeated for the VSG with the voltage amplitude, output power, and Alternating Inertia controls under the severest characteristics condition of voltage sags. To let the voltage amplitude control be quick enough, the LPF of the voltage reference loop of Fig. 4.7 was not included during the simulations. Fig. 4.9 shows the current of the VSG subjected to a critical sag type A. The overcurrent that appeared during and after voltage sag in Fig. 4.3 was eliminated effectively by the additional controllers. The current position in phase plane was moved from its normal position toward the origin of the phase plane. This small distance from the normal position caused a slight transient after voltage recovery that was damped slowly.

In the case of unsymmetrical voltage sags, without the LPF in voltage control loop,

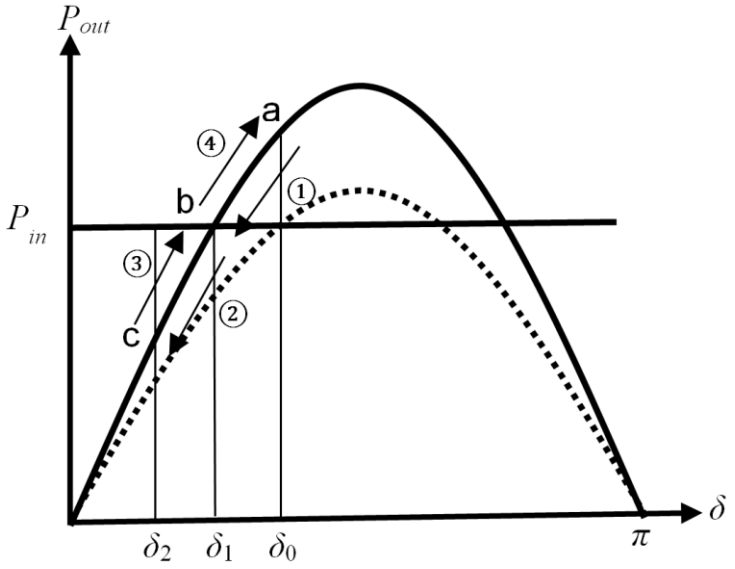

Fig. 4.8- Power-angle curve of a synchronous machine subjected to a fault. When a fault happens, operating point moves on the dotted line and reaches to the point δ_0. After fault clearance, it returns to the original curve and oscillates around the equilibrium point δ_1.

Table 4.2. Machine modes during oscillation.

Segment		$\Delta\omega$	$d\omega_m/dt$	Mode	J
①	a→b	$\Delta\omega < 0$	$d\omega_m/dt < 0$	Accelerating	J_{big}
②	b→c	$\Delta\omega < 0$	$d\omega_m/dt > 0$	Decelerating	J_{small}
③	c→b	$\Delta\omega > 0$	$d\omega_m/dt > 0$	Accelerating	J_{big}
④	b→a	$\Delta\omega > 0$	$d\omega_m/dt < 0$	Decelerating	J_{small}

the calculated RMS voltage will be oscillatory. On the other hand, using the LPF imposes a delay in following the grid voltage and consequently, overcurrent appears at the sag starting moment. It means that the effectiveness of the controller is reduced. Fig. 4.10 shows the simulation result for the severest voltage sag of type B. It is observed that the overcurrent was reduced compared to Fig. 4.5. However, because of the oscillatory voltage reference, it was not reduced as effectively as sag type A.

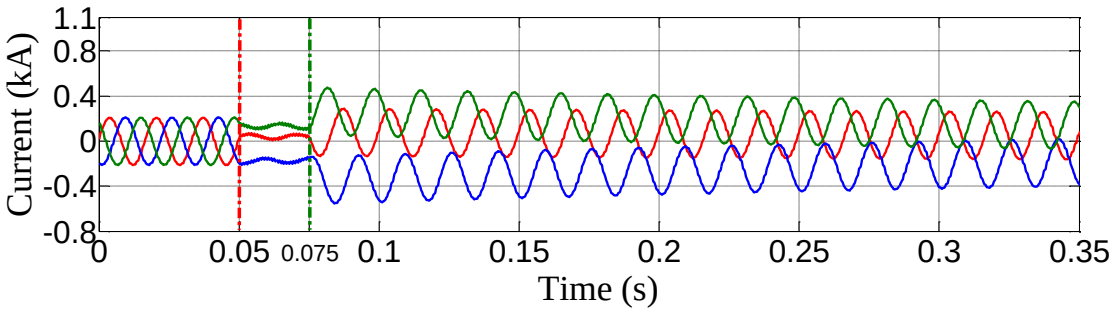

Fig. 4.9- Currents of the VSG with the voltage amplitude, output power, and Alternating Inertia controls, subjected to a voltage sag of type A with the duration of 1.5 cycles and h=0.1 (the severest case).

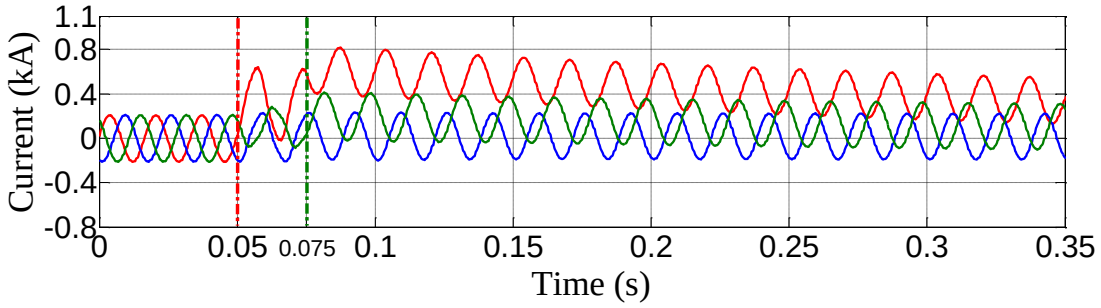

Fig. 4.10- Currents of the VSG with the voltage amplitude, output power, and Alternating Inertia controls, subjected to a voltage sag of type B with the duration of 1.5 cycles, initial point-on-wave of zero and h=0.1 (the severest case).

4.5- Simulation Results

A simulation model similar to the experiment system of next section was built in PSCAD/EMTDC. The system configuration and parameters are shown in Figs. 4.11 and 4.12 and Table 4.3. In the simulation, the transformer was replaced by its equivalent reactance, X_T and all system operated at 207 V nominal voltage. Furthermore, the fault path resistance was chosen 3 Ω to have deep voltage sags. To see the voltage profile during fault, the VSG was disconnected from the Point of Common Coupling (PCC) and three-phase fault stablished for 10 cycles of system frequency. The phase-to-neutral voltages of PCC affected by the fault are shown in Fig. 4.13. The remained voltage in this case is 45% of the rated voltage (h = 0.45). However, the voltage drop in the presence of VSG is less due to the compensation by VSG.

In the next step, the VSG system without the additional controller was connected and a fault happened while the VSG was injecting 2.6 kW power to the grid. The RMS voltage at PCC, VSG current, and the dc link voltage waveforms are presented in Fig. 4.14. In this simulation, the RMS voltage is calculated by (4.10) with a smoothing time constant of 3 ms. As it is observed, the RMS

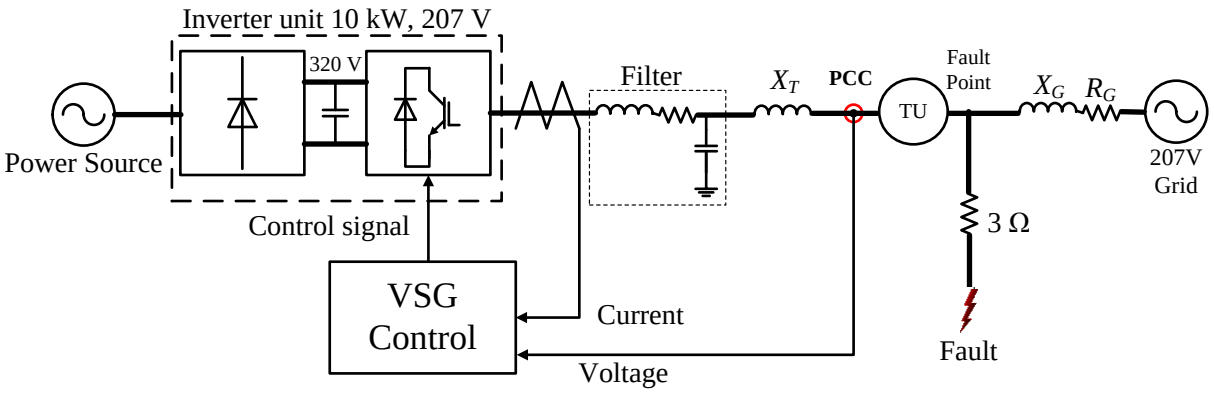

Fig. 4.11- Simulation system.

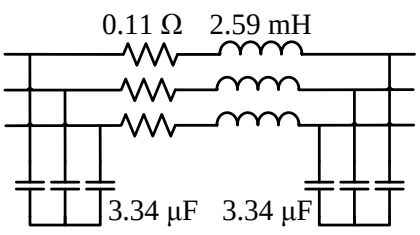

Fig. 4.12- The π model of a 40 km transmission line.

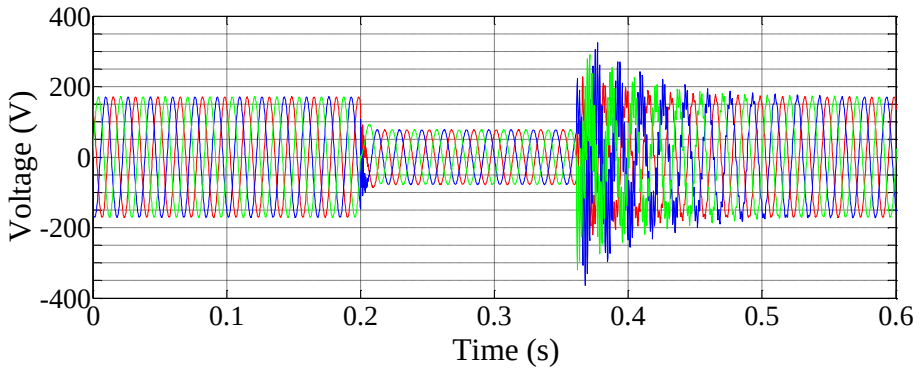

Fig. 4.13- Symmetrical voltage sag at PCC of simulated system due to the three-phase fault.

Table 4.3- The specifications of the simulation system.

Base Power	10 kVA
Base Frequency	60 Hz
Base Voltage	207 V
Switching Frequency	14 kHz
Dc-link Voltage	320 V
Dc-link Capacitor	4.7 mF
Filter Stray Resistance	0.23%
Filter Inductive Reactance	8.8%
Filter Capacitor VAR	1.62%
Resonance Frequency of LC Filter	1.59 kHz
X_T	9.68%
Grid Inductive Reactance, X_G	44%
Grid Resistance, R_G	46%
Damping factor	17 pu
Moment of inertia J	0.563 kgm^2
J_{big}	0.563 kgm^2
J_{small}	0.1 kgm^2

current raised immediately up to 70 A when voltage drop at PCC happened. Moreover, when the voltage magnitude was recovered, the current transient went to negative level (reverse current) and increased the dc-link voltage. The transient during voltage sag may result in the overcurrent failure and the transient after voltage recovery may result in the dc-link overvoltage failure.

The waveforms of the VSG angular velocity, power reference calculated by the governor, VSG output active power, and VSG output reactive power are shown in Fig. 4.15. During transients, the governor calculates the power reference in opposite of the frequency oscillation to fix the VSG frequency at system nominal frequency. The active power of VSG has a waveform similar to the I_d of Fig. 4.14. The reverse power that increases the dc-link voltage is observed more clearly in the

power waveform of Fig. 4.15. The reactive power transient is similar to the transient of I_q of Fig. 4.14.

To mitigate the possible failures, the proposed voltage amplitude control and output power control were added to limit the overcurrent current during voltage sag, and the Alternating Inertia control were added to eliminate the after sag transients and prevent dc-link overvoltage. The RMS voltage at PCC, VSG current, and the dc link voltage waveforms are shown in Fig. 4.16. The PCC voltage sag was deeper because the current injected by VSG was reduced by additional controllers. With the voltage amplitude and output power controls, although the transient current peak at the sag starting moment was reduced to some extent, however because of the delay in RMS voltage calculation, the voltage amplitude control was not able to apply the voltage reference equal to the PCC voltage promptly and the overcurrent prevention performance was limited by this delay. During the voltage sag, since the voltage reference followed the grid voltage, the overcurrent fell down with a steep ramp. The dc-link voltage rise was reduced by around 190 V via the Alternating Inertia control. However, by setting a smaller value for J_{small} this controller is more effective.

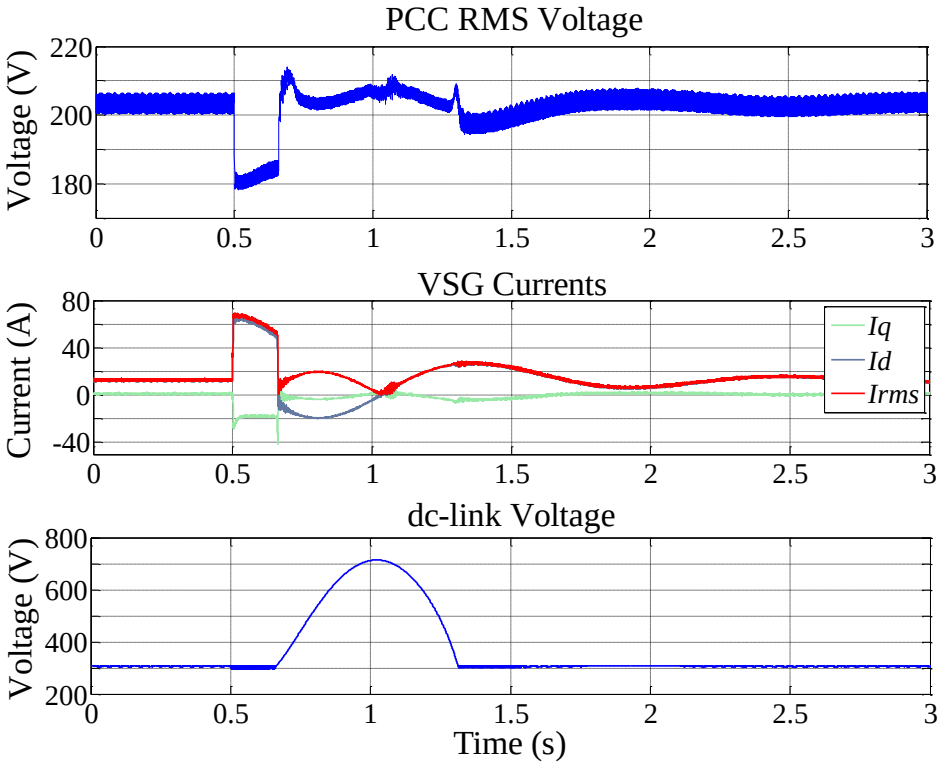

Fig. 4.14- PCC RMS voltage, VSG currents, and dc-link voltage of the system with VSG without the additional controllers, affected by voltage sag.

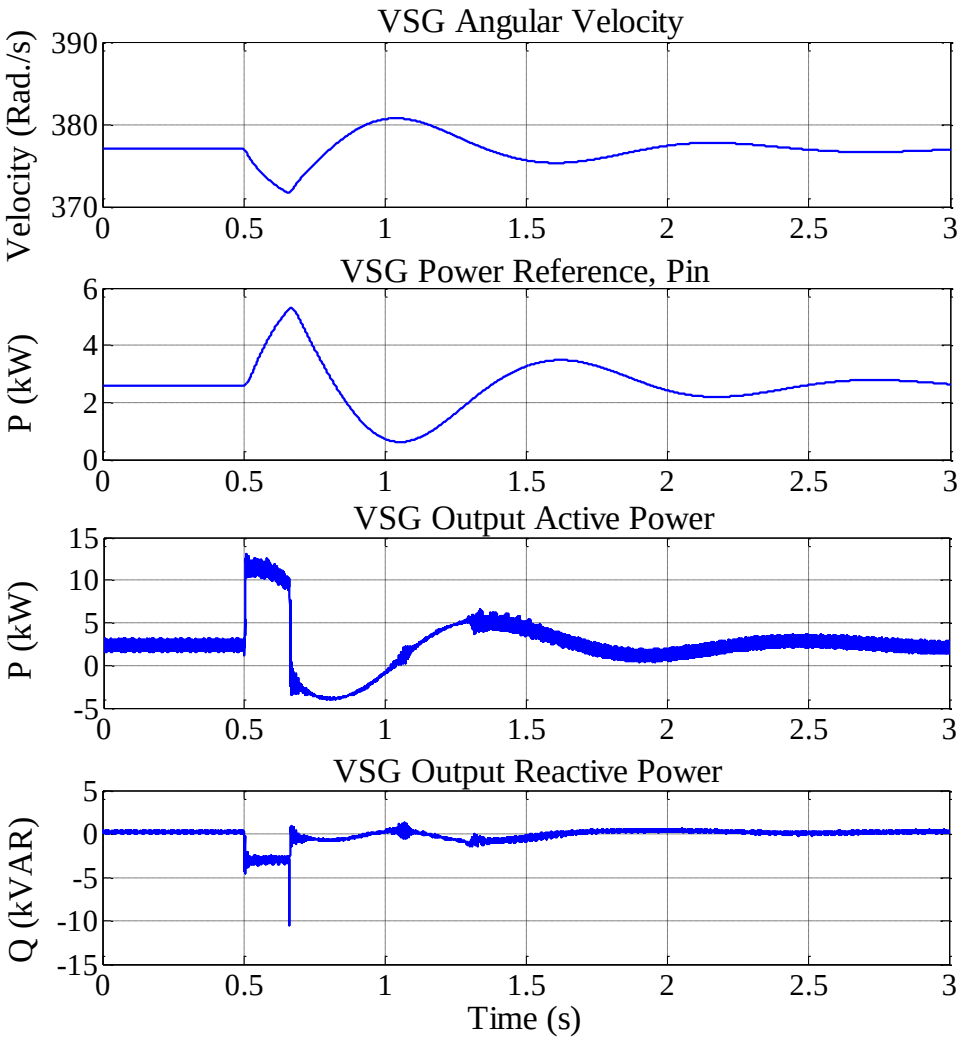

Fig. 4.15- VSG angular velocity, power reference calculated by the governor, VSG output active power, and VSG output reactive power of the system with VSG without the additional controllers, affected by voltage sag.

The VSG angular velocity, power reference calculated by the governor, VSG output active power, and VSG output reactive power are shown in Fig. 4.17. The Alternating Inertia control suppressed the VSG angular velocity quickly. By the output power control, the power reference calculated by governor is reduced at the sag starting moment proportional to the square of the PCC voltage. However the power reference was increased after a short while to regulate the frequency. Similar to I_d, the active power transient during voltage sag was reduced by the additional controllers. After voltage recovery, the transient of output active power had the negative amplitude almost equal to the curve of Fig. 4.15 that was without additional controllers. However, this transient was suppressed quickly by the Alternating Inertia control and did not last for the same

while as Fig. 4.15. Therefore the reverse energy and consequently the dc-link voltage rise is reduced. The *J* calculated by Alternating Inertia control is shown in Fig. 4.18.

As mentioned before, the delay in sensing, calculating and filtering the PCC voltage to calculate the VSG voltage reference is the main obstacle of the effectiveness of the voltage amplitude control. To see the effect of this delay, the smoothing time constant of the RMS voltage calculation was reduced to 1 ms and the simulation was performed. The result is shown in Fig. 4.19. It is observed the delay in RMS voltage calculation was reduced and thereby, the overcurrent at the sag starting moment was reduced considerably. The LPF is essential especially in case of unsymmetrical voltage sags that the calculated RMS voltage has oscillation with double system frequency which must be removed. Moreover, in practical systems, the delay is not only by the filter, but also the sensors and measurement devices comprise considerable delays.

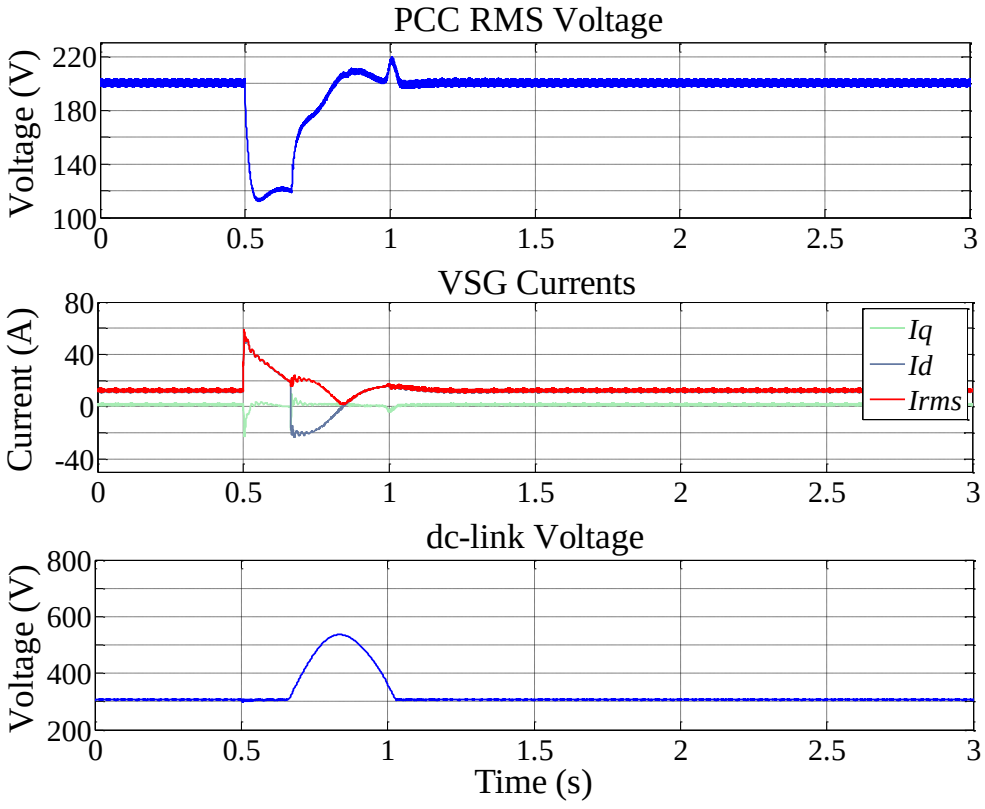

Fig. 4.16- PCC RMS voltage, VSG currents, and dc-link voltage of the system with VSG with the additional controllers, affected by voltage sag.

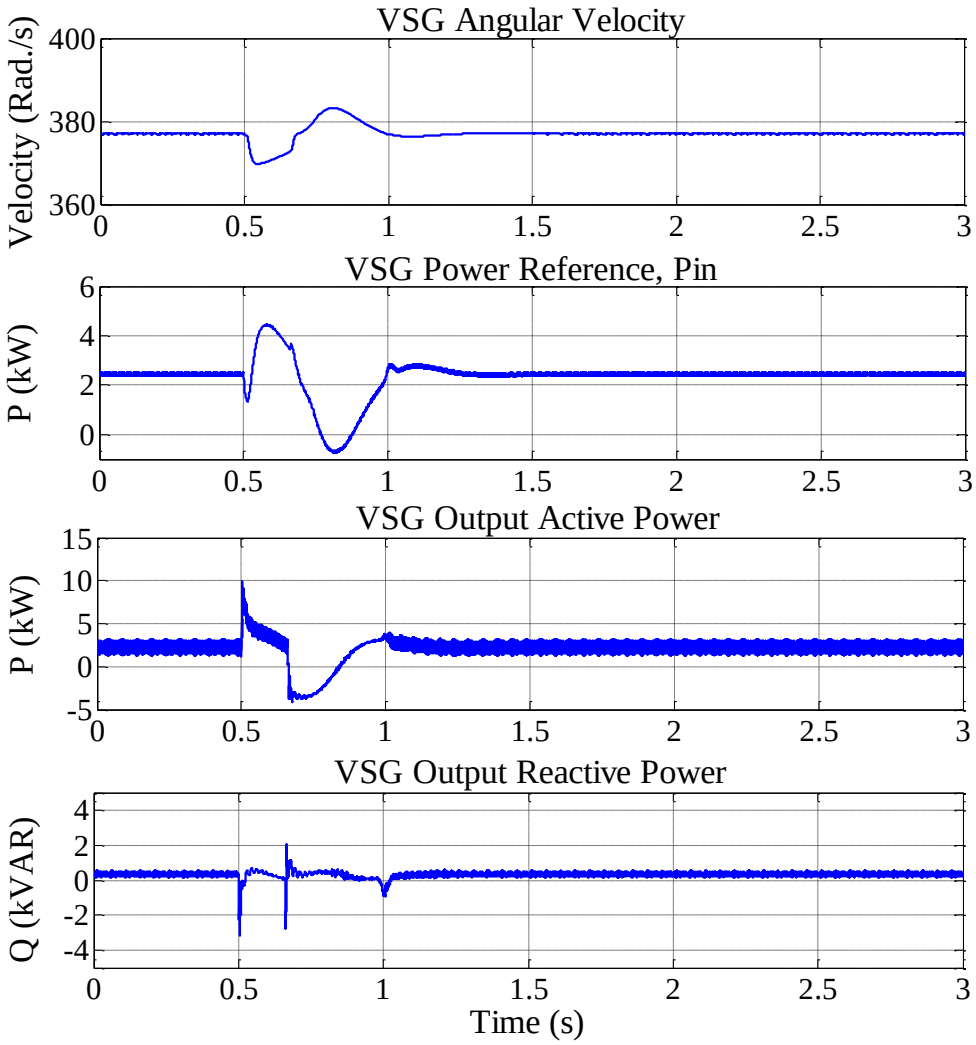

Fig. 4.17- VSG angular velocity, power reference calculated by the governor, VSG output active power, and VSG output reactive power of the system with VSG with the additional controllers, affected by voltage sag.

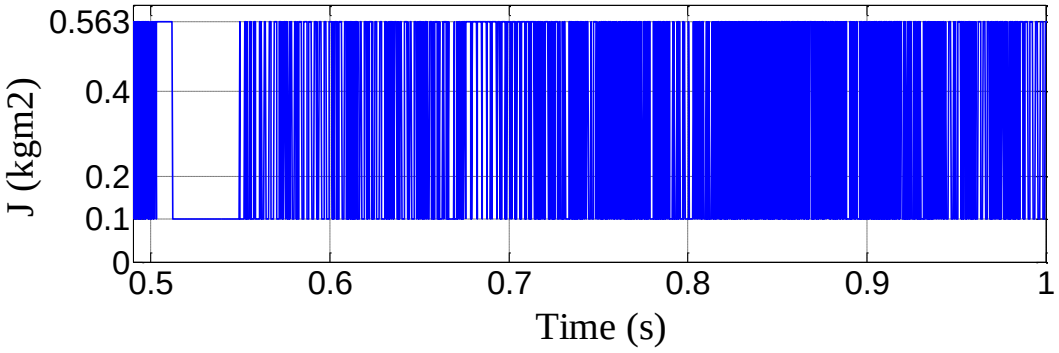

Fig. 4.18- *J* calculated by Alternating Inertia scheme to suppress the oscillation after voltage recovery quickly.

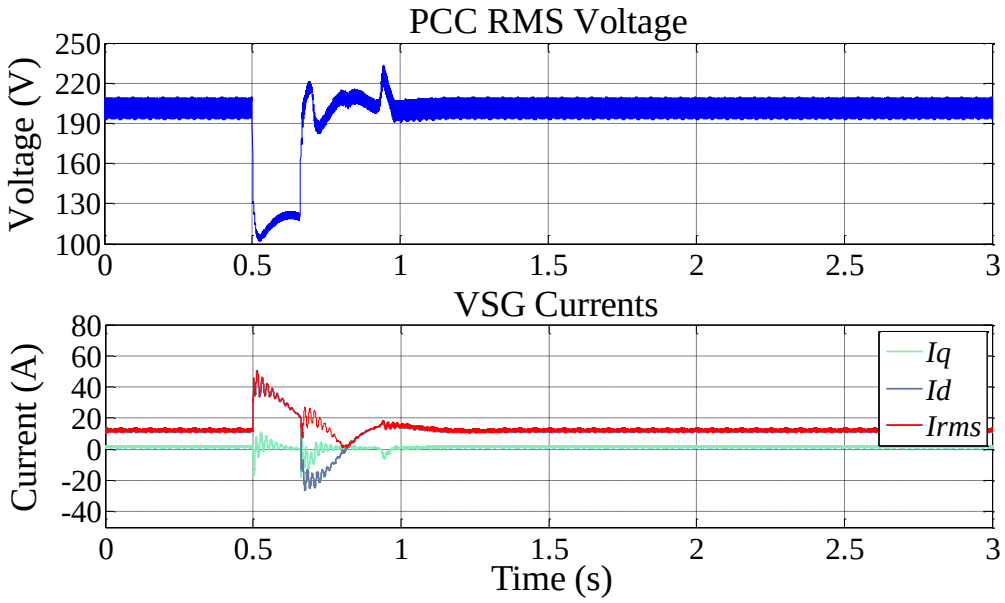

Fig. 4.19- PCC RMS voltage and VSG currents of the system with VSG with the additional controllers (with RMS voltage calculation time constant 1 ms), affected by voltage sag.

4.6- Experimental Results

A laboratory-scale system is used to investigate the voltage sag ride-through performance of the VSG. The overall system configuration is depicted in Fig. 4.20 and the main parameters of the system are presented in Table 4.4. The transmission unit (TU) in Fig. 4.20 simulates the π model of a 40 km transmission line shown in Fig. 4.12.

Due to the strict overcurrent limitation of the inverter unit, when a deep voltage sag happens, the VSG unit is stopped by its protection system. Therefore, mild voltage sags with magnitudes bigger than 90% with the duration of 10 cycles were tested on this system and voltage sag ride-through performance of the VSG unit was evaluated. For light voltage sags, since the state variable position in phase plane at the sag ending moment does not change considerably by the characteristics, the characteristics do not affect the severity of transient oscillation. The voltage amplitude control in experiments has a LPF with 10 Hz cut-off frequency (T = 0.0159 s in Fig. 4.7).

4.6.1- Symmetrical Voltage Sag

The voltage sag shown in Fig. 4.22 appeared due to three-phase short circuit happened at the fault point and measured at the Point of Common Coupling (PCC) indicated in Fig. 4.20. The voltage magnitude during voltage sag is 92% of the normal value. The fault was controlled by

switching thyristors in the fault path. The initial point-on-wave can be adjusted by a phase detection algorithm in the DSP unit. Since the exact turn-off point of the thyristors can not be controlled by the gate signal, the duration of the voltage sag will have utmost a half-cycle error. However, as mentioned before, the duration and initial point-on-wave are not effective for shallow voltage sags. Therefore, the effects of the characteristics of voltage sags were not investigated in the experiments.

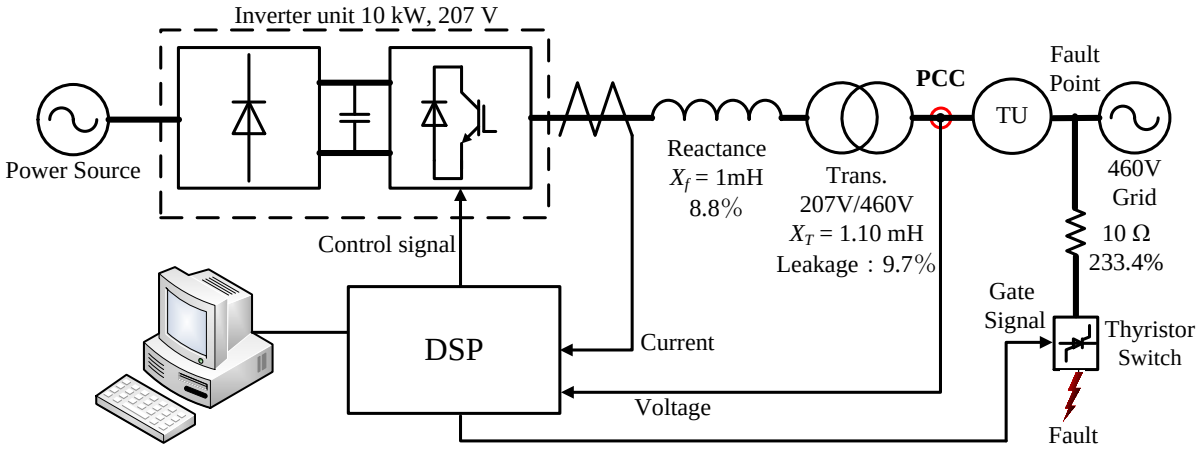

Fig. 4.20- Experimental system.

Table 4.4- The specifications of the simulation system.

Base Power	10 kVA
Base Voltage	207 V
Base Frequency	60 Hz
Switching Frequency	14 kHz
Dc-link Voltage	320 V
Dc-link Capacitor	4.7 mF
Filter Stray Resistance	0.23%
Filter Inductive Reactance	8.8%
Filter Capacitor VAR	1.62%
Resonance Frequency of LC Filter	1.59 kHz
Transformer Reactance	9.68%
Damping factor	17 pu
Moment of inertia J	0.563 kgm^2
J_{big}	0.563 kgm^2
J_{small}	0.1 kgm^2

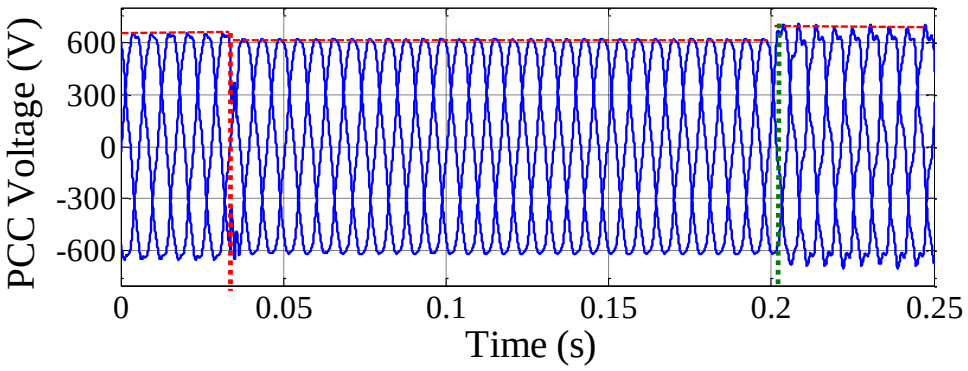

Fig. 4.21- Type A (symmetrical) voltage sag at PCC due to symmetrical three-phase fault.

To assess the performance of the additional controls, first the VSG unit without the controllers is subjected to the voltage sag presented in Fig. 4.21. As stated formerly, two transient states happen: the transient during voltage sag and the one after voltage recovery. To see the importance of the transient after voltage recovery, the VSG was subjected to the voltage sag while injecting 1 kW power to the grid and its current in synchronous *dq*-coordinate was monitored. Fig. 4.22 shows the currents and dc-link voltage in this condition. The oscillations after voltage recovery caused power and current oscillation which went to negative value. This reverse current increased the dc-link voltage and resulted in the failure. Using an energy storage unit with high rate of charging or a larger dc-link capacitor can prevent the dc-link overvoltage failure. However, the objective is to prevent the failure of the existing system by a proper control scheme. It is observed later that Alternating Inertia control will prevent this kind of failure.

During the voltage sag, the VSG current is raised due to the voltage difference between the VSG and the grid. Since the voltage sag amplitude (the remained voltage) is high in this research (that means a mild voltage sag), the initial current of the VSG affects the fault ride-through performance. When the VSG unit was loaded at 2.6 kW, the voltage sag type A was applied. Fig. 4.23 shows that the VSG current raised sharply and VSG was stopped. It can be concluded that for lower loading levels, the oscillations after fault recovery causes the failure and for higher loading levels, the overcurrent during voltage sag results in the failure.

In the next step, only the voltage amplitude control and output power control are activated. When the VSG output power was the inconsiderable value of 1 kW, the type A voltage sag

happened. As it is observed in Fig. 4.24, the oscillation after voltage sag fell to the negative level and activated the dc-link voltage protection.

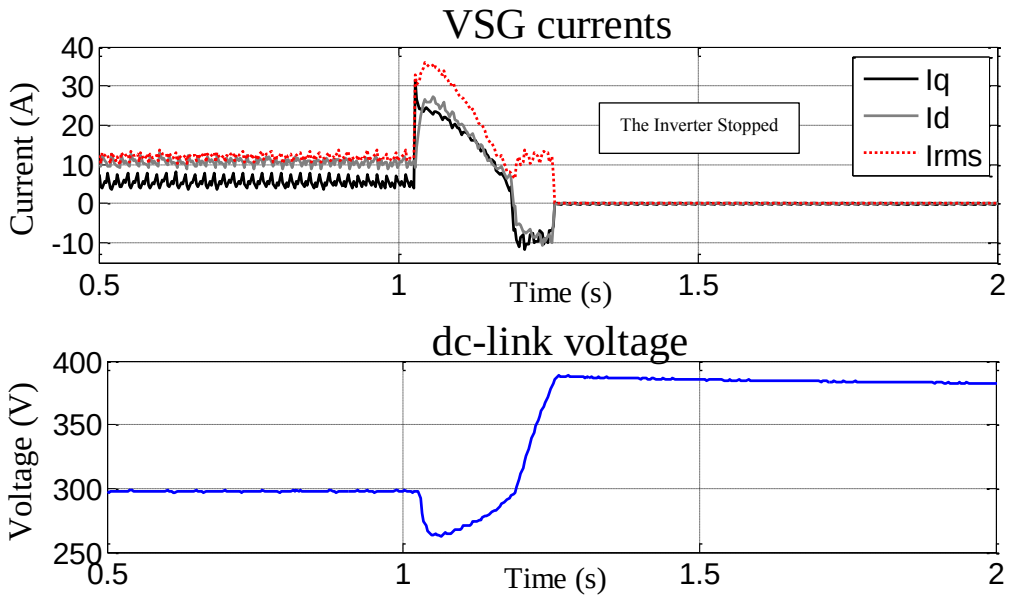

Fig. 4.22- Currents and dc-link voltage of the VSG with 1 kW output power and without additional controller subjected to voltage sag type A.

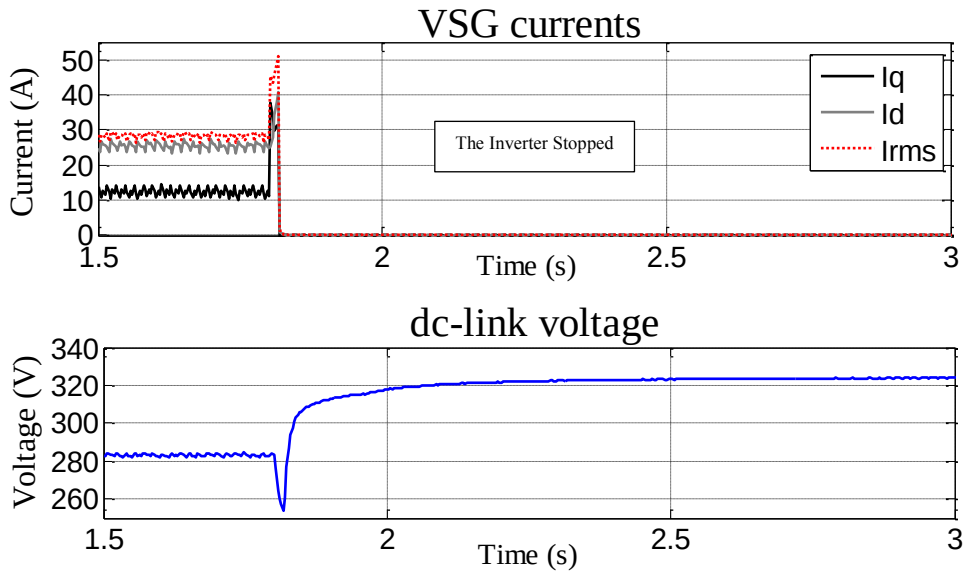

Fig. 4.23- Currents and dc-link voltage of the VSG with 2.6 kW output power and without additional controller subjected to voltage sag type A.

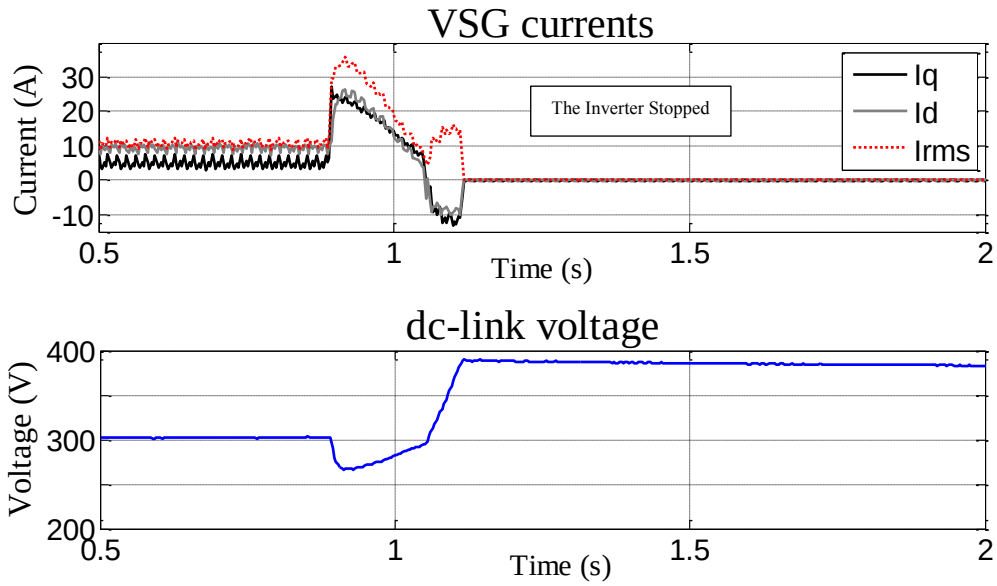

Fig. 4.24- Currents and dc-link voltage of the VSG with 1 kW output power and with voltage amplitude and output power controller subjected to voltage sag type A.

The VSG current and dc-link voltage affected by voltage sag when the VSG power is 2.6 kW is shown in Fig. 4.25. In this condition, the voltage amplitude and power control banned the overcurrent to some extent and the VSG was able to pass-through the fault. Voltage amplitude control of the experiments has a smoothing LPF with the cut-off frequency and transfer function of 10 Hz and $1/(1+0.0159s)$, respectively. When the voltage sag starts, it is expected that the voltage amplitude controller calculate the grid RMS-voltage and apply it as the voltage reference of the inverter. Although the overcurrent magnitude was reduced slightly; however, severe current transient happened. It is because of the delay in sensing, filtering, and applying the voltage reference. In spite of this technical shortcoming, the VSG unit was able to ride-through this voltage sag. It should be noted that the RMS value of I_d and I_q is concerned as the threatening overcurrent.

In the next experiment, all of the additional controllers were activated. First the VSG with the low output power of 1kW was subjected to the voltage sag type A. As it is observed in Fig. 4.26, the Alternating Inertia control suppressed the after sag oscillations by imposing a damping effect. By quick suppression of the after sag transient, the negative current (and the reverse power) was limited and as a result the raise in the dc-link voltage was limited effectively as observed in Fig. 4.26.

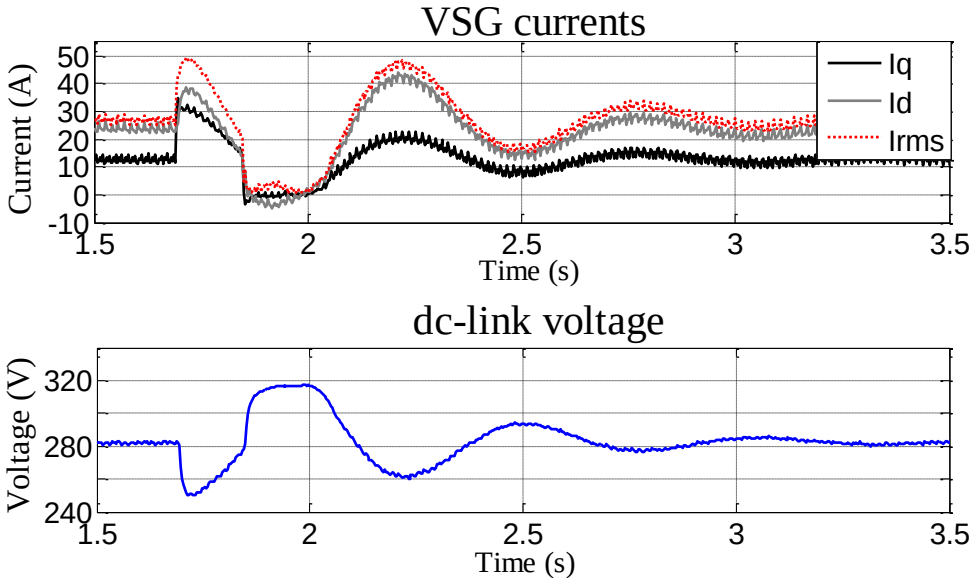

Fig. 4.25- Currents and dc-link voltage of the VSG with 2.6 kW output power and with voltage amplitude and output power controller subjected to voltage sag type A.

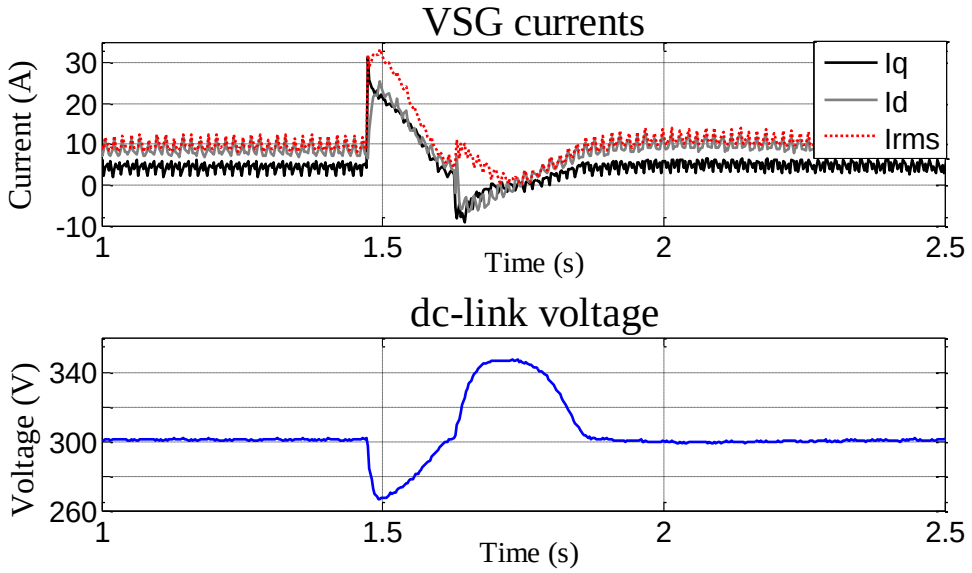

Fig. 4.26- Currents and dc-link voltage of the VSG with 1 kW output power and with voltage amplitude, output power, and Alternating Inertia controller subjected to voltage sag type A.

PCC RMS voltage, power reference calculated by governor, Alternating Inertia, angular velocity, VSG output active power, and VSG output reactive power for the experiment case with 1 kW output power reference and with voltage amplitude, output power, and Alternating Inertia controllers subjected to voltage sag type A are depicted in Fig. 4.27. It is observed that when the voltage dropped, the power reference calculated by governor has been slightly reduced at first,

because it is proportional to the square of RMS voltage by the output power control. However, it has been increased by governor afterwards to compensate the frequency drop. It should be noted that the overcurrent at the sag starting moment has maximum value and should be limited. Accordingly, the reduction in the power reference at the beginning of voltage sag was effective enough to prevent the overcurrent failure in this case. Although, the oscillation after voltage

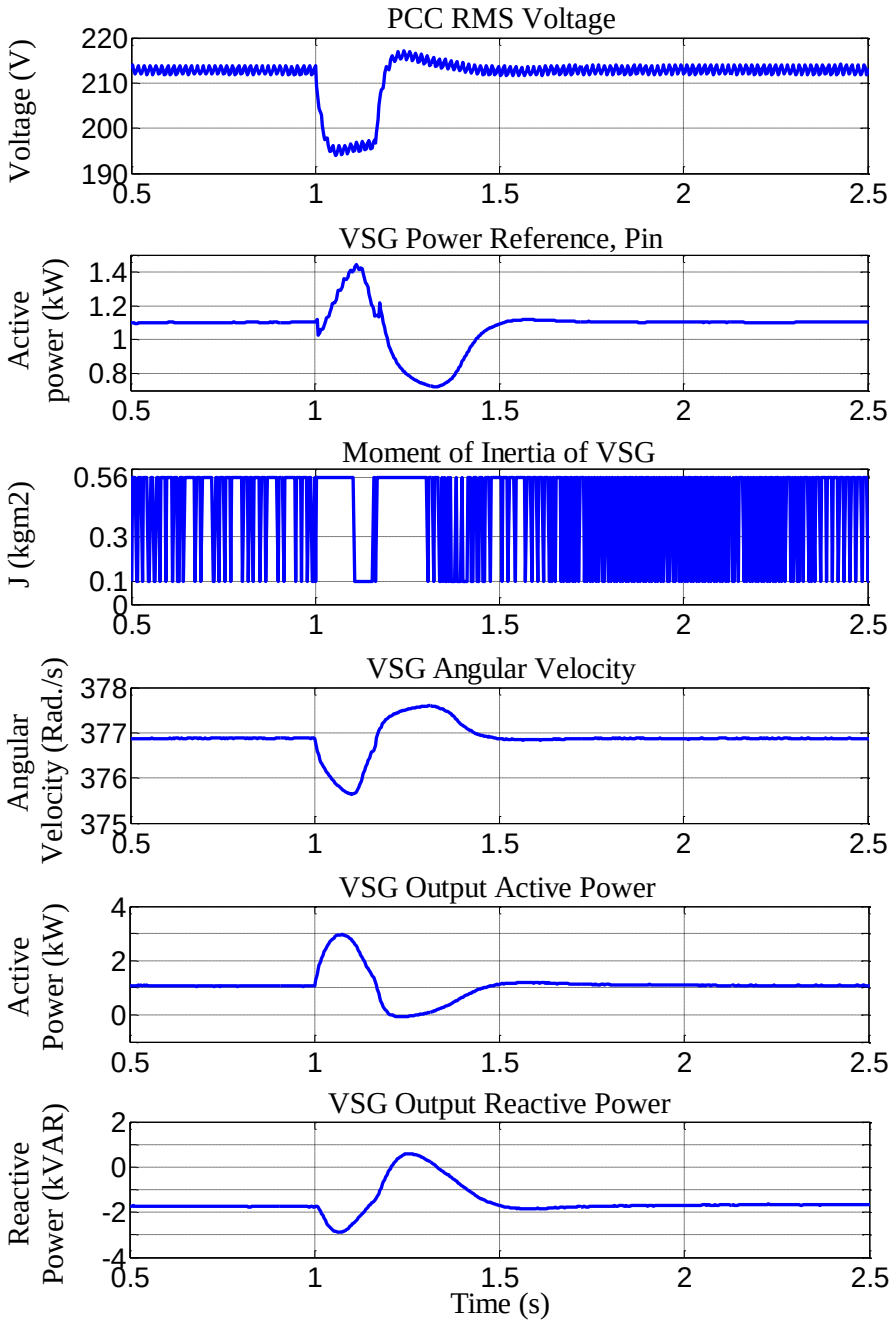

Fig. 4.27- PCC RMS voltage, power reference calculated by governor, Alternating Inertia, angular velocity, VSG output active power, and VSG output reactive power for the experiment case with 1 kW output power reference and with voltage amplitude, output power, and virtual inertia controller subjected to voltage sag type A.

recovery was suppressed by Alternating Inertia, still transient excursions are observed in the active and reactive power waveforms. However, the magnitude of the transients was reduced and the inverter was able to ride-through them. It will be shown in the unsymmetrical voltage sag experiment that the Alternating Inertia control is so effective that even for very lower output power (200 W), the oscillation after voltage recovery does not cause a failure.

In high loading condition, the overcurrent at the sag starting moment is perilous. Fig. 4.28 shows the currents and dc-link voltage of the VSG with 3 kW output power equipped with the additional controllers subjected to the voltage sag type A. Because of the delay in voltage control, output voltage did not follow the grid voltage promptly; therefore, overcurrent appeared right away when the sag starts. However, it fell down quickly and the VSG passed through the voltage sag even with high output power of 3 kW. In this case also, the transient after voltage recovery was damped quickly by Alternating Inertia. At the voltage recovery moment, the inconsiderable current caused a temporary raise in the dc-link voltage. However, the transient current did not go to the negative level and the dc-link voltage was raised up to its rated value.

PCC RMS voltage, power reference calculated by governor, Alternating Inertia, angular velocity, VSG output active power, and VSG output reactive power for the experiment case with 3 kW output power reference and with voltage amplitude, output power, and Alternating Inertia

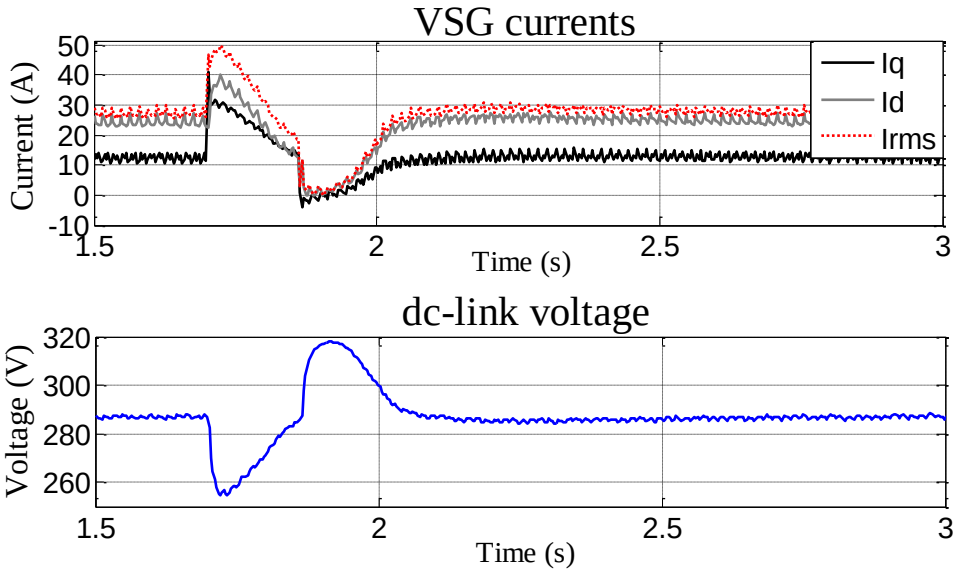

Fig. 4.28- Currents and dc-link voltage of the VSG with 3 kW output power and with voltage amplitude, output power, and Alternating Inertia controller subjected to voltage sag type A.

controllers subjected to voltage sag type A is shown in Fig. 4.29. The PCC RMS voltage value shown in this figure is used by voltage amplitude and power controls. As it is observed, the calculated RMS voltage had a delay that resulted in a high current at the beginning of the voltage sag. Nonetheless, the additional controllers limited this current peak to some extent so that the inverter was able to ride-through the voltage sag.

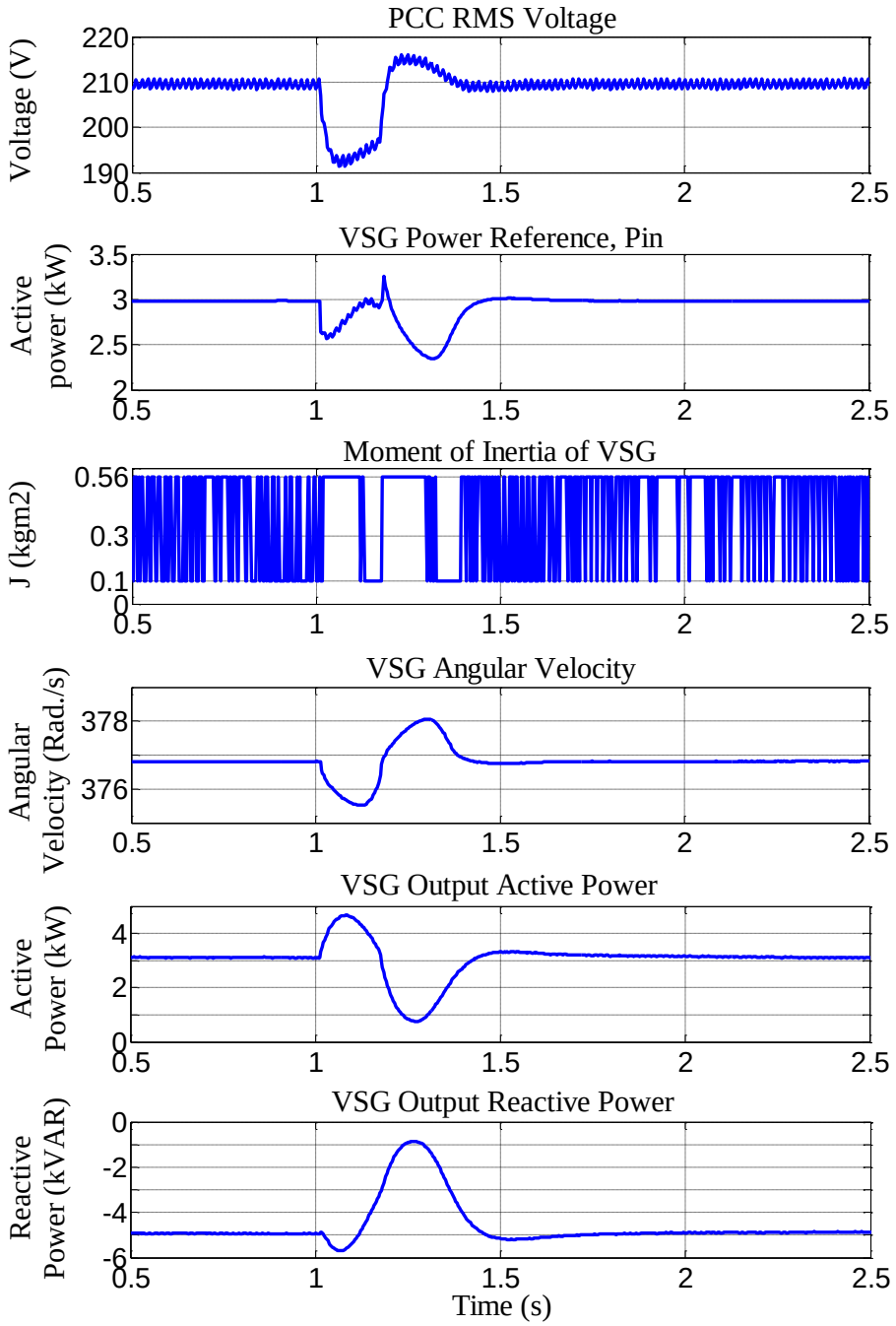

Fig. 4.29- PCC RMS voltage, power reference calculated by governor, Alternating Inertia, angular velocity, VSG output active power, and VSG output reactive power for the experiment case with 3 kW output power reference and with voltage amplitude, output power, and virtual inertia controller subjected to voltage sag type A.

4.6.2- Unsymmetrical Voltage Sag

The VSG unit was also evaluated under unsymmetrical voltage sag condition. A phase-to-phase fault (2LS) with the line-to-line resistance of 20 Ω happened at the fault point of Fig. 4.20 which produced type C voltage sag at PCC with 93% remained voltage at phases "*a*" and "*b*" as shown in Fig. 4.30.

Figs. 4.31 and 4.32 show the experiment results of VSG subjected to voltage sag type C at 1 kW and 2.6 kW output power, respectively. In these cases, the behavior of the VSG without any additional controller was similar to that of the symmetrical voltage sag. The only difference is the form of overcurrent during voltage sag that has an oscillatory component with twice of the system frequency. The VSG unit with output power less than 1 kW failed due to the transients after the sag, and it failed due to overcurrent during the sag when the output power is higher than 2.6 kW.

Fig. 4.33 depicts the current and dc-link voltage of the VSG with voltage sag ride-through controllers, at low output power of 200 W, subjected to the unsymmetrical voltage sag type C. It is observed that when the additional controllers were activated, the oscillation after voltage recovery was eliminated and hence, the failure because of the dc-link overvoltage was prevented.

The same experiment was done when the VSG works at 2.6 kW output power and the results are represented in Fig. 4.34. It is observed that the additional controllers improved the voltage sag ride-through capability of the VSG system effectively. However, there might be a problem in calculating the RMS voltage of the grid during unsymmetrical voltage sag. Since the *dq*-component voltages oscillate with double system frequency during unsymmetrical voltage sag, the RMS value

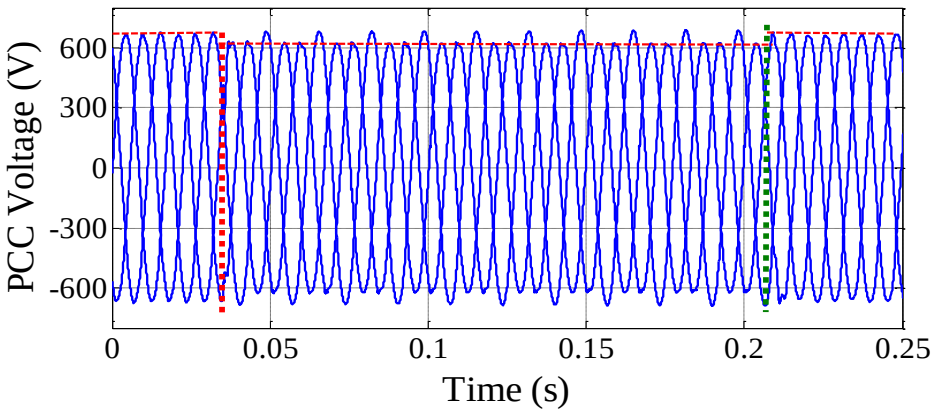

Fig. 4.30- Type C voltage sag at PCC due to phase-to-phase fault.

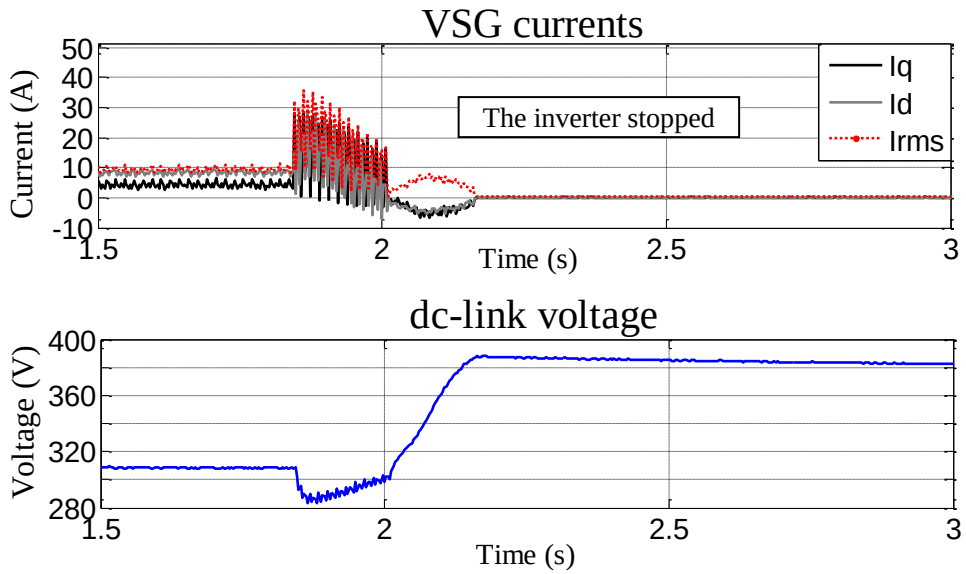

Fig. 4.31- Currents and dc-link voltage of the VSG with 1 kW output power and without additional controller subjected to voltage sag type C.

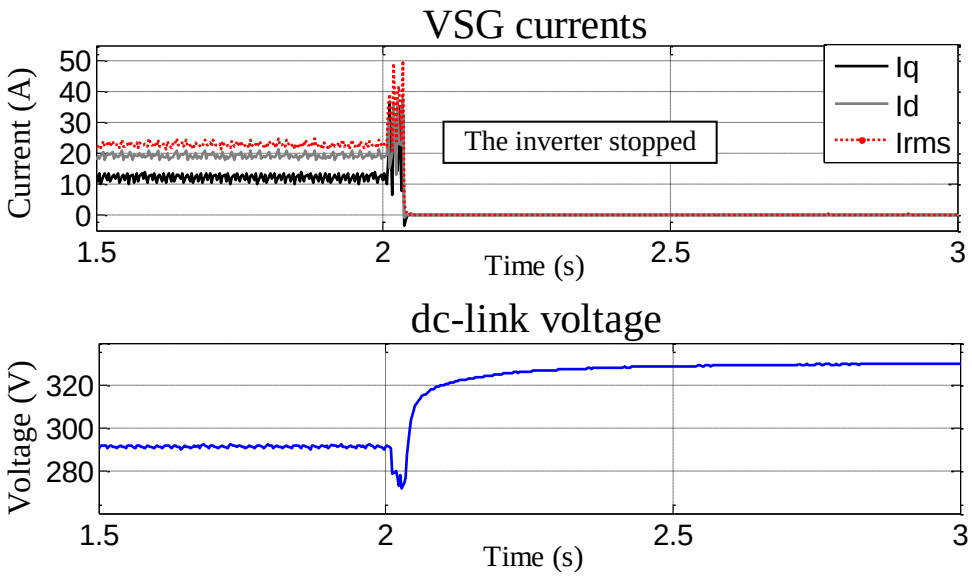

Fig. 4.32- Currents and dc-link voltage of the VSG with 2.6 kW output power and without additional controller subjected to voltage sag type C.

calculated by (4.10) will be oscillatory as well. The oscillatory RMS voltage is not suitable to be used as the voltage reference of VSG. The LPF of the voltage amplitude controller removes this oscillation. However, in accordance with the theoretical analysis of section 4.3, the transient current during unsymmetrical voltage sag has double system frequency component that is observed in Figs. 4.31 to 4.34.

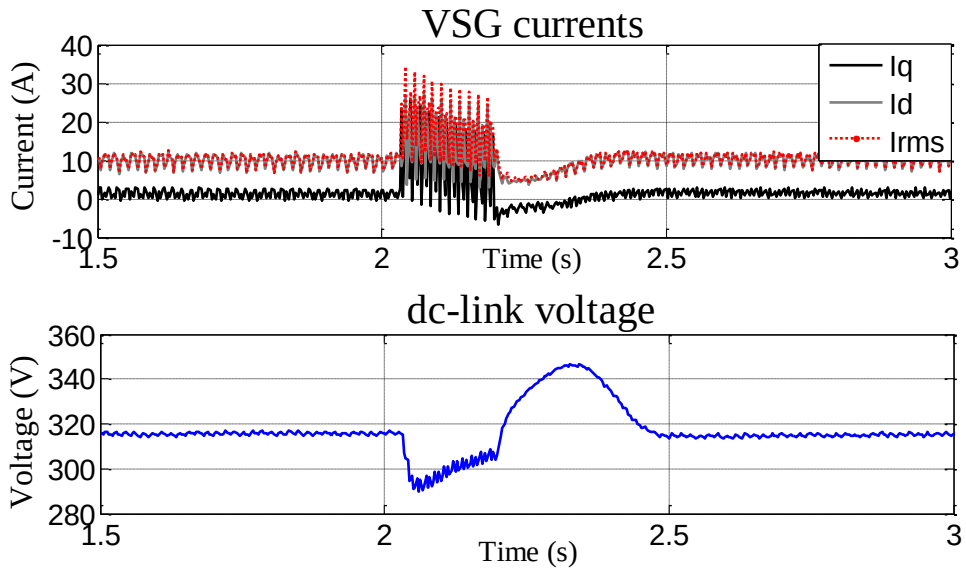

Fig. 4.33- Currents and dc-link voltage of the VSG with 200 W output power and with voltage amplitude, output power, and Alternating Inertia controller subjected to voltage sag type C.

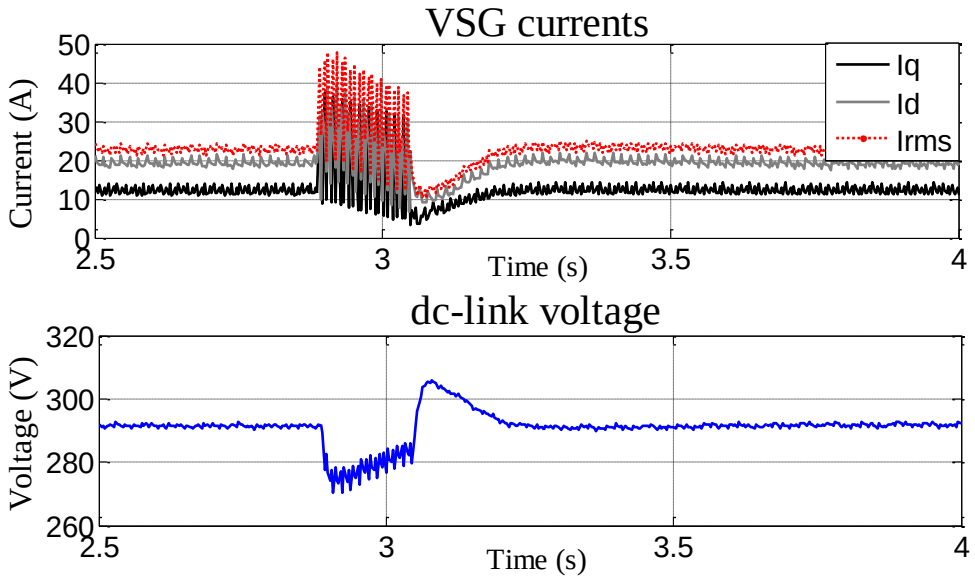

Fig. 4.34- Currents and dc-link voltage of the VSG with 2.6 kW output power and with voltage amplitude, output power, and Alternating Inertia controller subjected to voltage sag type C.

4.7- Conclusion

VSG has been invented to support grid stability by inserting virtual inertia into power system. VSG may be vulnerable in fault condition because of its power electronics basis. Evaluation of voltage sag consequences is the first step of VSG protection in fault condition. Symmetrical and

unsymmetrical types of voltage sag were applied to the VSG and its response was monitored by checking the transient current. It was observed that when a VSG unit is subjected to a voltage sag, two sorts of transients appear during and after voltage sag that their severity depends on the characteristics of the voltage sag. If a symmetrical voltage sag (type A) lasts a half cycle more than a multiple of full cycles, severest current oscillation appears after voltage recovery. For unsymmetrical voltage sags, initial point-on-wave is also important. The initial points-on-wave of zero and π result in the severest transients during and after voltage sag for both voltage sag types B and D; whereas for type C, $\pi/2$ and $3\pi/2$ are the critical ones. With the stated critical initial points-on-wave, the durations of a half cycle more than any multiple of full cycles produce the severest transients after voltage recovery. The origin of the transients was explained by analyzing the state variable trajectory in phase plane. By extracting the radius of the circulations of the transient current in phase plane, the severity of the transients can be evaluated. Finally, voltage amplitude control and output power control were added to the VSG system to suppress the overcurrent during voltage sag and Alternating Inertia control was implemented to eliminate the oscillation after voltage recovery. Simulations and experimental results showed that the additional controls improved voltage sag ride-through capability of VSG effectively for symmetrical and unsymmetrical voltage sags.

References

[1] K. J. P. Macken, M. H. J. Bollen, and R. J. M. Belmans : "Mitigation of voltage dips through distributed generation systems", IEEE Transactions on Industry Applications, vol. 40, no. 6, pp. 1686-1693, (2004)

[2] B. Renders, K. De Gusseme, W. Ryckaert, K. Stockman, L. Vandevelde, and M.H.J. Bollen : "Distributed generation for mitigating voltage dips in low-voltage distribution grids", IEEE Transactions on Power Delivery, vol. 23, no. 3, pp. 1581-1588, (2008)

[3] B. Renders, W.R. Ryckaert, K. De Gusseme, K. Stockman, and L. Vandevelde : “Improving the voltage dip immunity of converter-connected distributed generation units”, Elsevier, Renewable Energy, vol. 33, no. 5, pp.1011 -1018, (2007)

[4] M.H.J. Bollen : "Voltage recovery after unbalanced and balanced voltage dips in three-phase systems", IEEE Transactions on Power Delivery, Vol. 4, No. 18, pp. 1376–1381, (2003)

[5] M. H. J. Bollen : "Characterization of voltage sags experienced by three-phase adjustable-speed drives", IEEE Transactions on Power Delivery, Vol. 12, No. 4, pp.1666 -1671, (1997)

[6] Das, J. C., "Effects of momentary voltage dips on the operation of induction and synchronous motors," *IEEE Trans. Industry Appl.*, Vol. 26, No. 4, pp. 711–718, 1990.

[7] J. Alipoor, A. Doroudi, and S. H. Hosseinian, "Identification of the critical characteristics of different types of voltage sags for synchronous machine torque oscillations," Journal of *Electric Power Components and Systems, Taylor & Francis*, Vol. 42, No. 13, PP. 1347-1355, 2014.

[8] J. Alipoor, Y. Miura, T. Ise, "Power system stabilization using virtual synchronous generator with alternating moment of inertia," *IEEE Journal of Emerging and Selected Topics in Power Electronics*, vol. PP, no. 99, pp. 1-8, 2014.

Chapter 5

Summary and Future Challenges

Since the generated electricity of some types of DGs/RESs is not suitable to be connected to the power system directly, incorporating inverter-based generating units in new power systems is inevitable. It has been detected that the large number of inverter-based units without rotating inertia causes instability problem. Moreover, majority of existing control techniques for grid-connected inverters do not contribute in frequency regulation of power system. Load sharing and parallel operation of inverters are other challenging issues. The VSG idea emerged to mitigate the problems with inverter-based DGs. Based on the VSG concept, an inverter is controlled in a manner that it emulates the behavior of a synchronous generator as much as possible to utilize its advantages in stabilization and controllability.

Because the VSG is a power-electronics device inherently, it is not possible to operate in conditions exactly similar to a SG in terms of loading, tolerance, and reliability. Therefore, its control should be improved to enhance its performance. In this direction, Alternating Inertia was introduced that alternates the value of the moment of inertia considering the angular frequency mismatch and its rate of change. Alternating Inertia selects a big value for the moment of inertia

during acceleration to reduce the acceleration and on the other hand, during deceleration, a small value for inertia factor was adopted to increase the deceleration effect. It was clarified by the energy function analysis that the system transient energy is reduced promptly by the reduction in the value of the moment of inertia. This scheme results in a fast reference frequency tracking, oscillation damping, and reliable performance preserving the original feature of VSG that is mimicking the behavior of a SG.

Using several numbers of VSGs in power systems involves new technical challenges. As the electric industry seeks to reliably integrate large amounts of DGs/RESs into the power system in regulated environment, considerable effort will be needed to effectively manage the installed VSG units. To address this matter, multi-VSG microgrid was introduced. Since the parameters of the swing equation used in the VSG control can be varied in real time, PSO was used to coordinate the inertia of the generators in order to first, achieve a smooth transition with minimum oscillations and second, maintain the integrity of the system in case of a change or disturbance. Although adjusting the inertia of the VSGs by PSO is not effective in stabilization of a seriously unstable power system (it is performed in power systems by stability constrained power dispatch), during short period transients that can result in out-of-step, the integrity of the system can be preserved. Furthermore, Alternating Inertia was applied to the multi-VSG microgrid and it showed remarkable performance in stabilization.

Continuous operation of grid connected inverters in case of faults and disturbances is an important issue. If a new design is not reliable enough, its application will be limited. Because of the low tolerance of power electronic devices of inverters, majority of the inverter control technologies are very vulnerable against voltage disturbances. It was tried to improve the voltage sag ride-through performance of VSG-controlled inverter with the existing control structure and system elements. Firstly, the VSG system was evaluated under symmetrical and unsymmetrical voltage sags with various characteristics and the severest characteristics of voltage sags for grid connected inverters was extracted. The results showed that two sorts of transients appear: during and after voltage sag. Three controls were designed to mitigate the hazardous transients and prevent inverter failures. At low loading level, the transient after voltage recovery caused a negative current and reverse power that increased the dc-link voltage and resulted in a failure. Using Alternating

Inertia, the transient after voltage recovery was suppressed. Therefore, reverse power and dc-link overvoltage failure was prevented. In high loading condition, the overcurrent due to voltage difference during voltage sag caused the failure. The voltage amplitude and output power controls limited the overcurrent during voltage sag and reduced the chance of failure. However, the time delay associated with RMS voltage calculation reduced the effectiveness of this controller.

Once a new product or topology such as VSG is introduced to the power system, the key aspect to utilize the potential advantages of it is to coordinate the new product with the rest of system and also to make the power grid robust and able to take advantage of the potential flexibility of distributed VSGs. Hereafter, a challenging issue that can be subject of future research to improve the performance of VSG concept is mentioned.

- *Optimal allocation of VSGs and Coordination between VSGs and SGs*

Recent researches addressed the optimal allocation of DGs in modern power systems. However, the VSG system has its own properties and features. Therefore, the method for allocating them should be revised and considerations such as weak areas that have high rate frequency variations should be included. Because usually VSG units incorporate an energy storage unit, optimal allocation of them is more concerned form the economic point of view.

The operation of VSG unit in a grid or microgrid will affect the performance of other generators including SGs. In the design and control of other generator, the effect of VSG units must be considered. For example, in case of supporting the frequency of system, an important feature of VSG units is the possibility of their fast active power injection. Following a power imbalance, the active power generated by VSGs quickly changes to recover the system frequency following a disturbance. As this increased/decreased power can last just for a few seconds, conventional SGs should eventually take charge of the huge changed demand by shifting their generation to compensate power imbalance. However, the fast power injection by VSGs may slow down to a certain extent the response of conventional SGs. To avoid this undesirable effect, coordination between VSGs and conventional SGs in the grid frequency control is needed. Another example is the stability studies consideration. As discussed in chapter 3, the VSG units insert an amount of inertia into the system that can change the frequency and angle of the center of inertia. When the

stability analysis is performed, to take a true preventing/correcting decision, the role of VSGs should be included.

Same concern exists for standards related to overall reliable performance of the power system as instituted by technical committees, reliability entities, regulatory bodies and organizations ensure the integrity of the whole power system is maintained for credible contingencies and operating conditions. There exist some principles to be taken into account in the future standards development on microgrid system in the presence of DGs/RESs and VSG units.

Appendix A

Transient-Response Parameters of a VSG Connected to Grid

For steady-state stability analysis, the small-signal model of VSG connected to the grid is extracted by linearizing the equations that describes the VSG behavior in the vicinity of the predisturbance operating point. Consider the VSG unit connected to the grid bus as shown in Fig. A1. The VSG injects power P_{out} to the grid based on the swing equation expressed as:

$$P_{out} - P_{in} = -J\omega_m \, d\omega_m / dt - D\Delta\omega \tag{A.1}$$

In steady-state condition, $P_{out} = P_{in}$. The power transferred to the grid bus is determined by the power transfer equation that is:

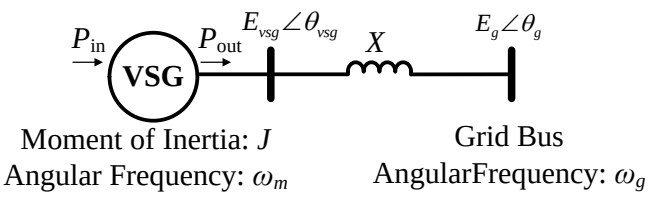

Fig. A.1- VSG connected to the grid bus.

$$\begin{aligned} P_{out} &= \frac{E_{vsg}E_g}{X}\sin\theta \\ &= P_{\max}\sin\theta \end{aligned} \tag{A.2}$$

Where $\theta = \theta_{vsg} - \theta_g$. Linearizing A.2 at the operating point with θ equal to θ_0 yields:

$$\Delta P_{out} = P_{\max}\cos\theta_0\Delta\theta \tag{A.3}$$

$\Delta\theta$ is the difference between the transient θ after the disturbance and θ_0 (θ_0 is the value of θ before the disturbance in steady-state and $\theta = \theta_0+\Delta\theta$). The change in the power ΔP_{out} is the difference between the VSG output power after the disturbance and its value before disturbance. The VSG output power before disturbance is equal to P_{in}. It can be concluded that ΔP_{out} is equal to the right-hand side of A.1. Substituting the right-hand side of A.1 in A.3, and considering $\omega = d\Delta\theta/dt$ results in the second order dynamic equation:

$$J\omega_m\frac{d^2\Delta\theta}{dt^2} + D\frac{d\Delta\theta}{dt} + P_{\max}\cos\theta_0\Delta\theta = 0 \tag{A.4}$$

Assuming the VSG angular velocity is equal to the system angular frequency ω_s, the eigenvalues of A.4 is written as:

$$\begin{aligned} \lambda_{1,2} &= \sigma \pm \sqrt{\sigma^2 - \omega_n^2} \\ &= -\frac{D}{2J\omega_s} \pm \sqrt{\left(\frac{D}{2J\omega_s}\right)^2 - \frac{P_{\max i}\cos\theta_{0i}}{J\omega_s}} \end{aligned} \tag{A.4}$$

The real part of the eigenvalue σ, the undamped natural frequency ω_n, and the damping ratio ξ that determine the VSG response can be written as:

$$\sigma = -\frac{D}{2J\omega_s}$$

$$\omega_n = \sqrt{\frac{P_{\max}\cos\theta_0}{J\omega_s}} \tag{3.2}$$

$$\xi = \frac{-\sigma}{\omega_n}$$

Publications

[1] J. Alipoor, A. Doroudi, S. H. Hosseinian, "Identification of the Critical Characteristic of Different Types of Voltage Sags for Synchronous Machine Torque Oscillations," *Electric Power Components and Systems*, vol. 42, no. 13, pp. 1347-1355, 2014.

[2] J. Alipoor, Y. Miura, T. Ise, "Power system stabilization using Virtual Synchronous Generator with Alternating Moment of Inertia," *IEEE Journal of Emerging and Selected Topics in Power Electronics*, Accepted for Publication.

Conference (with review)

[1] J. Alipoor, Y. Miura, T. Ise, "Distributed generation grid integration using virtual synchronous generator with adoptive virtual inertia," in Proc. *IEEE Energy Conversion Congress and Exposition (ECCE)*, pp. 4546-4552, 2013.

[2] J. Alipoor, Y. Miura, T. Ise, "Voltage sag ride-through performance of Virtual Synchronous Generator," in Proc. *IEEE Power Electronics Conference (IPEC-Hiroshima - ECCE-ASIA)*, pp. 3298-3305, 2014.

Other Presentations

[1] J. Alipoor, K. Sakimoto, Y. Miura, T. Ise, "Operation and Control of Virtual Synchronous generator under Different Types of Voltage Sag Conditions", Annual meeting of the Institute of Electrical Engineering of JAPAN (電気学会全国大会学会), Hiroshima, JAPAN, May, 2012.

[2] J. Alipoor, Y. Miura, T. Ise, "Evaluation of Virtual Synchronous Generator (VSG) Operation under Different Voltage Sag Conditions", IEEJ Conference on Power Technology and power systems (電力技術/電力系統技術合同研究学会), Tokyo, JAPAN, August, 2012.

[3] J. Alipoor, Y. Miura, T. Ise, "Real-Time Tuning of Multi-VSG by PSO Algorithm," In Proceeding of *Power and Energy Sector Conference of Institute of Electrical Engineers of Japan* (電気学会電力・エネルギー部門大会), Kyoto, September 2014.

[4] J. Alipoor, Y. Miura, T. Ise, "Optimization of Microgrid with Multiple VSG Units," In Proceeding of *IEEJ* power technology and power system technology (電力技術・電力系統技術合同研究会), PE-14-125, PSE-14-125, Osaka, September 2014.